2011

Advanced composites using non-autoclave processes: manufacturing and characterization

V. G. K. Menta

Department: Mechanical and Aerospace Engineering

ADVANCED COMPOSITES USING NON-AUTOCLAVE PROCESSES: MANUFACTURING AND CHARACTERIZATION

by

VENKATAGIREESH K MENTA

A DISSERTATION

Presented to the Faculty of the Graduate School of the

MISSOURI UNIVERSITY OF SCIENCE AND TECHNOLOGY

In Partial Fulfillment of the Requirements for the Degree

DOCTOR OF PHILOSOPHY

IN MECHANICAL ENGINEERING

2011

Approved by

K. Chandrashekhara, Advisor

L. R. Dharani

A. C. Okafor

V. A. Samaranayake

T. Schuman

PUBLICATION DISSERTATION OPTION

This dissertation has been prepared in the form of three papers using the styles utilized by the following publications as follows:

Pages 1 - 63 intended to submit to JOURNAL OF APPLIED POLYMER SCIENCE

Pages 64 - 87 intended to submit to JOURNAL OF REINFORCED PLASTICS

Pages 88 - 127 intended to submit to JOURNAL OF COMPOSITE MATERIALS

ABSTRACT

The objective of the present study is to develop non-autoclave processes to manufacture high performance composites for aerospace applications. In Paper 1, vacuum assisted resin transfer molding (VARTM) process was developed for elevated temperature composites. Use of VARTM process for fabricating high temperature resins presents unique challenges such as high porosity and low fiber volume contents. Two different vacuum bagging methods: Seeman Composite Resin Infusion Molding Process (SCRIMP) and Double Vacuum Bagging Infusion (DVBI) process were evaluated. Flow simulation tool was used to predict key flow parameters needed for the successful infusion. In Paper 2, honeycomb sandwich panels were manufactured using commercially available film adhesive and modified VARTM process. The resin incursion into the core openings is a major challenge for applying VARTM process to open cell core sandwich composites. Panels manufactured using the developed process did not show any resin accumulation in the core. The mechanical performance of the manufactured sandwich composites was evaluated. Results indicate that the VARTM process can be successfully used to manufacture honeycomb composite sandwich structures using currently available barrier adhesive films. In Paper 3, a new generation vacuum-bag-only cure out-of-autoclave (OOA) manufacturing process was studied. Physical and mechanical performance of the composites was evaluated. The influence of size, lay-up configuration, thickness and their interactions on the impact behavior of the composites was studied using Design of Experiments (DoE).

ACKNOWLEDGMENTS

I would like to express my heartfelt and deepest gratitude to my academic advisor, Dr. K. Chandrashekhara, for his invaluable guidance, advice, encouragement and generous financial support throughout the course of the investigation and successful completion of this dissertation research.

I would also like to express my sincere gratitude to the members of the advisory committee, Dr. L. R. Dharani, Dr. A. C. Okafor, Dr. V. A. Samaranayake, and Dr. T. Schuman for their guidance, assistance and their valuable time.

Many thanks to my colleagues Dr. S. Sundararaman, Dr. J. Hu, Dr. Chen, and Mr. R. R. Vuppalapati who never hesitated to help when needed. Also, I would like to thank our composite research group team for their support.

The author would also like to acknowledge the financial support received from the Department of Mechanical and Aerospace Engineering at Missouri University of Science and Technology for Graduate Research Assistantship (GRA). Also, the GRA received from National University Transportation Center (NUTC) and Center for Aerospace Manufacturing and Technology (CAMT) consortium at Missouri S&T is gratefully acknowledged.

I would also like to immensely thank my parents, family and friends for their encouragement and support to reach this milestone in my life.

TABLE OF CONTENTS

Page

PUBLICATION DISSERTATION OPTION iii

ABSTRACT iv

ACKNOWLEDGMENTS v

LIST OF ILLUSTRATIONS ix

LIST OF TABLES xii

SECTION

1. INTRODUCTION 1
2. SCOPE AND OBJECTIVES 5

PAPER

I. ELEVATED-TEMPERATURE VARTM PROCESS FOR HIGH PERFORMANCE AEROSPACE COMPOSITES 7

ABSTRACT 7

1. INTRODUCTION 8
2. EXPERIMENTAL 10
   - 2.1. RESIN CHARACTERIZATION 10
     - 2.1.1. Differential Scanning Calorimetry (DSC). 10
     - 2.1.2. Rheology. 11
     - 2.1.3. Mechanical Testing. 11
   - 2.2. MANUFACTURING OF COMPOSITES 11
   - 2.3. PERFORMANCE EVALUATION 13
3. RESULTS AND DISCUSSION 13
   - 3.1. DIFFERENTIAL SCANNING CALORIMETRY 13
   - 3.2. VISOCOSITY MEASUREMENT 14
   - 3.3. NEAT RESIN MECHANICAL TESTS 14
   - 3.4. FIBER VOLUME FRACTION TESTS 14
   - 3.5. TENSILE CHARACTERIZATION 15
   - 3.6. THREE POINT BENDING TESTS 15
   - 3.7. SHORT BEAM SHEAR TESTS 15
   - 3.8. IMPACT TESTS 15
   - 3.9. COMPRESSION-AFTER-IMPACT (CAI) TESTS 16

3.10. OPEN HOLE COMPRESSION (OHC) TESTS 16
4. FLOW SIMULATION 17
5. CONCLUSIONS 18
6. REFERENCES 19
II. EVALUATION OF HONEYCOMB SANDWICH COMPOSITE STRUCTURES MANUFACTURED USING VARTM PROCESS 63
ABSTRACT 63
1. INTRODUCTION 64
2. MATERIALS 65
3. MANUFACTURING 66
4. PERFORMANCE EVALUATION 67
4.1. FIBER VOLUME FRACTION TESTS 67
4.2. OPTICAL MICROSCOPY 67
4.3. FLATWISE TENSILE TESTS 67
4.4. FLATWISE COMPRESSION TESTS 68
4.5. EDGEWISE COMPRESSION TESTS 68
4.6. THREE-POINT BENDING TESTS 69
4.7. LOW VELOCITY IMPACT TESTS 69
5. CONCLUSIONS 70
6. REFERENCES 71
III. COMPOSITES USING OUT-OF-AUTOCLAVE PREPREGS 88
ABSTRACT 88
1. INTRODUCTION 89
2. MATERIALS 92
3. MANUFACTURING 93
4. CHARACTERIZATION 93
4.1. FIBER VOLUME FRACTION TESTING 93
4.2. TENSILE TESTS 94
4.3. FLEXURE TESTS 95
4.4. LOW VELOCITY IMPACT TESTS 95
4.5. COMPRESSION-AFTER-IMPACT (CAI) TESTS 95
5. STATISTICAL ANALYSIS 96

6. EXPERIMENTATION 97
7. RESULTS AND DISCUSSION 97
8. CONCLUSIONS 99
9. REFERENCES 100
SECTION
3. CONCLUSIONS 128
BIBLIOGRAPHY 130
VITA 132

LIST OF ILLUSTRATIONS

Page

PAPER I

Figure 1. Schematic Representation of SCRIMP Process 29
Figure 2. Cure Profile Obtained from Thermocouple of the Oven 30
Figure 3. Schematic Representation of DVBI Process 31
Figure 4. Dynamic Curing Curve of Cycom 977-20 Epoxy Resin 32
Figure 5. DSC Thermograms of Cycom 977-20 Epoxy Resin 33
Figure 6. Viscosity vs. Temperature Profile of Cycom 977-20 Resin System 34
Figure 7. Tensile Stress-Strain Curves of Cycom 977-20 Showing Reproducibility of Tensile Tests 35
Figure 8. Stress-Strain Curves of Cycom 977-20 in Three Point Bending and Showing Reproducibility 36
Figure 9. Tensile Stress-Strain Curves of Cycom 977-20/AS4-5HS Carbon Composites and Showing Reproducibility 37
Figure 10. Stress-Strain Curves of Cycom 977-20/AS4-5HS Carbon Composites in Three Point Bending and Showing Reproducibility 38
Figure 11. Load-Displacement Curves of Cycom 977-20/AS4-5HS Carbon Composites under Short Beam Shear Loads and Showing Reproducibility 39
Figure 12. Impact Energy History Curves of Cycom 977-20/AS4-5HS Carbon Composites 40
Figure 13. Contact Force History Curve of Cycom 977-20/AS4-5HS Carbon Composites 41
Figure 14. Displacement History Curve of Cycom 977-20/AS4-5HS Carbon Composites 42
Figure 15. Contact Force vs. Displacement of Cycom 977-20/AS4-5HS Carbon Composites 43
Figure 16. Damage on the Top Surface of the Impacted Samples of Cycom 977-20/AS4-5HS Carbon Composites 44
Figure 17. Damage on the Bottom Surface of the Impacted Samples of Cycom 977-20/AS4-5HS Carbon Composites 45
Figure 18. CAI Testing Set-up 46
Figure 19. Compression Load vs. Deflection of Cycom 977-20/AS4-5HS Carbon Composites during CAI Testing Process 47
Figure 20. Front View of the Tested of Cycom 977-20/AS4-5HS Carbon Composite Samples 48

Figure 21. Rear View of the Tested of Cycom 977-20/AS4-5HS Carbon Composite Samples 49
Figure 22. OHC Testing Coupons of Cycom 977-20/AS4-5HS Carbon Composites 50
Figure 23. OHC Compressive Stress-Strain Curves of Cycom 977-20/AS4-5HS Carbon Composites 51
Figure 24. Cycom 977-20/AS4-5HS Carbon Composite Specimens Before (Left) and After OHC Testing (Right) 52
Figure 25. Damaged Cycom 977-20/AS4-5HS Carbon Composite Specimen After OHC Testing (Side View) 53
Figure 26. Mesh of FEA model for VARTM Flow Simulation 54
Figure 27. Saturation Distribution at Time = 7 sec 55
Figure 28. Saturation Distribution at Time = 30 sec 56
Figure 29. Pore Pressure Distribution at Time = 7 sec 57
Figure 30. Pore Pressure Distribution at Time = 30 sec 58
Figure 31. Saturation Distribution of Cross-section at Time = 7 sec 59
Figure 32. Saturation Distribution of Cross-section at Time = 30 sec 60
Figure 33. Saturation Distribution of Cross-section at Time = 225 sec 61
Figure 34. Saturation Distribution of Cross-section at Time = 435 sec 62

Paper II

Figure 1. Schematic Representation of Out-of-Autoclave Bagging Procedure 78
Figure 2. Cure Profile of VARTM Manufacturing 79
Figure 3. Sandwich Composites Manufactured using VARTM Process 80
Figure 4. Photomicrograph (x20) of Core-to-Facing Adhesive Bond 81
Figure 5. Flatwise Compression Behavior of Honeycomb Sandwich Composites 82
Figure 6. Edgewise Compression Testing (Left); Facesheet Buckling Failure (Right) 83
Figure 7. Edgewise Compression Load Deflection Curves of Sandwich Composites 84
Figure 8. Three Point Bending Test Set-up 85
Figure 9. Three-Point Bending Load Deflection Curves of Sandwich Composites 86
Figure 10. Impact Test Results (a) Impact Energy History Curve, (b) Velocity History Curve, (c) Contact Force vs. Displacement 87

Paper III

Figure 1. Schematic of Out-of-Autoclave Bagging Procedure 109
Figure 2. Cure Cycle for Out-of-Autoclave Process 110

Figure 3. Flexural Stress-Strain Curves of MTM45-1/CF2412 Composites.....111
Figure 4. Energy-Time History of MTM45-1/CF2412 Composites.....112
Figure 5. Impact Load vs. Deflection of MTM45-1/CF2412 Composites 113
Figure 6. Velocity-Time History of MTM45-1/CF2412 Composites 114
Figure 7. Load vs. Deflection of MTM45-1/CF2412 Composites during CAI Testing Process 115
Figure 8. Front View of MTM45-1/CF2412 Composite Sample under CAI Testing 116
Figure 9. Impact Energy vs. Time of MTM45-1/CF2412 Composites 117
Figure 10. Contact Force vs. Time of MTM45-1/CF2412 Composites 118
Figure 11. Contact Force vs. Displacement of MTM45-1/CF2412 Composites.....119
Figure 12. Main Effect Plots for Absorbed Energy 120
Figure 13. Interaction Effect Plots for Absorbed Energy 121
Figure 14. Significant Main Effect Plots for Peak Force.....122
Figure 15. Size vs. Thickness Interaction Effect Plot for Peak Force 123
Figure 16. Significant Main Effect Plots for Contact Duration.....124
Figure 17. Size vs. Thickness Interaction Effect Plot for Contact Duration.....125
Figure 18. Significant Main Effect Plots for Maximum Deflection 126
Figure 19. Size vs. Thickness Interaction Effect on Maximum Deflection.....127

LIST OF TABLES

Page

Table 1.1. Properties of Conventional Structural Materials and FRP Composites.....2

PAPER I

Table 1. Differential Scanning Calorimetry Results of the Cycom 977-20 Epoxy Resin 21

Table 2. Fiber Volume Fraction Test Results 22

Table 3. Tensile Properties of AS4-5HS/Cycom 977-20 Composite 23

Table 4. Flexural Test Results in Longitudinal and Transverse Directions.....24

Table 5. Summary of Impact Test Results.....25

Table 6. CAI Strength Values at Different Impact Energies 26

Table 7. OHC Test Results 27

Table 8. Type and Number of Elements for Parts 28

PAPER II

Table 1. Core Properties 73

Table 2. Fiber Volume Fraction Test Results 74

Table 3. Ultimate Flatwise Tensile Strength.....75

Table 4. Flexural Test Results 76

Table 5. Low Velocity Impact Test Results.....77

PAPER III

Table 1. Fiber Volume Fraction Test Results 102

Table 2. Tensile Properties 103

Table 3. Flexural Test Results 104

Table 4. CAI Strength Values at 32J Energy Level.....105

Table 5. Factors and their Levels.....106

Table 6. Experimental Treatments for Testing 107

Table 7. Analysis of Variance (ANOVA), p-values.....107

SECTION

1. INTRODUCTION

Composite materials can be defined as "a combination of two or more materials that form a new material system with enhanced material properties." Typically, composite materials contain discontinuous phases embedded in a continuous phase. The discontinuous phase is called the "reinforcement" while the continuous phase is called the "matrix" [1].

Composite materials offer several advantages over conventional metals like: high strength to weight ratio, light weight, greater corrosion resistance, low life-cycle costs, extended service life. Another outstanding advantage of composite materials is that they offer design flexibility in that they can be tailored to provide properties in the desired direction [2-3]. Composite materials have been considered as an excellent alternative for heavy and costly metals in many applications. The properties of conventional structural materials and fiber reinforced polymer (FRP) composites are shown in the Table 1.1 [4].

Composite materials are being used in marine, aircraft, automotive, construction, bio-medical and consumer applications. Presently, composites are used in almost every industry. Published reports show that there is a rapid increase in the global use of composite materials with a 3,800 percent growth over a period of 45 years since their first commercial use in late 1940's [6]. History has shown that the use of composite materials increased from 158,800 metric tons (350 million lb) in 1960 to 6.1 million metric tons (13.5 billion lb) in 2004 [2].

Sandwich composites are extensively used in aerospace applications due to their exceptional strength and high stiffness-to-weight ratios as compared to conventional materials [6-7]. Sandwich construction typically consists of thin facesheets separated by a lightweight core. The facesheets carry the bending loads and the core carries the shear/compressive loads. The facesheets are made of metal or composites. Balsa wood, foam, and honeycomb are commonly used core materials. The composite materials offer at least the same or even higher strengths as metals such as aluminum or steel, but their moduli are often much lower giving poor stiffness performance. By using sandwiched composites this problem can easily be overcome.

Table 1.1. Properties of Conventional Structural Materials and FRP Composites

Material	Tensile Modulus (E) (GPa)	Tensile Strength (σ_u) (GPa)	Density (ρ) (g/cm^3)	Specific Modulus (E/ρ)	Specific Strength (σ_u/ρ)
Mild Steel	210	0.45-0.83	7.8	26.9	0.058-0.106
Aluminum 2024-T4	73	0.41	2.7	27	0.152
Aluminum 6061-T6	69	0.26	2.7	25.5	0.096
E-glass–epoxy	21.5	0.57	1.97	10.9	0.26
Kevlar 49–epoxy	40	0.65	1.4	29	0.46
Carbon–epoxy	83	0.38	1.54	53.5	0.24
Boron-epoxy	106	0.38	2	53	0.19

The continuous support of the facesheet, unlike a stiffened structure, implies that surfaces remain flat even under high compressive stress without buckling. This is important in e.g. aircraft structures in which control surfaces should remain smooth even under loading. Sandwich structures in several applications have shown superior acoustic insulation. The use of cellular core materials means that no additional thermal insulation needs to be added to the structure thus ensuring a low structural weight, since most cellular cores have a very low thermal conductivity. Sandwich structures can be manufactured in large sheets, giving large smooth areas without the need for connections like rivets and bolts. This means fewer parts are needed and the assembly of the structure is simplified, which in turn saves money. When using fiber composite faces, even large structures can be manufactured in more or less than one piece, thus reducing assembly costs and ensuring smooth and continuous load paths without disturbing stress concentrations [8]. Sandwich structures are used in almost every industrial sector ranging from building to aerospace applications.

In spite of all the advantages, the high costs involved in the manufacturing of composite materials limit their use to specific applications. Studies show that the cost of composite structures can be significantly reduced by decreasing the part count and

fastener count [9]. The decrease in the part count rapidly lowers the assembly labor cost. Non-autoclave processes are the cost effective composite manufacturing techniques. The widely used non-autoclave processes in the aerospace industry are: Filament Winding, Resin Transfer Molding (RTM) process, Vacuum Assisted Resin Transfer Molding (VARTM) process and Out-of-Autoclave (OOA) vacuum-bag-only prepreg process.

Filament winding is a composite fabrication process which involves winding filaments under varying amounts of tension over a male mould or mandrel. The mandrel rotates while a carriage moves horizontally, laying down fibers in the desired pattern. One of the major advantages of filament winding is its suitability to automation [10]. However, the profiles of the parts that can be manufactured by this process are limited to those with symmetric shapes. Currently, filament winding is used in manufacturing fuselages, pipes, pressure vessels etc [11].

In the RTM process, a two-sided mold that fits together to produce a mold cavity is used. The fiber preforms are placed into this cavity and the mold set is closed. Then the liquid resin is pumped into the preforms using positive pressure. RTM process offers several advantages such as tighter dimensional tolerances, more reproducibility and faster production cycles [1-2]. However, the expensive molds and difficulties in pumping the resin through the fiber preforms are major disadvantages that limit the use of this process.

The VARTM process is a modification of RTM process in which the matched metal mold is replaced by a flexible vacuum bag material. The vacuum pressure is used as the driving force for the resin flow instead of the positive pressure as in RTM process. The VARTM process offers several advantages over RTM and filament winding processes [12] like low tooling costs, low capital, reduced volatile emissions, scalability to large complex structures, reduced filling time, and high fiber volume fractions (60%). The VARTM process was first used in the marine industry to make boat hulls and large complex structures. The coast guard patrol boat hulls were infused by the Marco method in the 1940s. In 1989, Seeman Composites developed a VARTM infusion process called Seeman Composite Resin Infusion Molding Process (SCRIMP). The SCRIMP process is the first to use a highly porous flow medium for resin flow which increased the infusion speed, thus saving significant amount of time. The VARTM process enables integral fabrication and reduces the number of fasteners. Studies report that using this process in

manufacturing complex parts reduced the part count from 61 to one and eliminated more than 376 fasteners resulting in cost savings of up to 75% without sacrificing quality [13].

In addition to these low cost manufacturing processes, another technique called ‘out-of-autoclave’ process using oven curing of pre-impregnated tapes has been recently developed [6]. The out-of-autoclave manufacturing process offers time and cost benefits and does not require skilled labor. The quality of the manufactured part is repeatable irrespective of the manufacturer. Also, the out-of-autoclave (OOA) process uses only atmospheric pressure and hence eliminates the need for expensive tooling thus reducing capital costs [14-15]. The scalability of the process to manufacture large structures makes the OOA process an attractive alternative.

In recent years, increasing demands of the aerospace industry to reduce the weights of aircraft has made VARTM and OOA processes as valuable methods for the manufacture of high-quality composites for structural applications. High performance aircraft parts have been manufactured using the autoclave process for many years [3]. But the autoclave process is costly and is limited to small size parts. Non-autoclave processes offer the potential for reduced cost and cycle time, especially for large complex parts. These processes have been receiving increased attention as an alternative for producing aerospace quality parts. A key challenge for commercial implementation of VARTM and OOA parts is the need to achieve mechanical and thermal performance equivalent to the autoclaved parts [16].

2. SCOPE AND OBJECTIVES

Autoclaves have been commonly used to manufacture high performance composites for aerospace applications. However, high capital and tooling costs make these composites very expensive. In spite of numerous application possibilities, the usage of composites has been limited because of high costs. While the material costs sum to 8-10% of the total costs, manufacturing and processing costs contribute to the majority of the overall costs of the composites [17]. Cost savings of up to 75% have been achieved by using low-cost composite manufacturing techniques and by making integral parts. Hence, several studies have been devoted over the past few decades in developing non-autoclave manufacturing techniques. Developing low cost advanced composites will allow to fully utilize the advantages of composites and to advance the usage of composites in several applications. To become a viable alternative, the non-autoclave process should achieve consistent part quality, low void content and high fiber volume fractions as obtained in an autoclave. Very few processes can match that of an autoclave. Previous work at Missouri S&T has shown that aerospace quality composite parts were successfully produced by VARTM process. The VARTM process offers several advantages such as lower tooling and capital costs, net shape manufacturing of large complex parts and environmentally friendly operating conditions. Studies report that using this process, in manufacturing complex parts, reduced the part count from 61 to one and eliminated more than 376 fasteners resulting in cost savings of up to 75% without sacrificing quality [18-19].

VARTM has traditionally been used for general temperature applications. With the constant rising demand for light-weight strong materials in the aerospace industry, composites are being employed in the primary structures. And the need for the usage of composites at higher operating temperatures has also increased. Application of VARTM to the processing of high temperature (≥350°F) resin systems faces unique challenges. High viscosities of resins, difficulties involved with removing volatiles from solvents during the processing, high processing temperatures, preform spring-backs, dimensional variations due to large part sizes are the issues that challenge the usage of VARTM process for producing affordable aerospace quality parts [20]. Another hindrance to the

adoption of the VARTM technology in the aerospace industry is the lack of material property databases. The focus of the present work in Paper I is to develop a VARTM set-up to obtain high performance elevated-temperature composites and to develop a material property database of the current resin and composite system. Flow simulation tool was developed and implemented in ABAQUS commercial finite element codes.

In Paper II, VARTM process was applied to honeycomb sandwich composite manufacturing. The conventional manufacturing of open-cell core sandwich composites generally includes several steps such as fabricating laminates followed by secondary bonding of facesheets to the core. Co-curing techniques coupled with low cost manufacturing methods are ideal for reduced cost and cycle time. A key challenge in applying liquid molding processes for the open-cell core sandwich materials is to prevent resin from entering the hollow cells during the infusion process [21]. The resin infiltration will cause undesirable increase in the weight of the composite. Some of the solutions include filling the hollow cells with closed-cell foam, sealing the core with surface veils and polymer film barriers [22-23]. These solutions often resulted in increase in the weight or cost of the final products. The objective of the study is to develop a one-step process for manufacturing high performance sandwich structures using low cost liquid molding processes and to evaluate the manufactured parts.

In Paper III, a new oven cure vacuum-bag-only out-of-autoclave (OOA) process composite manufacturing is explored. Although the current OOA prepreg systems offer variable cure cycle capability, mechanical and physical property variations have been observed with changes in cure cycle. Data has shown that porosity levels and laminate void content are highly influenced by processing conditions, including the achieved vacuum level in the oven vacuum bag, the pre-heat vacuum hold, the cure temperature heat-up rate, and the part temperature variance due to tool mass or oven temperature variations [14]. In the present study, high performance composites have been manufactured employing the OOA manufacturing process. Physical and mechanical tests have been conducted to evaluate the performance of the manufactured composites. The influence of size, lay-up configuration and thickness and their interactions on the low velocity impact behavior of OOA composites has been investigated using 2^3 full factorial DoE approach.

PAPER

I. ELEVATED-TEMPERATURE VARTM PROCESS FOR HIGH PERFORMANCE AEROSPACE COMPOSITES

V.G.K. Menta and K. Chandrashekhara
Missouri University of Science and Technology, Rolla, MO 65409-0050, USA

ABSTRACT

The objective of the present work is to develop a low cost and reliable vacuum assisted resin transfer molding (VARTM) process to manufacture elevated-temperature composites for aerospace applications. VARTM is commonly used for general temperature (<300°F) applications such as boat hulls and secondary aircraft structures. With growing demands for applications of composites in elevated-temperature environments, significant cost savings can be achieved by employing VARTM process. However implementation of VARTM process for fabricating elevated-temperature composites presents unique challenges such as high porosity and low fiber volume contents. In the present work, two different vacuum bagging methods: Seeman Composite Resin Infusion Molding Process (SCRIMP) and Double Vacuum Bagging Infusion (DVBI) process were evaluated. Issues related with the manufacturing process were presented. Density and fiber volume fraction testing of manufactured panels showed that high quality composite parts with void content less than 1% have been consistently manufactured. A property database of the resin system and the composites was developed. A three dimensional mathematical model has also been developed for flow simulation and implemented in the ABAQUS finite element package code to predict the resin flow front during the infusion process and to optimize the flow parameters. The results of the present study indicate that aircraft grade composite parts with high fiber volume fractions can be manufactured using the developed elevated-temperature VARTM process.

1. INTRODUCTION

In recent years, composite materials have been increasingly used in a wide variety of applications due to their light weight, high specific strength, specific modulus, corrosion resistance and excellent fatigue properties. With the rising demand for more environmentally friendly and less petroleum dependent products, researchers are constantly finding ways to apply lightweight-strong composite materials in new areas [1]. In the aerospace industry, composites are being employed in primary structures [2]. The need for the usage of composites at higher operating temperatures has also increased. Traditionally, composite aircraft parts have been manufactured using the autoclave process. However, high capital and tooling costs and part size limited by autoclave chamber volume make these composites very expensive [3]. Non-autoclave processes offer the potential for reduced cost and cycle time and have been receiving increased attention as an alternative for producing aerospace quality parts. Compared to resin transfer molding (RTM) and out-of-autoclave (OOA) vacuum-bag-only prepreg processes, vacuum assisted resin transfer molding (VARTM) is rapidly emerging as a competitive low cost alternative for autoclave process [4-5]. VARTM process uses one-sided vacuum sealed mold and resin is then drawn into the mold by vacuum to infuse the preform. The VARTM process offers several advantages such as lower tooling and capital costs, net shape manufacturing of large complex integral parts and environmentally friendly operating conditions. Studies report that by using VARTM process in manufacturing complex structures, part count was reduced from 61 to one and eliminated more than 376 fasteners resulting in cost savings of up to 75% without sacrificing quality [6-7].

VARTM has traditionally been used for general temperature applications such as boat hulls, windmill blades etc. Application of VARTM to the processing of elevated and high temperature resin systems faces unique challenges. Elevated-temperature composites are defined in the literature in different ways. In the present work, glass transition temperature (T_g) of the material is taken as the basis: general temperature applications if $T_g < 300°F$, elevated-temperature applications if $300°F \leq T_g \leq 600°F$, and high temperature applications if $T_g > 600°F$. High melt viscosities of resins, high

processing temperatures, preform spring-backs, dimensional variations are some of the issues that challenge the usage of general temperature VARTM process for manufacturing aerospace quality composite parts for elevated and high temperature applications [8]. Most of the work presented in literature to date concentrated on high temperature polyimide resin systems [8-14]. Fu et al. manufactured phenylethynyl terminated imides (PETIs) using in-flow and through-thickness resin flow methods to manufacture parts. The authors were able to manufacture parts with fiber volume fractions of around 60% and void content ranging from 3-4% [10]. Cano et al. manufactured PETI composites using LARC^{TM} PETI-8 (Langley Research Center Phenylethynyl Terminated Imide- 8), with fiber volume fractions around 60% and void content ranging from 4 – 10% [11].

While the polyimide materials are the leading high temperature resin systems for usage in aerospace industry, they are also expensive and time consuming to process. Significant time and cost savings can be achieved by using lower cost elevated-temperature resin systems in applications where such high temperatures (>600°F) are not required. Processing of elevated-temperature composites is different from high temperature materials. Hence, addressing the issues related with the processing of these composites and developing a reliable and affordable VARTM process is of importance. Li et al. presented the new Benzoxazine elevated-temperature resin with Tg ~ 374°F for RTM/VARTM applications [15]. The authors used double vacuum bagging process to manufacture panels. However, the details of the manufacturing process and related issues were not presented. Another hindrance to the adoption of the VARTM technology in the aerospace industry is the lack of material property database.

The focus of the present work is to improve the VARTM set-up to obtain high performance elevated-temperature composites and to develop a material property database of the current resin system. Carbon/epoxy composite flat panels were manufactured using AS4-5HS carbon fabric and Cycom 977-20 toughened epoxy resin system. Flat panels were chosen for the study to understand the critical factors and parameters of the process. Two different vacuum bagging methods, Seeman Composite Resin Infusion Molding Process (SCRIMP) and Double Vacuum Bagging Infusion (DVBI) process were evaluated. SCRIMP is a modification of VARTM process that uses

a high-permeability layer to rapidly distribute the resin on the part surface and then allow it to penetrate through-thickness of the part [16]. As the name suggest, DVBI uses two vacuum bags instead of one [17]. The second bag helps in maintaining the vacuum integrity of the part at high temperatures. The manufactured panels were then tested for density, fiber volume fraction, and void content. Viscosity and Differential scanning calorimetric (DSC) tests were conducted to evaluate the infusion and cure temperatures of the resin system. Mechanical performance of the composites was evaluated using tensile, flexure, short beam shear, impact, compression-after-impact and open hole compression tests.

Simulation of the vacuum infusion process is a necessary tool to optimize the process parameters and to minimize costly and time-consuming trial-and-error processes [18-20]. A three dimensional mathematical model has been developed for flow simulation and implemented in the ABAQUS finite element package code to predict the resin flow front during the infusion process and to optimize the flow parameters. Tensile tests on coupons were performed to determine the elastic constants required for finite element structural analysis. The flow simulation results are compared with the experimental findings for a flat panel. The results of the present study indicate that aircraft grade elevated-temperature composite parts with high fiber volume fractions can be manufactured using the VARTM process and that flow modeling can be successfully developed and implemented into the ABAQUS finite element analysis code.

2. EXPERIMENTAL

2.1. RESIN CHARACTERIZATION

Cycom 977-20, a one-part toughened epoxy resin system obtained from Cytec Industries Inc. was used in the present study. Initially Dynamic Scanning Calorimetry (DSC) and rheology tests were performed on the resin system to evaluate the cure profile and infusion temperatures.

2.1.1. Differential Scanning Calorimetry (DSC). DSC tests were performed on the resin system using a TA Instrument model 2010. Three samples of 10-15mg of Cycom 977-20 epoxy resin were each placed into an aluminum crucible. The curing

exotherms were made at a rate of 10° C/min from 35°C to 310°C. The onset of cure, heat of reaction, and end of cure was measured for each sample. Once the samples were cured in the DSC, the cell was quickly cooled using liquid nitrogen and subjected to subsequent scanning from -50°C to 300°C to measure the resulting glass transition temperature.

2.1.2. Rheology. Viscosity measurements were conducted using Brookfield DV-III Ultra Rheometer. The temperature of the resin system was varied from 85°F to 220°F and the viscosity was measured at different temperature intervals.

2.1.3. Mechanical Testing. Tension and flexure tests were performed on the coupons according to ASTM D3039 and ASTM D792 at a crosshead speed of 2.54 mm/min and 1.27 mm/min respectively. All the neat resin samples were heated to 350°F at a ramp rate of 5°F/min and cured for 3 hours.

2.2. MANUFACTURING OF COMPOSITES

Cycom 977-20 and AS4-5HS-6K satin weave carbon fabric were used to manufacture Carbon/epoxy composites. SCRIMP and DVBI processes were evaluated. Producing reliable bagging/sealing, low void content, and high fiber volume fractions had been the focus in manufacturing elevated-temperature composite parts. The schematic of the SCRIMP process is shown in Figure 1.

In the SCRIMP process, the aluminum mold was first cleaned with acetone and was sanded to obtain a smooth surface finish. Any burrs on the aluminum mold will be reflected in the final part and should be avoided. Tacky tapes were placed along the perimeter of the mold. The mold was coated with Frekote mold release agent three times with an interval of 15 minutes between coats. The carbon fabric was cut to the required dimensions and stacked on the mold. A layer of peel ply was then placed on the top of the preform. The peel ply serves as a release layer and also gives uniform texture to the final composite panel. Resin can flow through the peel ply but the peel ply is not hardened with the composite panel. A distribution flow medium was placed on the top of the peel ply, to speed up the resin infusion through the preform. Resin infusion and vacuum lines were then placed in the selected positions. Single resin line and single vacuum line were

used in the manufacturing of all the panels. After locating the lines, a vacuum bag was placed over the mold and sealed around the perimeter. The vacuum line was then connected to a resin trap and vacuum pump. The resin trap collects any excess resin that comes from the part and avoids resin entering the vacuum pump and spoiling it. Vacuum of 737 mm Hg was applied to the bag which evacuates all air from the bag and the bag tightly collapsed onto the part. The bag was then checked for any leaks. Vacuum outlet was then connected to the resin container. Resin was drawn into the mold by vacuum to infuse the preform. Resin flow is assisted by microgrooves built into a distribution medium placed beneath the vacuum bag. The flow of resin occurs both in the inplane and the short-transverse directions of the preform. After full infiltration of the resin was achieved, the mold was heated to the curing temperature and the part was solidified.

To enable elevated-temperature processing, all the tooling and bagging materials (peel ply, distribution medium, tacky tape, inlet and outlet tubes etc.) were replaced with the materials that can withstand the processing temperatures. Since the viscosity of the resin was high at room temperatures, the resin was preheated in a separate oven and was degassed. Also grippers that are convenient to open or shut the resin inlet/vacuum outlet at elevated temperatures were used. Using disposable valves is a better option. Also, elevated-temperature resins usually exhibit exothermic behavior. Hence, care should be taken not to leave resin container in the oven especially if it is a closed container. Flat composites panels of 12'' x 14'' were manufactured using 6 layers of AS4-5HS carbon fabric and Cycom 977-20 resin system. The part was infused at 167°F. Figure 2 shows the cure profile followed for the elevated-temperature VARTM process. The vacuum bag failed several times using SCRIMP process at 350°F cure. Replacing one layer with two layers of tacky tape did not minimize the vacuum bag failures enough. However the panels still had low fiber fractions, high void content and large variations in thickness along the resin flow direction.

DVBI process employs two vacuum bags instead of one and allows the usage of caul plate. An extra bag in the DVBI process provides a redundancy of vacuum and maintains high vacuum integrity during the process avoiding any air leaks which would adversely affect the quality of the parts. The double bag uses a caul plate and thus provides parts with uniform and constant thickness. The schematic representation of the

DVBI setup is shown in Figure 3. In the DVBI process, the resin and the vacuum lines are shut-off once full infusion of the part is achieved while the vacuum on the outer bag will be maintained throughout the manufacturing process. No vacuum bag failure was observed when the DVBI was implemented in elevated-temperature VARTM process. The panels from DVBI process were free from any visible dry spots and initial panels showed consistent high fiber volume fractions and low void contents. Also the thickness was consistent throughout the part. Hence the characterization panels were manufactured using DVBI process.

2.3. PERFORMANCE EVALUATION

Density and fiber volume fraction contents of the manufactured panels were calculated to evaluate the quality of the manufactured panels. Tensile, flexure, short beam shear, low velocity impact, compression-after-impact (CAI) and open hole compression (OHC) tests were conducted.

3. RESULTS AND DISCUSSION

3.1. DIFFERENTIAL SCANNING CALORIMETRY

Figure 4 shows the DSC spectrum of Cycom 977-20 epoxy resin. Two peaks have been observed in the curing exotherm as opposed to a single peak representing that two reactions are taking place. The peak that has been observed on the high-temperature shoulder of the curing exotherm peak can be considered to be the reaction happening between the epoxy groups and the additives (or toughening agents). This indicates that the material will have good particle matrix interface which in turn results in improved toughness of the resin. Similar observation has been reported for an epoxy anhydride resin system with epoxidized hyper branched polymer (HBP) as an additive [21].

Figure 5 shows the glass transition curve of the resin system. The glass transition temperature was reported as the inflection point on the glass transition region. A very small peak that is present right next to the endothermic step-like change in Figure 5 can be explained as relaxation of polymer chains from residual stresses induced during the

fast curing/cooling process (during DSC testing). Onset, peak maximum, end set, glass transition temperatures and heat of reactions have been tabulated in Table 1.

3.2. VISOCOSITY MEASUREMENT

Figure 6 shows the viscosity profile of the resin system obtained from two different runs. The resin system was solid at room temperature and had an average viscosity of 74.82 Pa-s at 85°F. At 167°F, the resin reaches low viscosity value of 0.322 Pa-s making it the suitable infusion temperature.

3.3. NEAT RESIN MECHANICAL TESTS

Since no data was available on the Cycom 977-20 resin system, neat resin coupons were cast for mechanical performance evaluation. The stress-strain curves for the neat resin samples were showed in Figure 7. The samples had an average tensile modulus of 3.273 GPa and strength of 77.62 MPa. Six specimens were tested for flexural properties at a crosshead speed of 1.27 mm/min and a support span of 51 mm. Figure 8 shows the flexural stress versus flexural strain trends for the neat resin samples. Neat resin samples had an average flexural strength of 148.36 MPa, flexural modulus of 3.62 GPa and an average failure strain of 5.6%.

3.4. FIBER VOLUME FRACTION TESTS

Density and fiber volume fraction tests were conducted on the manufactured composite panels in accordance with ASTM D792 and ASTM D3171 nitric acid digestion method respectively. Four specimens each weighing 1.7 to 2 gm was cut from the panel. The samples had an average density of 1.5635 g/cm^3. Table 2 shows the density, fiber volume fraction, matrix volume fraction and void content of the composite samples. The samples had an average fiber volume fraction of 59.42 %, resin content of 39.97 % and a void content of 0.61 %. The fiber volume fractions obtained are typical of high performance composite parts.

3.5. TENSILE CHARACTERIZATION

Tensile tests were conducted on the coupons using Instron 4204 testing machine in accordance with ASTM D 3039. Samples were tested at a crosshead speed of 1.27 mm/min. Three coupons each of size 25.4 mm x 2.54 mm were used. The stress-strain curves are shown in Figure 9 and the values are tabulated in Table 3. The samples had an average tensile modulus, strength and strain to failure of 81.84 GPa, 618.86 MPa and 0.77 % respectively.

3.6. THREE POINT BENDING TESTS

Flexure tests were performed on an Instron testing machine according to ASTM D790 standard. Three samples each of 12.7 mm x 152 mm size were cut in longitudinal (0°) and transverse (90°) directions of the sample and were tested for their flexural properties. The samples had an average thickness of 2.26 mm. The flexural stress-strain curves of the samples are shown in Figure 10 and the results are tabulated in Table 4. The samples had an average flexural strength of 929.53MPa and 670.6 MPa and an average flexural modulus of 60.31 GPa and 44.25 GPa in longitudinal and transverse directions respectively.

3.7. SHORT BEAM SHEAR TESTS

Short beam shear tests were performed according to ASTM D2344. The tests were performed on Instron test machine. Six coupons of size 6.35 mm x 25.4 mm were tested. A span length four times the thickness was used. All the tests were performed at a cross-head speed of 1.27 mm/min. The samples had average short-beam strength of 473.07 MPa with a standard deviation of 25MPa. The load-displacement curves obtained during the tests were shown in Figure 11.

3.8. IMPACT TESTS

Low velocity impact tests were performed according to ASTM D7136. Laminate construction consists of 12 fabric plies with a stacking sequence of $[(+45/-45)/(0/90)]_{3S}$. Three energy levels were selected for the tests. Impact energy per unit thickness of 6672

J/m, an industry standard for evaluating thick, quasi-isotropic laminates, was selected as one energy level. 12J of energy which is corresponding to maximum load (E_p) and 6J (50% E_p) were selected as the other two energy levels. Three samples were tested at each energy level. Energy, load and displacement history curves are shown in Figures 12-14, respectively. Load vs. displacement curve is shown in Figure 15. Damage on the top and bottom surfaces of the impacted samples is shown in Figures 16-17. While damage was visible for 29J of energy, only a small delamination of a fiber was observed at 12J of impact energy. No visible damage was observed at 6J and hence not included in the figures. Results obtained from the curves are tabulated in Table 5.

3.9. COMPRESSION-AFTER-IMPACT (CAI) TESTS

CAI tests were conducted according to ASTM D7137. Specimens of size 152.4 mm x 152.4 mm used to evaluate the low velocity impact properties were machined to 152.4 mm x 101.6 mm and were utilized for the CAI tests. The test fixture is edge-loaded between the flat platens as shown in Figure 18. Compressive loads were applied to the ends of the specimen/fixture assembly at a cross-head speed of 1.27 mm/min. Compression load vs. deflection curves are shown in Figure 19. The ultimate compression-after-impact strength values of the specimens at different energy levels are tabulated in Table 6. The failure modes of the tested samples are also shown in Figures 20-21.

3.10. OPEN HOLE COMPRESSION (OHC) TESTS

OHC tests were conducted according to ASTM D6484 -Procedure B. Specimens were of 304.8 mm x 38 mm x 4.32 mm dimensions with a hole of 7.62 mm diameter. Laminates are quasi-isotropic with $[(+45/-45)/(0/90)]_{3S}$ stacking sequence. Four samples each were tested at a cross-head speed of 1.27 mm/min. The test coupons were shown in Figure 22. The specimen is placed in the fixture and the required torque was applied to the bolts. The specimen/fixture assembly was placed between the flat platens and a compressive preload of 445 N was applied prior to the tests. The specimens were then subjected to compressive loads until failure. The stress-strain curves are shown in Figure

23 and the results obtained from the tests are listed in Table 7. The failed specimens are shown in Figures 24-25. In all the specimens, the failure had occurred at the hole which is the only acceptable failure mode for OHC tests.

4. FLOW SIMULATION

A three-dimensional porous media model has been developed for the flow simulation of VARTM process and implemented in the FEA commercial code ABAQUS to predict the resin flow front during the infusion process. Simulation of vacuum infusion process is a necessary tool to optimize the process parameters and to minimize the costly and time-consuming trial-and-error processes. In the present work, a refined three-dimensional porous media model has been developed to track the flow of the resin through the distribution medium and the preform in VARTM manufacturing process. The governing equations for the flow simulation are:

Continuity equation for an incompressible fluid:

$$\vec{v} = \frac{\vec{f}}{\phi} = -\frac{S}{\phi\mu}\frac{\partial u_w}{\partial \vec{x}}$$

Darcy's law of flow through a porous medium:

$$\nabla \cdot \vec{v} = 0$$

where, $\vec{v}$ - interstitial velocity vector of the resin

$\vec{f}$ - superficial velocity vector

ϕ - porosity of the porous preform

μ - viscosity of the fluid

S - permeability tensor of the preform

u_w - resin pressure

The flow model was implemented in commercial FEA code ABAQUS. Flat panel (305 mm x 356 mm) considered for the simulation was made of AS4-5HS carbon fiber fabric and CYCOM 977-20 resin. The per-ply-thickness was taken as 0.356 mm and the thickness of distribution medium as 1.52 mm. The in-plane and transverse permeability of the distribution medium were assumed to be 1.2926×10^{-7} m^2 and 5.36×10^{-7} m^2, respectively. The porosity of the distribution medium was taken as 0.75. The 8-node

brick element is used to mesh the preform, distribution medium and the inlet. The number of elements for each part is shown in Table 8.

The mesh of preform, distribution medium and inlet is shown in Figure 26. Resin is infused from the inlet and then fills the distribution medium and preform. Figures 27 and 28 show the saturation distribution after 7 and 30 seconds respectively. The red zone in these figures presents the saturation part of the preform and the flow distribution medium. Figures 29 and 30 show the pore pressure distribution during the flow process. The flow front along the cross-section of the panel at different times is shown from Figures 31-34. It takes about 7 minutes for resin to fully infuse the preform, which agrees well with the result from the experiment.

5. CONCLUSIONS

A set-up to manufacture elevated-temperature composites has been developed and high performance composites were successfully manufactured. SCRIMP and DVBI processes were evaluated. Composite panels of low void content, high fiber volume contents and uniform thickness were manufactured employing DVBI process. Viscosity and differential scanning calorimetric (DSC) tests were conducted to evaluate the infusion and cure behavior of the resin system. Mechanical performance of the neat resin coupons was evaluated. Density and fiber volume fraction tests showed that composites with void content less than 1% were performed to evaluate the quality of the manufactured parts. Mechanical performance of the composites was evaluated using tensile, flexure, short beam shear, impact, compression after impact and open hole compression tests. A database of these properties will help manufacturers and designers to employ low cost elevated-temperature VARTM process. A three dimensional flow simulation of VARTM process was developed and implemented in ABAQUS commercial code. The flow simulation results are compared with the experimental findings for a flat panel and the simulation results are in good agreement with experimental results. Initial flow modeling study performed in the present work helps in understanding the process and can aid in manufacturing large composite parts.

6. REFERENCES

1. B. D. Agarwal, L. J. Broutman and K. Chandrashekhara, "Analysis and Performance of Fiber Composites," John Wiley & Sons, Inc., Hoboken, NJ, Third Edition, 2006.
2. Pederson C, Lo Faro C, Aldridge M, Maskell R, "A novel route to aerospace primary structures via liquid resin infusion processes," Proceedings of the SAMPE Conference, Dayton OH, SAMPE Covina CA 2003.
3. V. G. K. Menta, S. Sundararaman, K. Chandrashekhara, N. Phan, and T. Nguyen, "Hybrid Composites using Out-of-Autoclave Process for Aerospace Sub-structures," SAMPE International Symposium, 53 (2008): 1 – 11.
4. Tatum, S., "VARTM Cuts Costs," *Reinforced Plastics*, 45(5) (2001): 22.
5. V.G.K. Menta, R. R. Vuppalapati, K. Chandrashekhara, D. Pfitzinger, and N. Phan, "Evaluation of Honeycomb Sandwich Structures Manufactured using VARTM Process," Proceedings of the 55th International SAMPE Technical Conference, 17 – 20 May 2010, Seattle, WA, pp. 1 – 12.
6. Brosius D, "Boeing 787 Update", High Performance Composites, May 2007
7. W. D. Brouwer, E. C. F. C. van Herpt, and M. Labordus, "Vacuum Injection Molding for Large Structural Applications," *Composites Part A: Applied Science and Manufacturing*, 34 (2003): 551-558.
8. T. Prasad, "Investigation of VARTM Processing of High Temperature RP-46 Resin System," Master's Thesis, 2004.
9. J. Criss, R. Koon, P. Hergenrother, J. Connell, J. Smith Jr., "High Temperature VARTM of Pheylethynyl Terminated Imide Composites," Proceeedings of 33rd International SAMPE Technical Conference, Seattle, WA, USA, 5-8 Nov. 2001, pp. 1009 – 1021.
10. Fu, X., Zhang, C., Liang, R., Wang, B. and Fielding, J. C., "High Temperature Vacuum Assisted Resin Transfer Molding of Phenylethynyl Terminated Imide Composites," *Polymer Composites*, 32 (2011): 52-58.
11. R.J. Cano, B.W. Grimsley, B.J. Jensen, and C.B. Kellen, "High Temperature VARTM with LaRC Polyimides," NASA technical report (2004).

12. S. Ghose, R. J. Cano, K. A. Watson, S. M. Britton, B. J. Jensen, J. W. Connell, J. G. Smith Jr., A. C. Loos, and D. Heider, "Processing and Characterization of PETI composites Fabricated by High Temperature VARTM," Proceedings of the 56th International SAMPE Technical Conference, 23 – 23 May 2011, Long Beach, CA, pp. 1 – 15.
13. S. Ghose, K. A. Watson, R. J. Cano, S. M. Britton, B. J. Jensen, J. W. Connell, H. M. Herring, Q. J. Lineberry, "High Temperature VARTM of Pheylethynyl Terminated Imides," High Performance Polymers, October 2009, Vol. 21, No. 5, pp. 653-672.
14. J. Criss, R. Koon, P. Hergenrother, J. Connell, and J. Smith Jr., "High temperature VARTM of phenylethynyl terminated imide composites (vacuum assisted resin transfer molding)," 33rd International SAMPE Technical Conference; Proceedings, Seattle, WA; UNITED STATES; 5-8 Nov. 2001. pp. 1009-1021. 2001.
15. W. H. Li, A. Wong and D. Leach, "Advances in Benzoxazane Resins for Aerospace Applicatioins," Proceedings of the 55th International SAMPE Technical Conference, 17 – 20 May 2010, Seattle, WA, pp. 1 – 9.
16. H. Seemann, "Unitary vacuum bag for forming fiber reinforced composite articles," U.S. Patent, 5,316,462 (1994).
17. T. Hou, and B. J. Jensen, "Double vacuum bag process for resin matrix composite manufacturing," US Patent 7186367, March 6, 2007.
18. J. Hu, S. Sundararaman, K. Chandrashekhara, T. Berkel, G. Bilow and J. Fielding, "A Refined porous Media Model for Mold Filling in Vacuum Infusion Process," Proceedings of the SAMPE Conference, pp. 1-11, Baltimore, MD, June 3-7, 2007.
19. X. Song, "Vacuum Assisted Resin Transfer Molding (VARTM): Model Development and Verification," Ph. D Dissertation, Virginia Polytechnic Institute and State University, 2003.
20. X. Song, A. C. Loos, B. W. Grimsley, R. J. Cano, and P. Hubert, "Modeling the VARTM Composite Manufacturing Process," SAMPE Technical Conference, Long Beach CA, pp. 1-13, 2004.
21. R. J. Varley and W. Tian, "Toughening of an Epoxy Anhydride Resin System using an Epoxidized Hyperbranched Polymer", Polymer International, Vol. 53, pp. 69 - 77, 2004.

Table 1. Differential Scanning Calorimetry Results of the Cycom 977-20 Epoxy Resin

Sample	**T_{onset} (°C)**	**T_{peak} (°C)**	**T_{end} (°C)**	**T_g (°C)**	**Heat of reaction (H) (J/g)**
1	181.47	227.65	291.18	199.72	502.7
2	182.22	225.66	291.44	199.99	465.6
3	181.74	226.00	289.87	199.53	587.0
Average	181.81	226.44	290.83	199.75	518.43
Standard Deviation	0.38	1.06	0.84	0.23	62.21

Table 2. Fiber Volume Fraction Test Results

Sample	**Density of composite sample (g/cm^3)**	**Fiber volume fraction (%)**	**Matrix volume fraction (%)**	**Void content (%)**
1	1.5645	59.6828	39.6985	0.6186
2	1.5662	59.3780	40.2355	0.3865
3	1.5629	59.0861	40.3735	0.5404
4	1.5604	59.5424	39.5731	0.8845
Average	1.5635	59.4223	39.9702	0.6075
Standard Deviation	0.0025	0.2564	0.3935	0.2083

Table 3. Tensile Properties of AS4-5HS/Cycom 977-20 Composite

Sample	**Modulus (GPa)**	**Strength (MPa)**	**Strain to failure (%)**
1	82.20	643.00	0.7948
2	87.04	597.93	0.7060
3	76.29	615.64	0.8135
Average	81.84	618.86	0.7714
Standard Deviation	5.38	22.71	0.0574

Table 4. Flexural Test Results in Longitudinal and Transverse Directions

Sample		**Flexural Strength (MPa)**	**Flexural Strain to Failure (%)**	**Flexural Modulus (GPa)**
Longitudinal	1	901.5	1.762	59.874
	2	941.0	1.624	58.742
	3	946.1	1.649	62.331
	Average	929.5	1.678	60.316
Transverse	1	760.2	1.712	46.122
	2	670.9	1.560	44.548
	3	580.7	1.406	42.079
	Average	670.6	1.559	44.250

Table 5. Summary of Impact Test Results

Energy Level	Energy Absorbed (J)	Peak Force (kN)	Contact Duration (ms)	Maximum Displacement (mm)
6J	3.35	4.73	5.23	2.37
12J	6.66	5.89	5.91	3.45
29J	24.23	6.10	8.18	6.87

Table 6. CAI Strength Values at Different Impact Energies

Sample	**Compression After Impact Strength (MPa)**		
	6J - Impact	**12J - Impact**	**29J - Impact**
1	295.1	228.16	179.78
2	307.8	229.98	208.43
3	318.25	232.13	183.57
Average	307.05	230.09	190.59
Standard Deviation	11.59	1.99	15.56

Table 7. OHC Test Results

Sample	**Strength (MPa)**	**Failure Strain (%)**
1	287.33	0.27
2	242.25	0.24
3	256.28	0.24
4	253.85	0.25
Average	259.92	0.25
Standard Deviation	19.27	0.01

Table 8. Type and Number of Elements for Parts

	Element Type (ABAQUS 6.7)	**Number of Elements**
Preform	**C3D8RP** (8-node brick, trilinear displacement, trilinear pore pressure, reduced integration, hourglass control)	1344
Distribution medium	**C3D8RP** (8-node brick, trilinear displacement, trilinear pore pressure, reduced integration, hourglass control)	672
Inlet	**C3D8RP** (8-node brick, trilinear displacement, trilinear pore pressure, reduced integration, hourglass control)	28

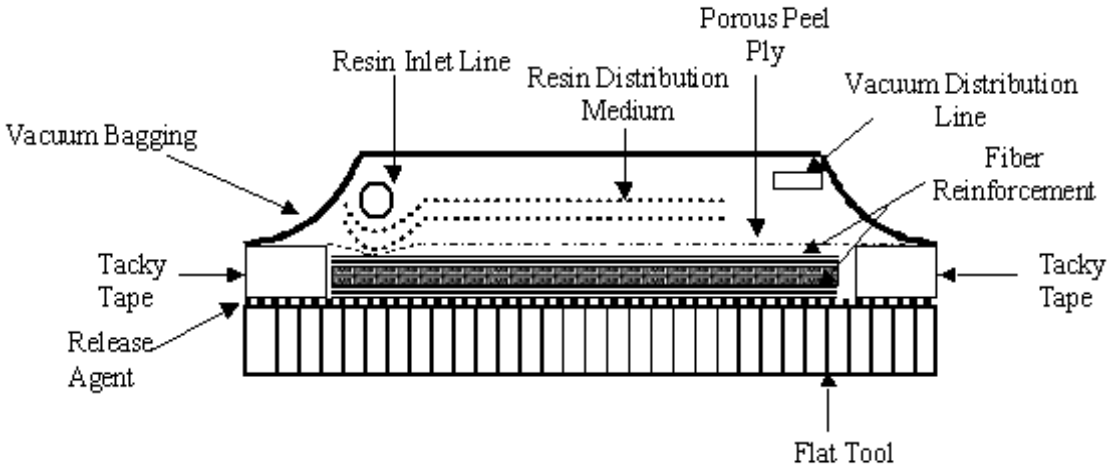

Figure 1. Schematic Representation of SCRIMP Process

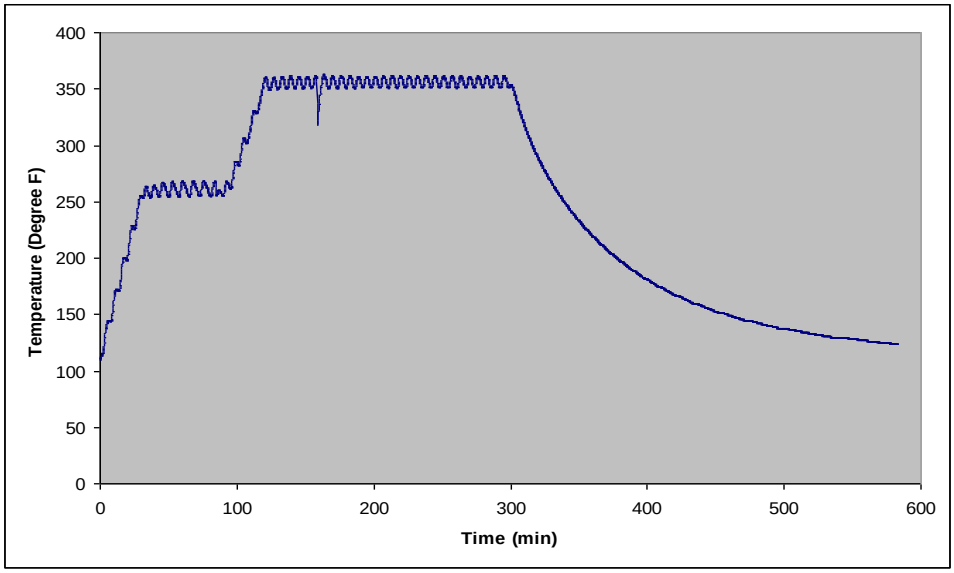

Figure 2. Cure Profile Obtained from Thermocouple of the Oven

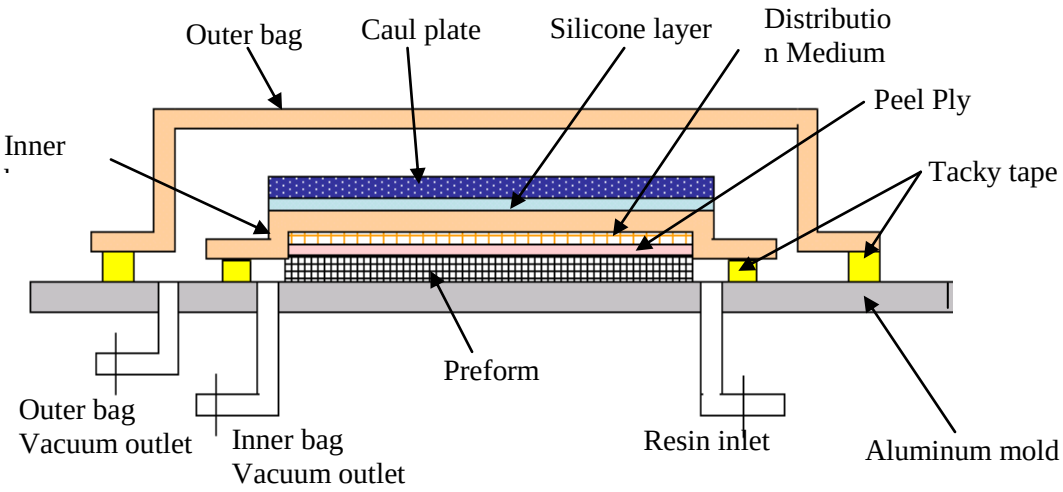

Figure 3. Schematic Representation of DVBI Process

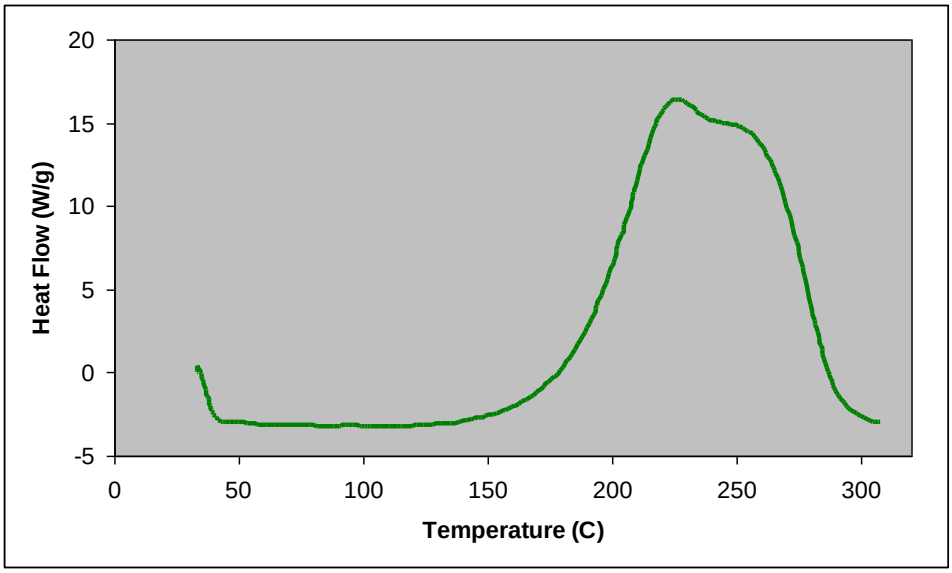

Figure 4. Dynamic Curing Curve of Cycom 977-20 Epoxy Resin

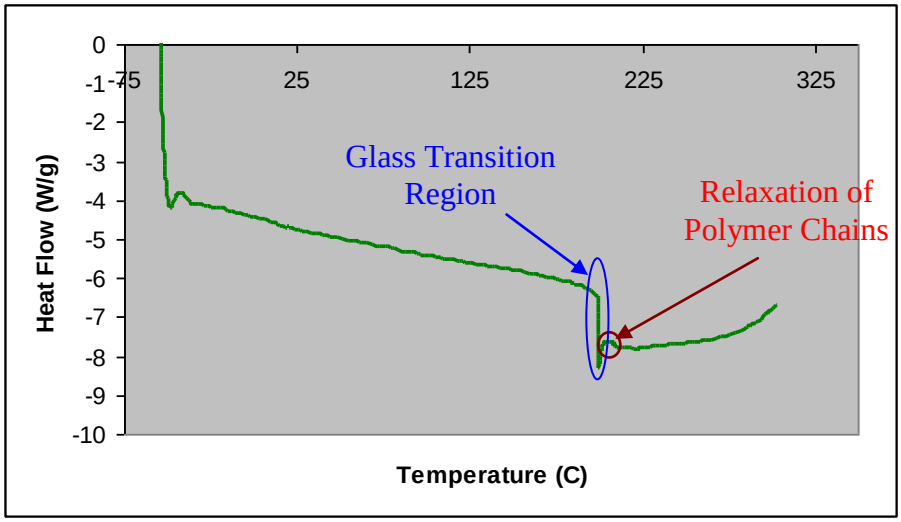

Figure 5. DSC Thermograms of Cycom 977-20 Epoxy Resin

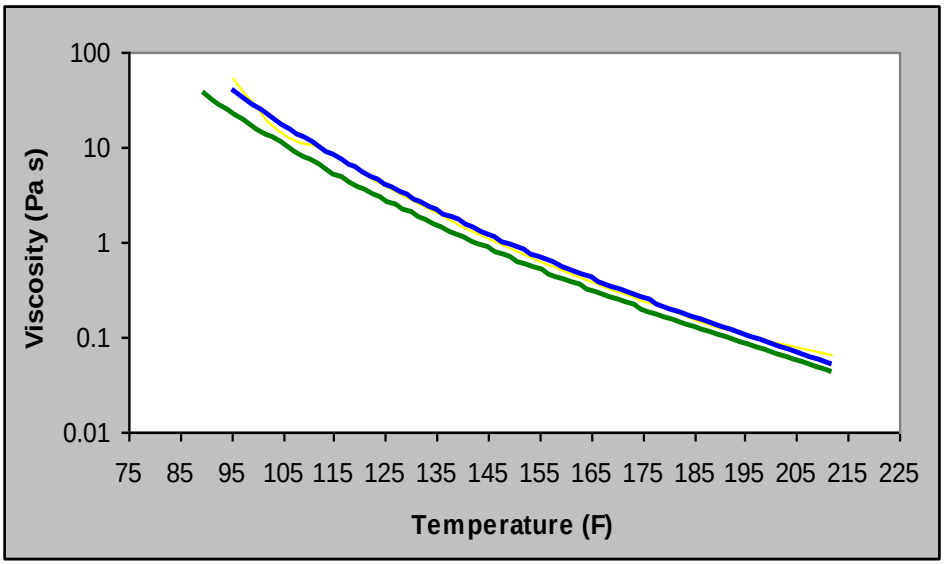

Figure 6. Viscosity vs. Temperature Profile of Cycom 977-20 Resin System

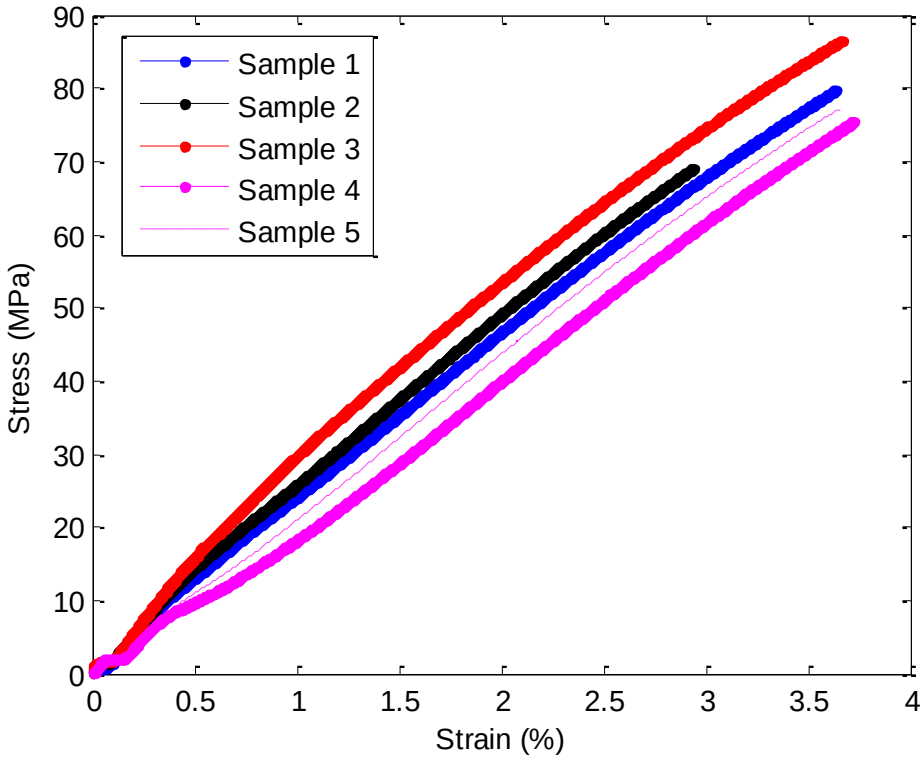

Figure 7. Tensile Stress-Strain Curves of Cycom 977-20 Showing Reproducibility of Tensile Tests

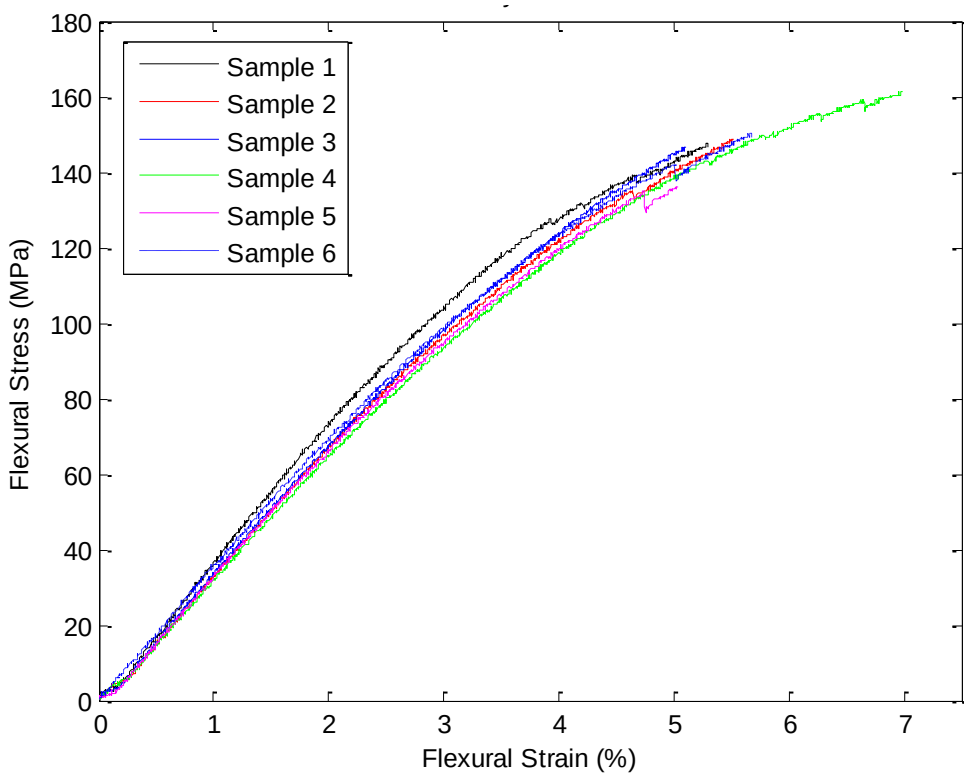

Figure 8. Stress-Strain Curves of Cycom 977-20 in Three Point Bending and Showing Reproducibility

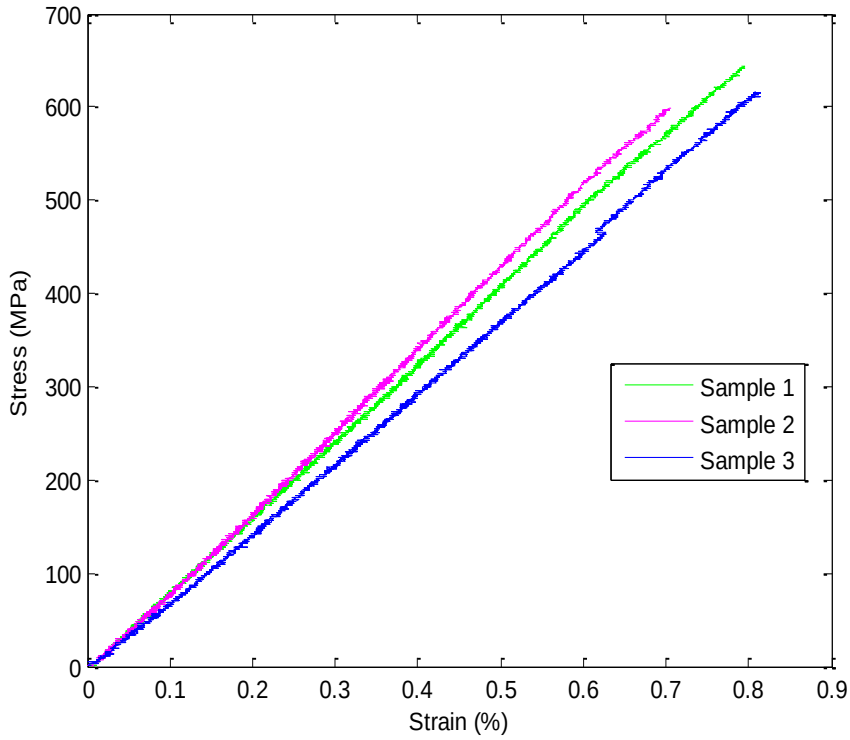

Figure 9. Tensile Stress-Strain Curves of Cycom 977-20/AS4-5HS Carbon Composites and Showing Reproducibility

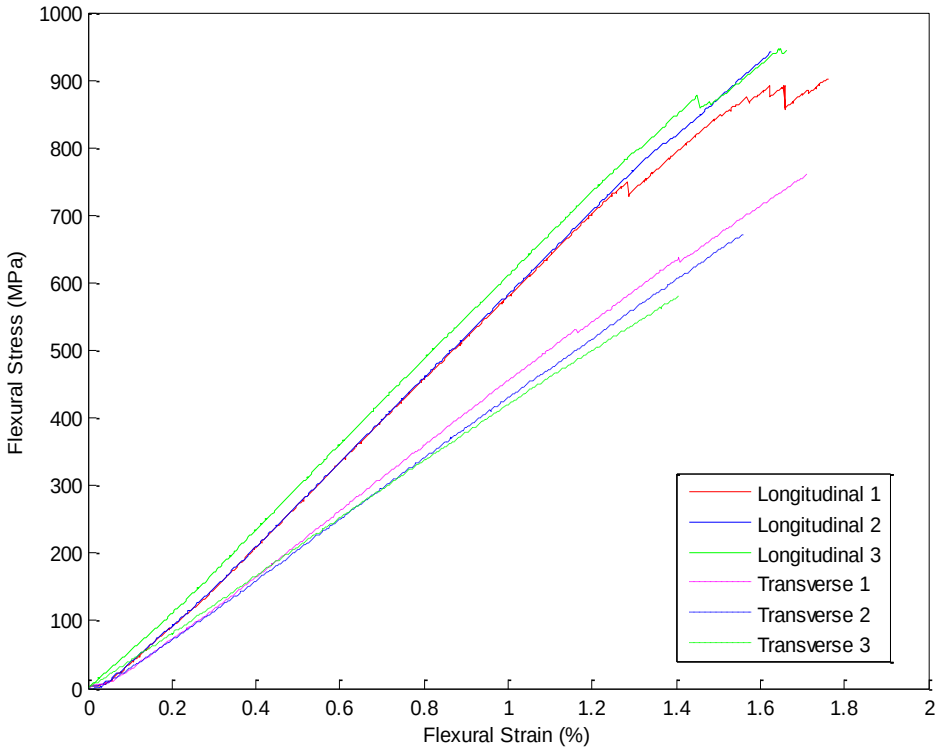

Figure 10. Stress-Strain Curves of Cycom 977-20/AS4-5HS Carbon Composites in Three Point Bending and Showing Reproducibility

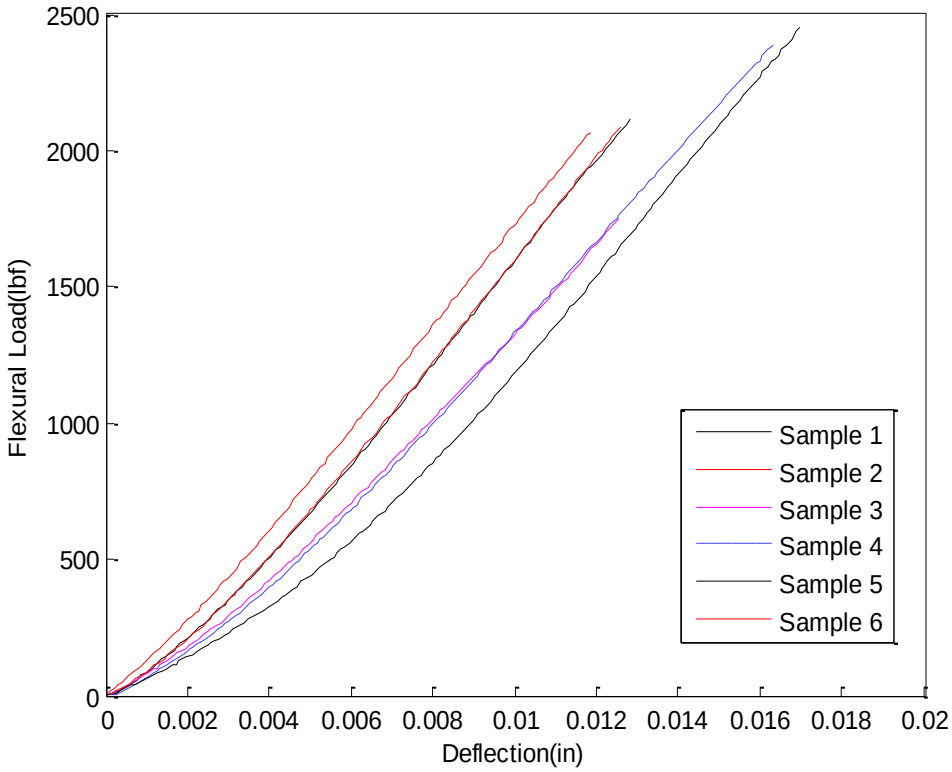

Figure 11. Load-Displacement Curves of Cycom 977-20/AS4-5HS Carbon Composites under Short Beam Shear Loads and Showing Reproducibility

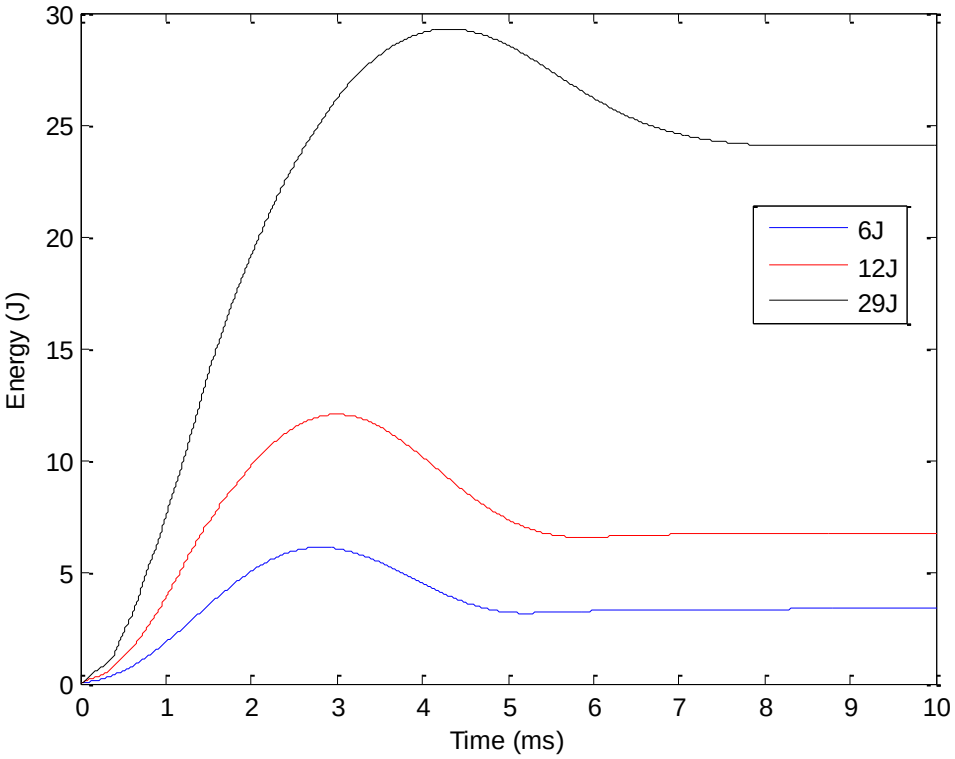

Figure 12. Impact Energy History Curves of Cycom 977-20/AS4-5HS Carbon Composites

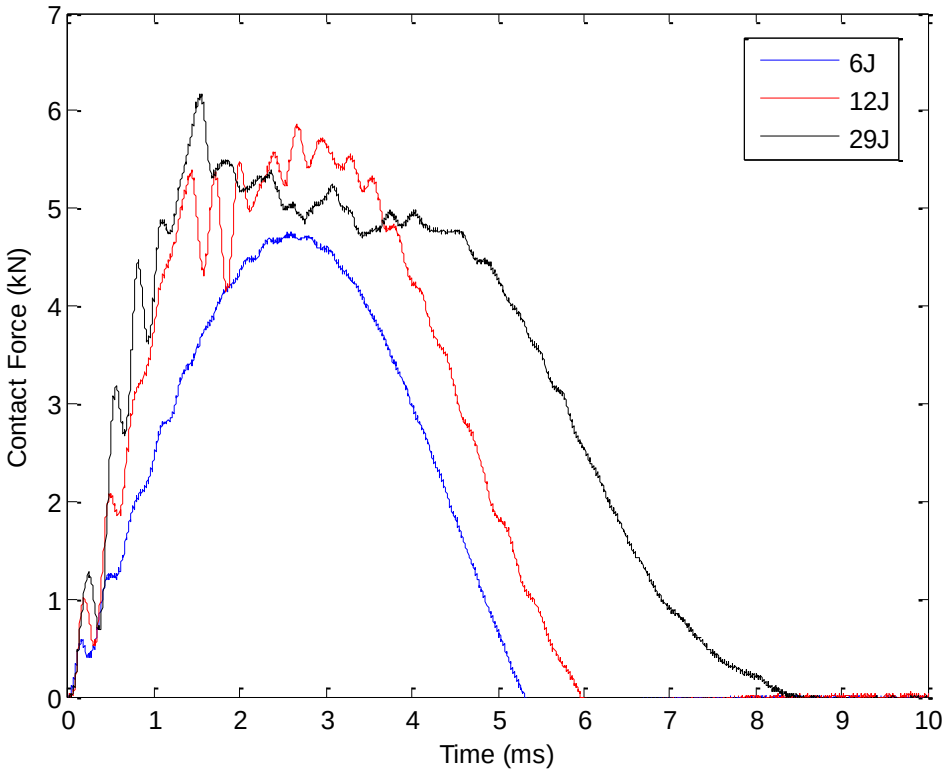

Figure 13. Contact Force History Curve of Cycom 977-20/AS4-5HS Carbon Composites

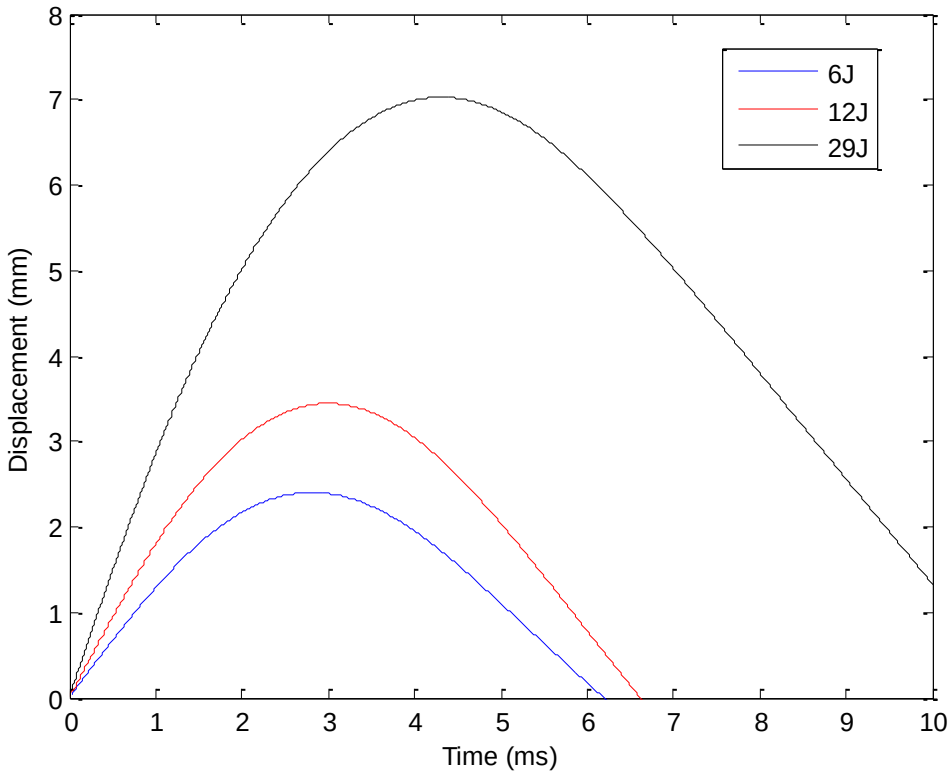

Figure 14. Displacement History Curve of Cycom 977-20/AS4-5HS Carbon Composites

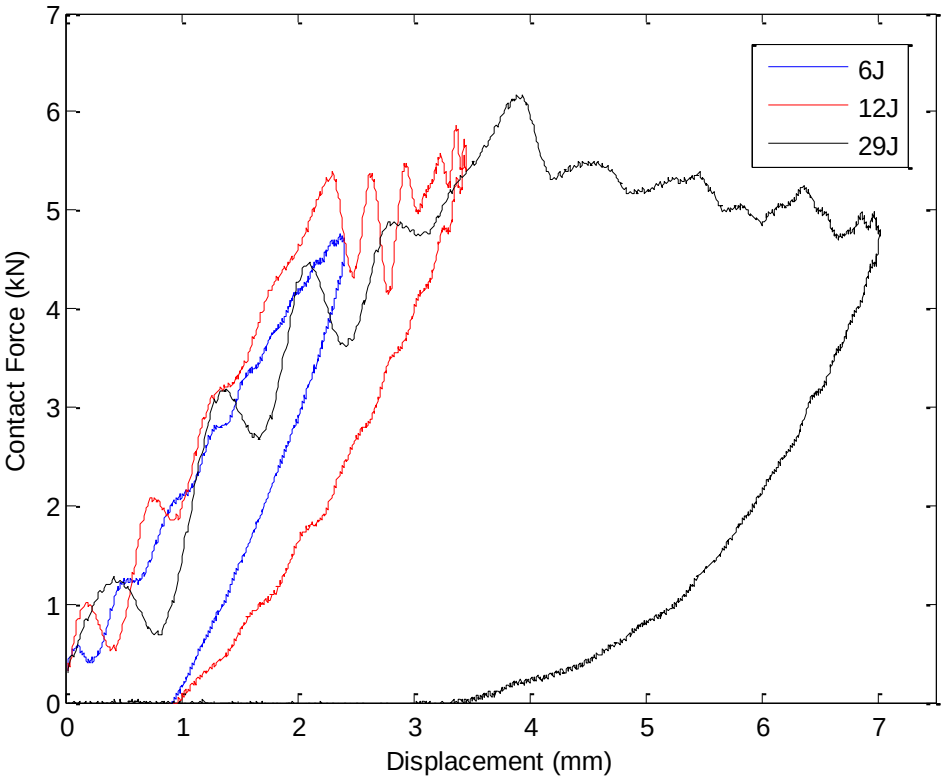

Figure 15. Contact Force vs. Displacement of Cycom 977-20/AS4-5HS Carbon Composites

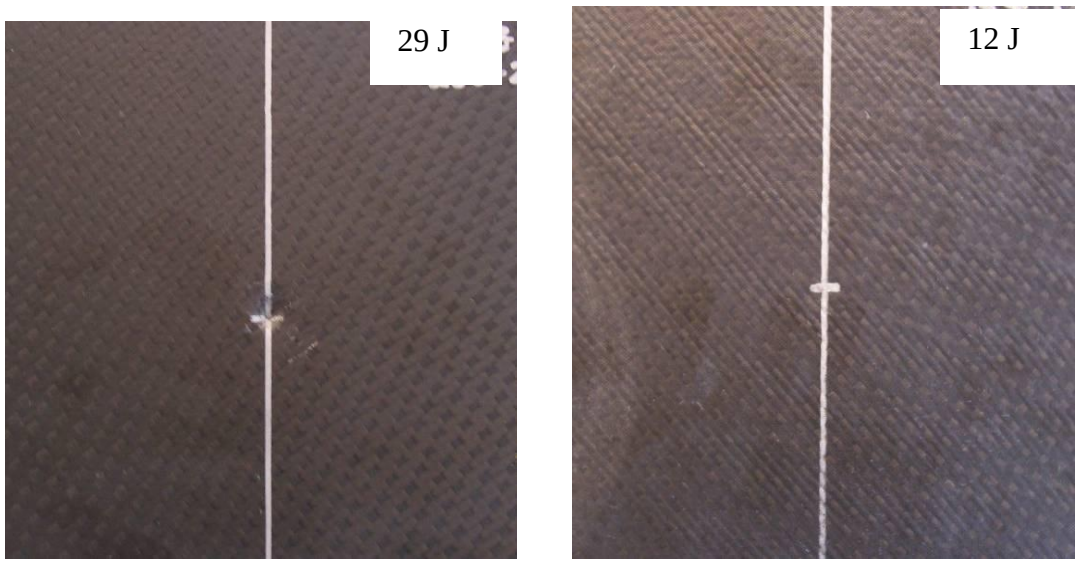

Figure 16. Damage on the Top Surface of the Impacted Samples of Cycom 977-20/AS4-5HS Carbon Composites

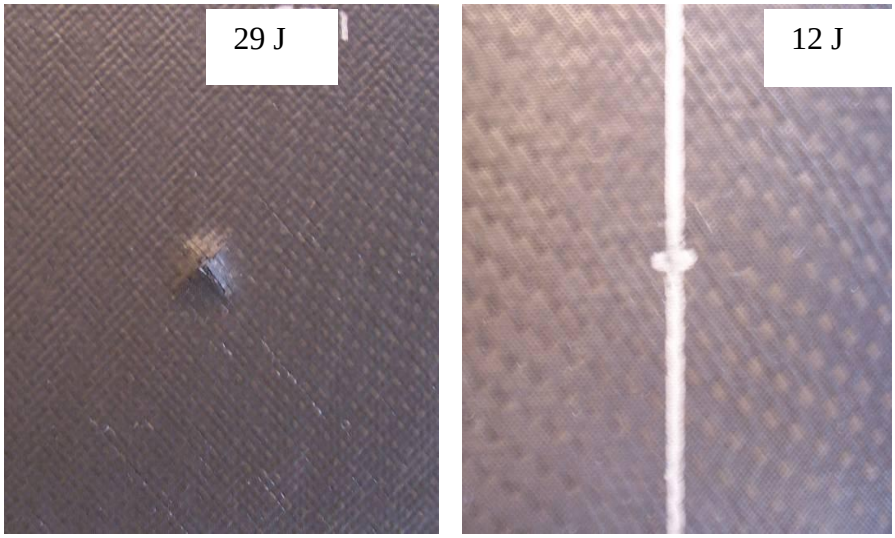

Figure 17. Damage on the Bottom Surface of the Impacted Samples of Cycom 977-20/AS4-5HS Carbon Composites

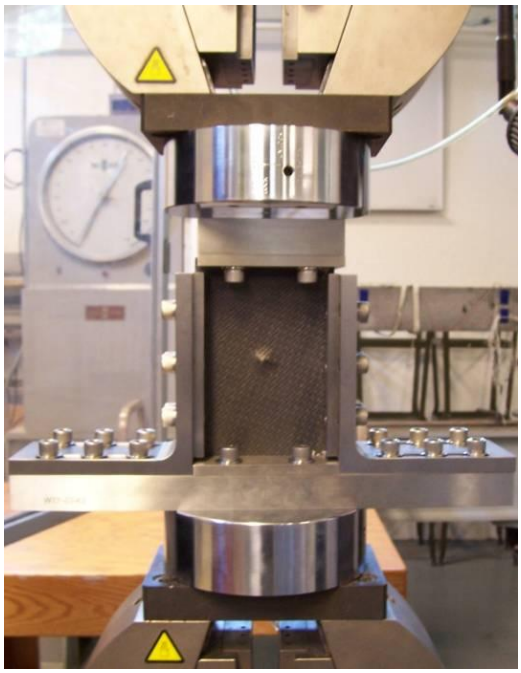

Figure 18. CAI Testing Set-up

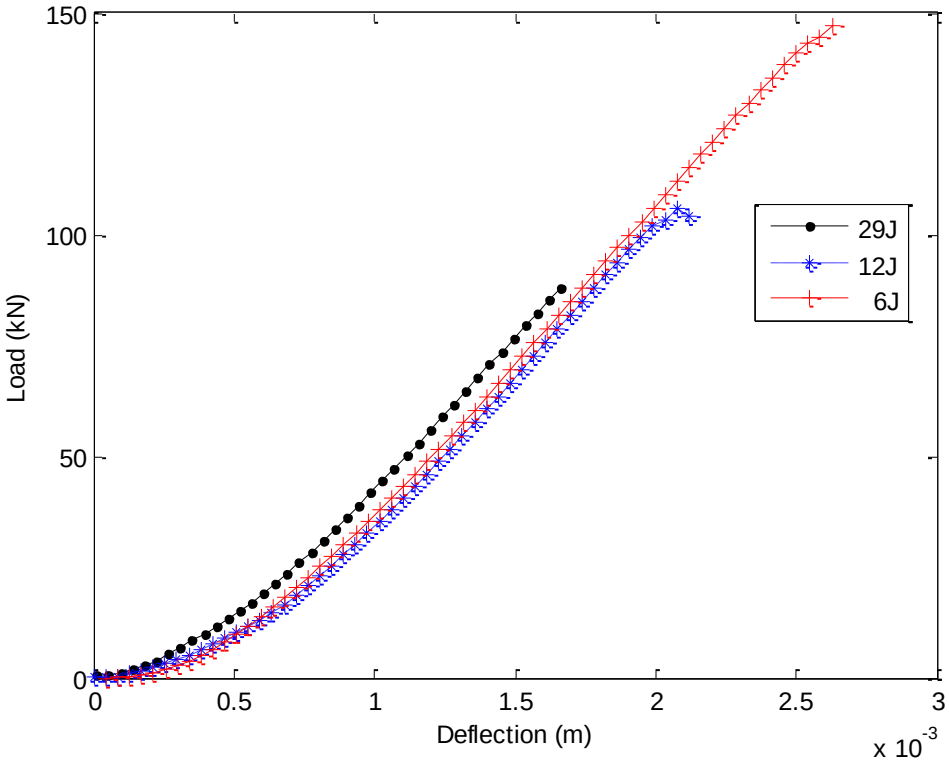

Figure 19. Compression Load vs. Deflection of Cycom 977-20/AS4-5HS Carbon Composites during CAI Testing Process

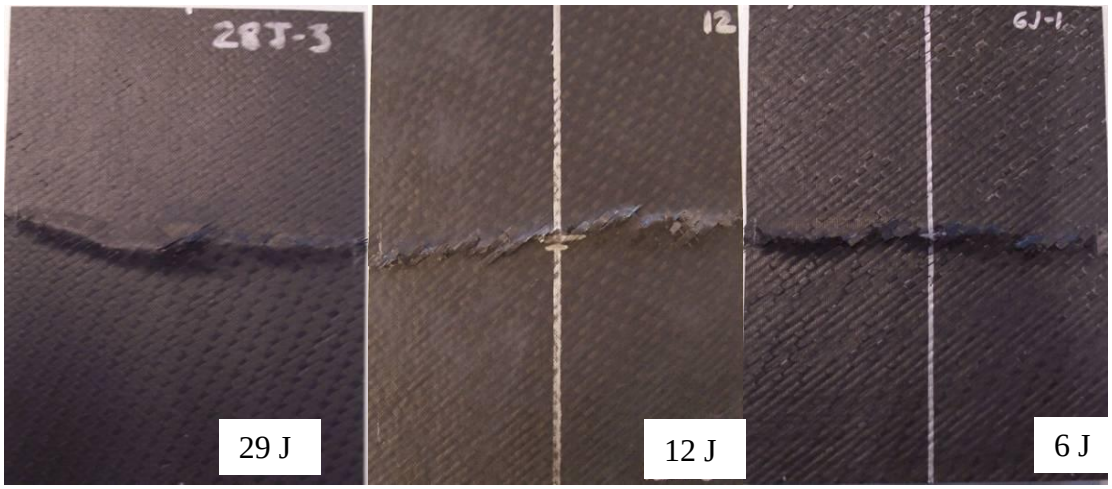

Figure 20. Front View of the Tested of Cycom 977-20/AS4-5HS Carbon Composite Samples

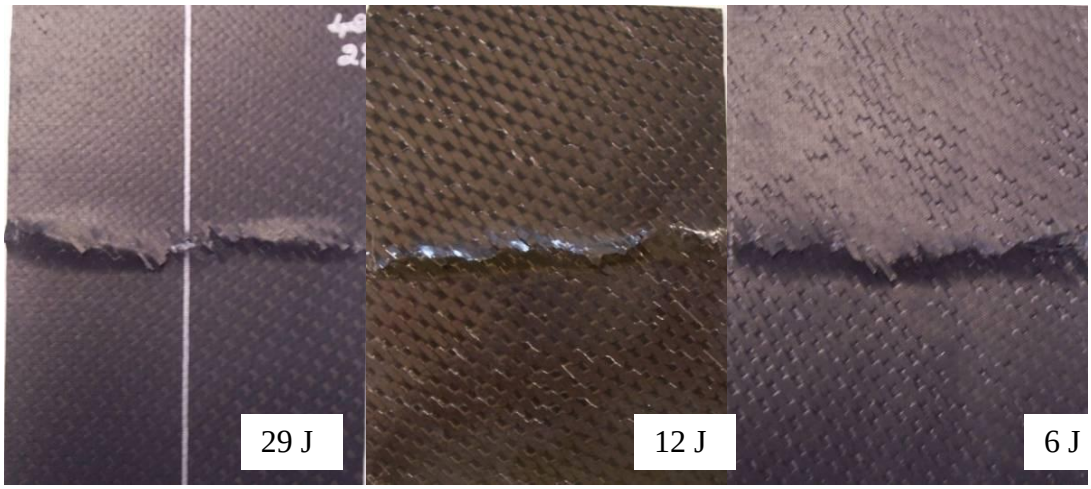

Figure 21. Rear View of the Tested of Cycom 977-20/AS4-5HS Carbon Composite Samples

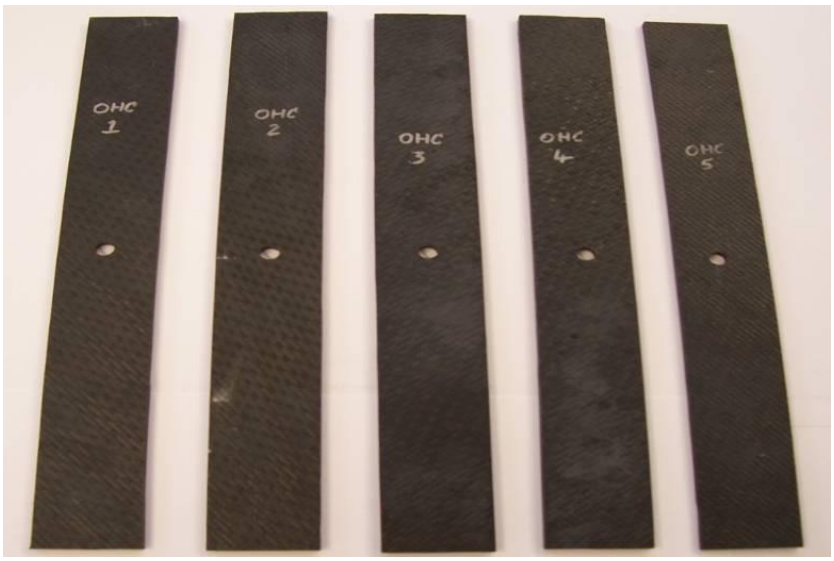

Figure 22. OHC Testing Coupons of Cycom 977-20/AS4-5HS Carbon Composites

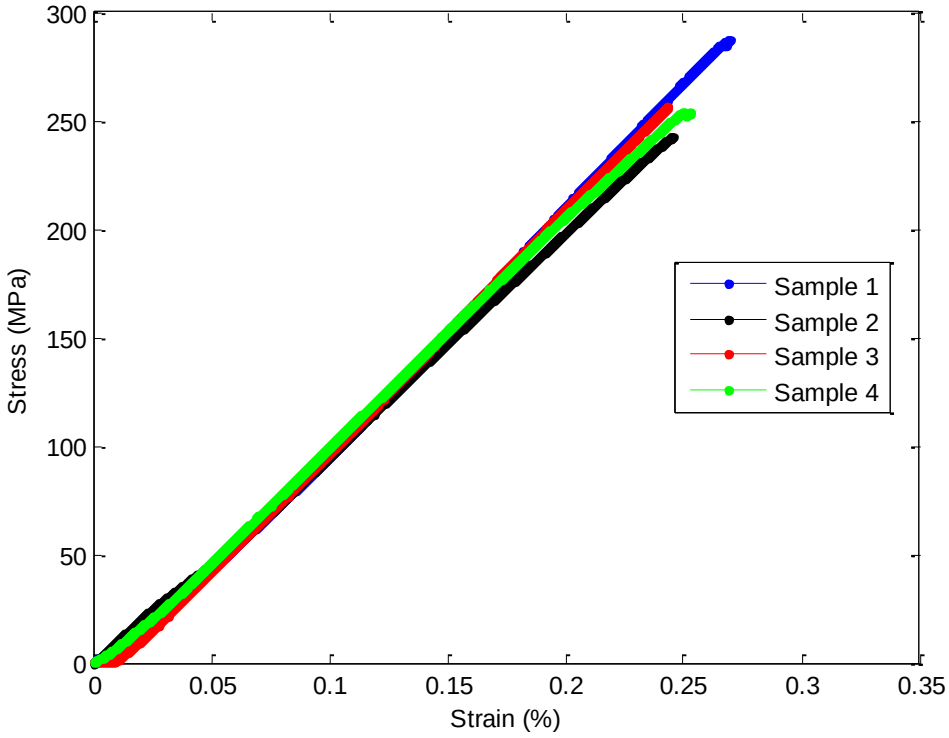

Figure 23. OHC Compressive Stress-Strain Curves of Cycom 977-20/AS4-5HS Carbon Composites

Figure 24. Cycom 977-20/AS4-5HS Carbon Composite Specimens Before (Left) and After OHC Testing (Right)

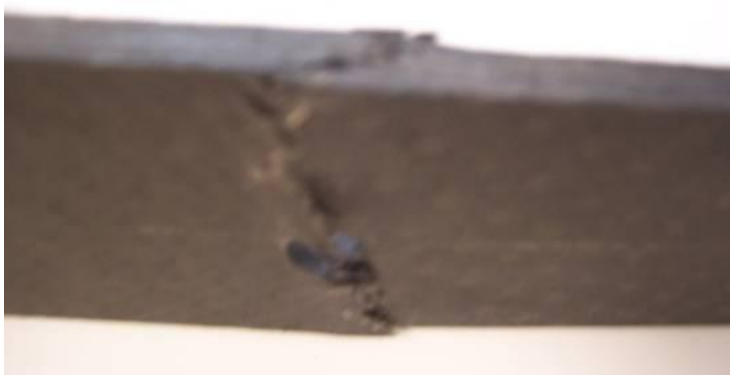

Figure 25. Damaged Cycom 977-20/AS4-5HS Carbon Composite Specimen After OHC Testing (Side View)

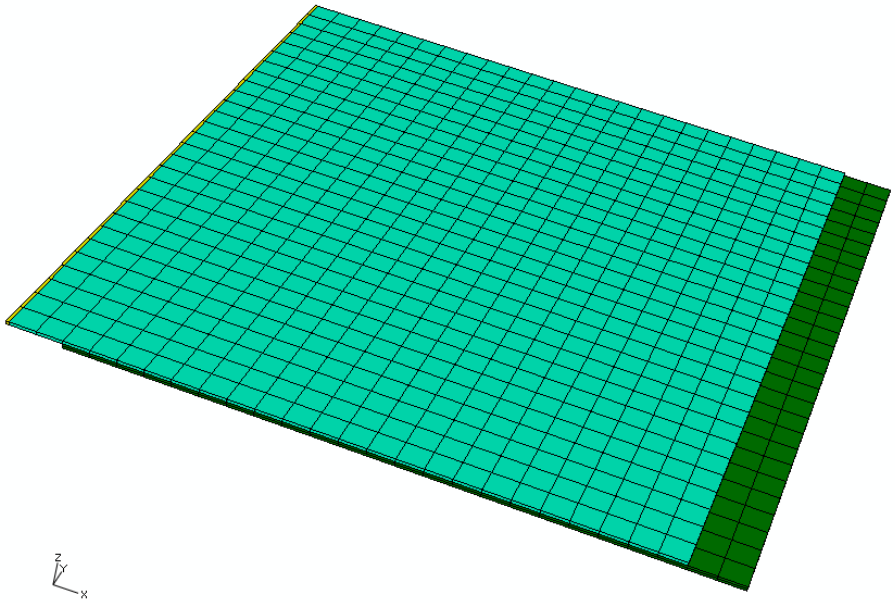

Figure 26. Mesh of FEA model for VARTM Flow Simulation

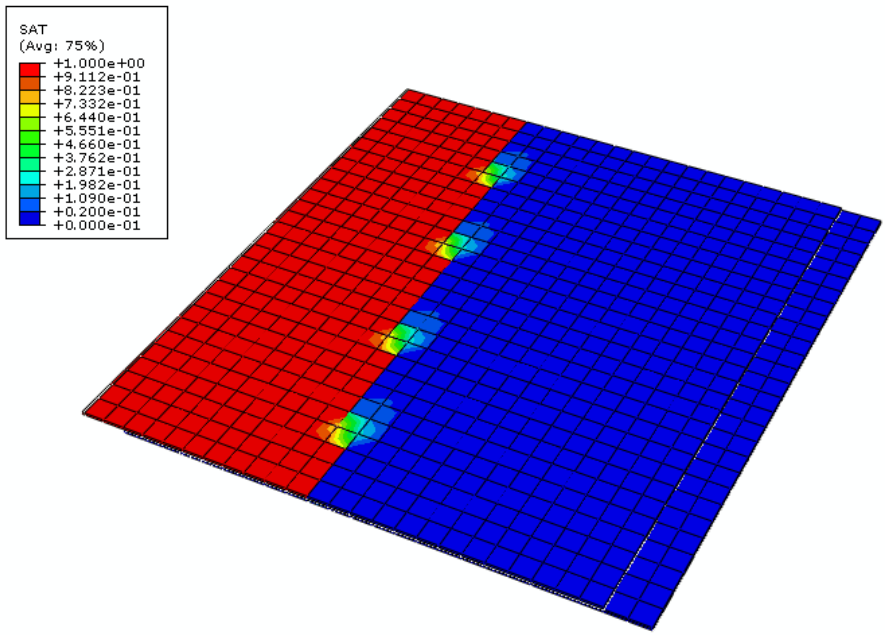

Figure 27. Saturation Distribution at Time = 7 sec

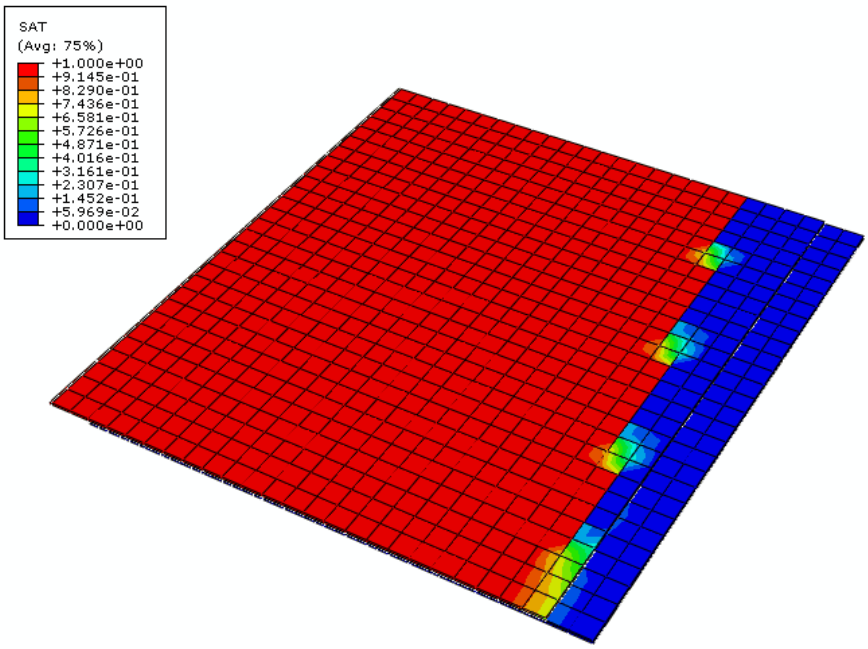

Figure 28. Saturation Distribution at Time = 30 sec

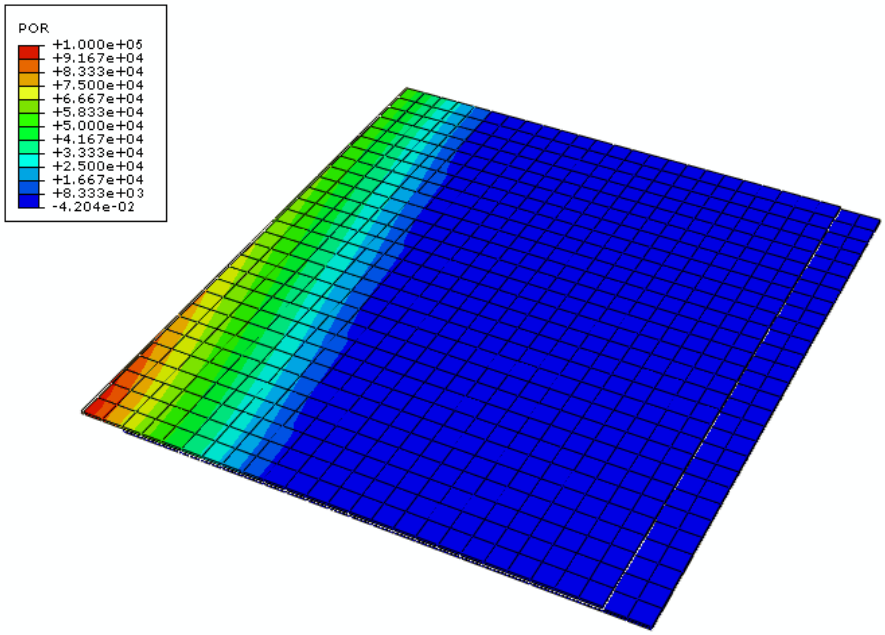

Figure 29. Pore Pressure Distribution at Time = 7 sec

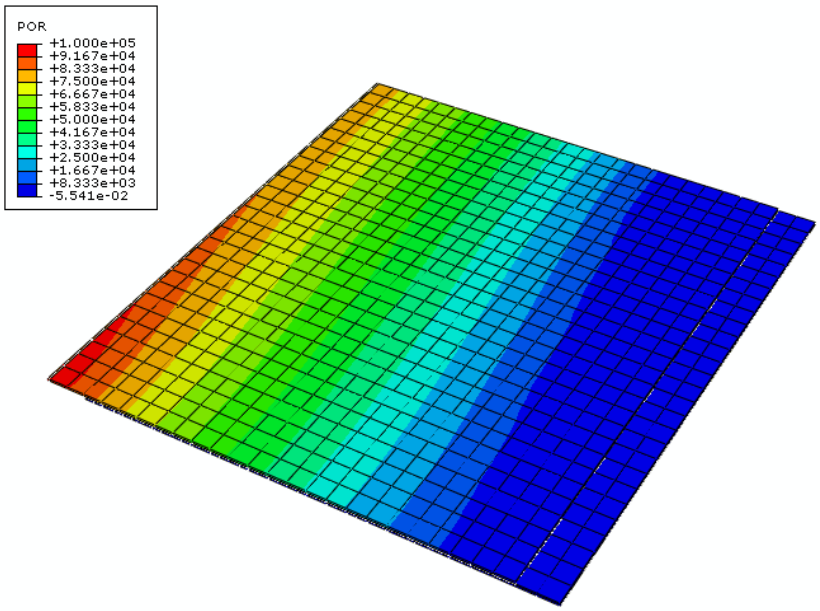

Figure 30. Pore Pressure Distribution at Time = 30 sec

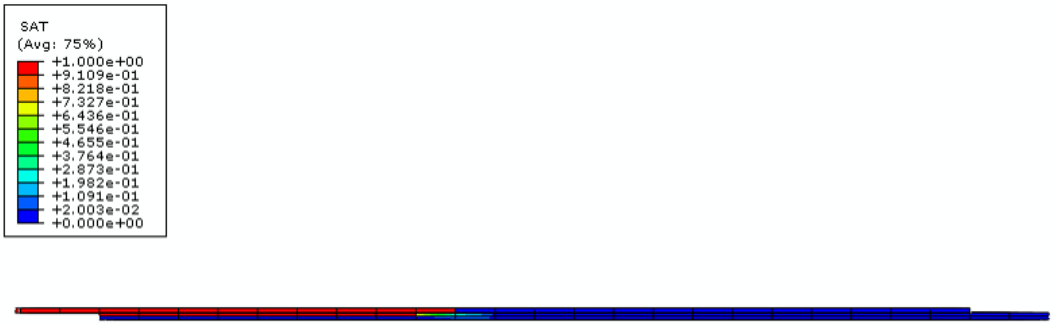

Figure 31. Saturation Distribution of Cross-section at Time = 7 sec

Figure 32. Saturation Distribution of Cross-section at Time = 30 sec

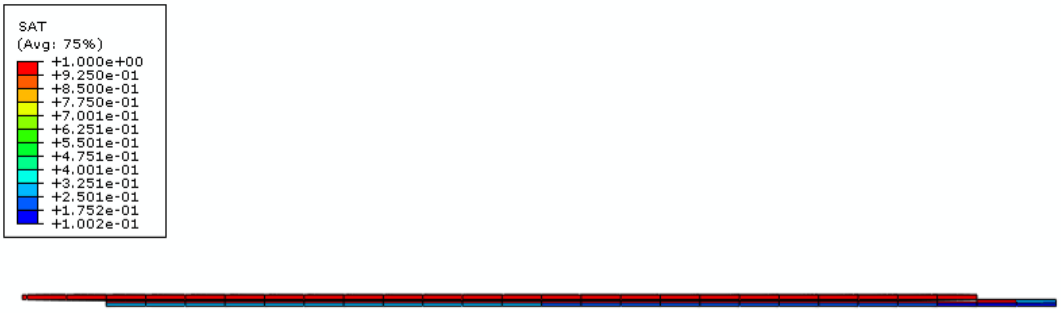

Figure 33. Saturation Distribution of Cross-section at Time = 225 sec

Figure 34. Saturation Distribution of Cross-section at Time = 435 sec

II. EVALUATION OF HONEYCOMB SANDWICH COMPOSITE STRUCTURES MANUFACTURED USING VARTM PROCESS

V.G.K. Menta and K. Chandrashekhara
Missouri University of Science and Technology, Rolla, MO 65409

ABSTRACT

In spite of numerous advantages of open-cell core sandwich composites, the applications have been limited due to the problems involved in manufacturing using low cost processes. Resin accumulation in the core is a major challenge in the fabrication of honeycomb sandwich panels using resin infusion techniques. Foam-filled cores and polymer film barriers are some of the methods used in the literature to address this issue. However, these techniques will increase the weight of the sandwich composites. In the present work, honeycomb sandwich panels were manufactured using commercially available film adhesive and modified vacuum assisted resin transfer molding (VARTM) process. The resin incursion into the core openings was investigated. No accumulation of resin was observed in the core. Flatwise tension, flatwise/edgewise compression, and three-point bending tests were conducted to evaluate the mechanical performance of the sandwich composites. The performance of sandwich panels during a low velocity impact event was also evaluated. Results indicate that the VARTM process can be successfully used to manufacture honeycomb composite sandwich structures using currently available barrier adhesive films.

1. INTRODUCTION

Sandwich composites are extensively used in aerospace applications due to their exceptional strength and stiffness-to-weight ratios as compared to conventional materials. Sandwich construction typically consists of thin facesheets separated by a lightweight core. The facesheets carry the bending loads and the core carries the shear/compressive loads. Fiber-reinforced composite laminates and aluminum are generally used as facesheets. Balsa wood, foam and honeycomb are commonly used core materials [1]. Containing 90-98% air in the core cells, honeycomb sandwich construction offers significant weight reductions over other foam materials while maintaining structural integrity [2]. Honeycombs from organic materials provide several other benefits such as greater design flexibility through thermal insulation, low electrical conductivity, sound and vibration dampening. In spite of all the advantages, the usage of honeycomb sandwich composites has been limited to specific applications due to the challenges involved in implementing low cost fabrication techniques such as liquid molding processes.

The conventional manufacturing of open-cell core sandwich composites generally includes several steps such as fabricating laminates followed by secondary bonding of facesheets to the core. Other complexities such as core moving, core crushing are also involved during the process. Co-curing techniques coupled with low cost manufacturing methods are ideal for reduced cost and cycle time [3]. Vacuum assisted resin transfer molding (VARTM) process has shown potential as a viable method for the manufacture of high-quality composites for structural aerospace applications at low production costs [4]. VARTM is a low cost and reduced volatile organic compound (VOC) emission manufacturing process. A key challenge in applying liquid molding processes for the open-cell core sandwich materials is to prevent resin from entering the hollow cells during the infusion process. The resin infiltration will cause undesirable increase in the weight of the composite. In the past, numerous efforts were made to address this issue [5-6]. Some of the solutions include filling the hollow cells with closed-cell foam, sealing the core with surface veils and polymer film barriers. These solutions often resulted in increase in the weight or cost of the final products [7].

The idea of wrapping the honeycomb core with an impermeable film during infusion process has been explored for several years. In 2002, the Boeing Company has patented a method, wherein a combination of film adhesive and solid bondable film was used with carbon prepregs [8]. Ebonee et al. [9] manufactured honeycomb sandwich composites using scrims in VARTM process. Authors reported that the resulting properties correlated with those manufactured using film adhesive. Most of the work reported in literature utilizes foam-filled core for liquid molding processes. Nida-Core Co. and Plascore Inc. offer thermoplastic extruded honeycomb cores with heat welded veil and barrier films for infusion processes [10]. Though these cores deliver a variety of advantages, applications can be limited due to the low mechanical and thermal properties. Much progress has been done with the adhesive films, and several moisture barrier film adhesives are currently available in the market. In the present work, attempts have been made to utilize FM 300MB, a commercially available moisture barrier film adhesive in VARTM process. In addition to properly permeating the core, the adhesive films are required to produce high bond strength without adding weight to the resulting sandwich composites. The objective of the study is to develop a one-step process for effective sealing of honeycomb core which is compliant with low cost liquid molding processes. The manufactured panels were cut at different cross-sections to visually inspect any presence of resin in the core. The sandwich core was free from any resin. Optical photomicrographs were used to examine the adhesive fillets at the core-to-facing interface. The compression, bending and low velocity impact behavior of the sandwich composites were also investigated.

2. MATERIALS

The facesheets were made from AS4-6K-5HS satin weave carbon fabric from Hexcel Co. Cycom 977-20, a one-part toughened epoxy resin system from Cytec Engineered Materials Inc. was used for infusion. FM 300MB adhesive film obtained from Cytec Engineered Materials Inc. was used to seal the core. HK 1/8’’- 4.5 pcf (2.8 mil N636) Kevlar honeycomb from M.C.Gill Co. was used as the core. The properties of the core obtained from the manufacturer are given in Table 1.

3. MANUFACTURING

Honeycomb sandwich composites have been manufactured using VARTM process. The schematic of the bagging procedure is shown in Figure 1. The facesheets consist of two layers of carbon fabric on each side. The process includes wrapping the honeycomb core with film adhesive and sealing the edges by applying heat. The core was preheated at 121°C (250°F) for one hour to remove any moisture absorbed and sealed water tight using the film adhesive. In the manufacturing process, a distribution medium followed by peel ply was first laid onto a mold that had been coated with release agent. Two layers of carbon fabric followed by sealed core and two more layers of fabric were placed on the top of peel ply. A layer of distribution medium and peel ply were placed over the preform. Resin inlet and vacuum outlet lines were placed in selected positions. After setting up the lines, a vacuum bag was placed over the mold and sealed around the perimeter with tacky tape. The vacuum line was connected to a resin trap and vacuum pump. The set-up was kept under vacuum for 1-2 hours. Vacuum was applied to the outlet of the mold and checked for any leaks. Before the infusion, resin was preheated to 65°C (150°F) and degassed to remove any entrapped air bubbles. The part was infused at 65°C (150°F).

After full infiltration of the resin had been achieved, the panels were placed inside the oven to cure. The cure cycle includes ramping the heat from 65°C (150°F) to 125±12°C (257±10°F) and held for 60±5 minutes. The temperature is then increased to 179±12°C (355±10°F) and held for 180±5 minutes. The part was then cooled to room temperature before removal from the oven. The cure profile is shown in Figure 2. The cured parts are shown in Figure 3. The manufactured sandwich composites have been visually inspected at several cross-sections for any presence of resin. No resin accumulation was observed inside the core.

4. PERFORMANCE EVALUATION

4.1. FIBER VOLUME FRACTION TESTS

The fiber volume fraction tests were conducted on the facesheets in accordance with ASTM D3171 nitric acid digestion method [11]. Four specimens weighing 0.5 to 1 gm were cut randomly from the panels for measurements. The edges of the specimens were polished to facilitate accurate measurements. The samples were dried in an oven for 1 hour at 149°C (300°F) to remove any surface moisture and then weighed. The specimens were then placed in a container filled with concentrated nitric acid and heated at 80°C (176°F) for 6 hours. After the resin was completely digested, the specimens were washed with water and acetone to remove excess acid and then dried in the oven for 1 hour at 100°C (212°F). Table 2 shows the fiber volume fraction of the laminate. The average density, fiber volume fraction and void content of the specimens were 1.56 g/cm^3, 59.42% and 0.61% respectively.

4.2. OPTICAL MICROSCOPY

The mechanical performance of sandwich panels depends on the quality of adhesive bond between the facesheets and core. In honeycomb sandwich composites, the proper flow of adhesive and filleting around the cell walls at the interface of core-to-facing determines the load transfer capability from facings to core. Formation of a symmetric, well-formed fillet is the main goal of any manufacturing process [12]. The relation between the adhesive fillet and sandwich properties is best described by Grimes et al. [13]. The manufactured sandwich composite samples were polished and examined under an optical microscope. The photograph of the adhesive fillet at magnification of x20 is shown in Figure 4. Symmetric adhesive fillets can be observed at the interface of core and facing.

4.3. FLATWISE TENSILE TESTS

Flatwise tensile strength primarily serves as a quality control parameter for bonded sandwich panels. These tests produce information on the quality and strength of

the core-to-facing bond. Coupons were subjected to uniaxial tensile forces normal to the plane of facesheets. Forces are transferred to the specimen through the loading blocks bonded to the coupons. Tests were carried out in accordance with ASTM C297 [14]. Five specimens of size 25 mm (1 in.) x 25 mm (1 in.) were tested at a crosshead speed of 0.5 mm/min (0.02 in/min) on Instron 4469 testing machine. Test results are shown in Table 3. The average ultimate flatwise tensile strength of the specimens was 1.013 MPa.

4.4. FLATWISE COMPRESSION TESTS

Flatwise compression tests produce information on the behavior of sandwich composites when subjected to uniaxial compressive loads normal to the plane of the facings. Tests were conducted on an Instron 4469 testing machine in accordance with ASTM C365 [15]. Five specimens of size 25 mm (1 in.) x 25 mm (1 in.) were tested. Tests were conducted at a crosshead speed for 0.5 mm/min (0.02 in./min). A preload of 44.5 N (10 lbf) was applied initially. The compressive load-deflection curves are shown in Figure 5. Linear elastic behavior was observed till the peak load followed by a steady crushing of the core. The oscillations in the crushing region of the curve correspond to the local buckling of the cells [16]. All the samples failed in uniform core compression. Samples had an average flatwise compression strength of 50.04 MPa (7258 psi).

4.5. EDGEWISE COMPRESSION TESTS

In the edgewise compression testing, compressive loads are applied in the direction parallel to the facing planes. Tests were conducted on Instron 5583 UTM according to ASTM C364 [17]. Four specimens of size 102 mm (4 in.) long x 76 mm (3 in.) wide were held in the end-fixture between the compression platens (Figure 6a). Compressive loads were applied at a crosshead speed of 0.5 mm/min (0.02 in/min). Initiated by facing to core debonding, the facesheet exhibited a buckling type of failure as shown in Figure 6b. The load-deflection curves are shown in Figure 7. The specimens had an ultimate edgewise compressive strength of 354.42 MPa with a standard deviation of 37.11 MPa.

4.6. THREE-POINT BENDING TESTS

Tests were conducted to determine the flexural and transverse shear stiffness of the sandwich construction (Figure 8). Tests were conducted on Instron 4469 machine in accordance with ASTM C393/D7250 [18, 19]. Four rectangular specimens with a width of 76 mm (3 in.) and a length of 203 mm (8 in.) were subjected to bending moments normal to the facing plane. A span length of 152 mm (6 in.) and a crosshead speed of 0.25 in/min were used. Force versus deflection curves are shown in Figure 9. The sandwich flexural stiffness and transverse shear rigidity values are presented in Table 4.

4.7. LOW VELOCITY IMPACT TESTS

A Dynatup Instron Model 9250 Impact Testing Machine with impulse control and data system was used to evaluate the resistance of sandwich composites to drop-weight impact events. The impact test instrument has a motor and twin screw drive for rapid crosshead retrieval after impact. The impulse control and data system includes impulse software controller panel for test set-up and high-speed impulse signal conditioning unit. The impact support fixture contains two steel plates with cut-outs of size 76 mm (3 in.) x 127 mm (5 in.). The hemi-spherical impactor had a mass of 6.48 kg and a diameter of 12.7 mm (0.5 in.). Specimens of size 152 mm (6 in.) x 102 mm (4 in.) were clamped in the support fixture along the perimeter and the impactor mass was raised to the desired drop height corresponding to the energy of impact. Three energy levels of 3J, 6J and 10J were selected such as to produce barely visible impact damage (BVID) causing a dent depth of 0.25 mm (0.01 in.) – 0.51 mm (0.02 in.), visible damage and facing penetration energy. Dent depths of 0.3 mm (0.012 in.) and 1.52 mm (0.06 in.) were observed at 3J and 6J of impact energy whereas the top facing was penetrated at 10J of energy. Three specimens were tested at each energy level.

Figure 10a shows the variation of impact energy with time. The loading phase of the curve (increasing energy) indicates the amount of energy absorbed by the specimen and the unloading phase is a measure of the amount of energy given out by the specimen while trying to regain its initial configuration due to its elasticity. Therefore, the flat region indicates the net energy absorbed by the specimen. The velocity history of the impactor is shown in Figure 10b. The velocity is observed to decrease as the time

progressed and reaches zero at maximum deflection. Negative values of velocity represent the rebounding of the impactor and that the sample is not perforated. The velocity values remain positive if the impactor penetrates through the sample. At 10J of energy, the velocity remained positive indicating the penetration of the top facesheet by the impactor. The same can be observed in contact force versus displacement plot in Figure 10c. At 3J of energy, the sudden drop after the peak load has been reached indicates the facesheet loss of load carrying capacity. Several oscillations were observed in the load-deflection curves. The data intervals have been increased to present the curves vividly. These oscillations can be attributed to the local crushing of the honeycomb core. The tests results are tabulated in Table 5.

5. CONCLUSIONS

Honeycomb sandwich composites have been manufactured using a modified one-step VARTM process. The method includes wrapping the core with film adhesive and sealing the edges. The sealed core was then used in the vacuum infusion process. Two layers of FM 300MB, commercially available moisture barrier film, were used for sealing the core. The resulting sandwich composites were free from any resin inside the core. The photomicrographs showed symmetric well-formed adhesive fillets. The quality of the adhesive bond was evaluated using flatwise tensile tests. Flatwise/edgewise compression, three-point bending and low velocity impact test results were presented. Fiber volume fraction and optical microscopy test results show that the facesheets have very low void content. The work shows that the currently available moisture barrier adhesive films can be used to implement a resin infusion process for honeycomb or open-cell core sandwich composite manufacturing.

6. REFERENCES

1. Bitzer, T., "Honeycomb Technology: Materials, Design, Manufacturing, Applications and Testing," *Chapman & Hall:* (1998).
2. Khan, S., and Loken, H. Y., "Bonding of Sandwich Structures - The Facesheet/Honeycomb Interface – A Phenomenological Study," *39rd International SAMPE Technical Conference,* Baltimore, MD (2007): 1-9.
3. Menta, V. G. K., Sundararaman, S., Chandrashekhara, K., Phan, N., and Nguyen, T., "Hybrid Composites using Out-of-Autoclave Process for Aerospace Sub-structures," *SAMPE International Symposium*, 53 (2008): 1-11.
4. Tatum, S., "VARTM Cuts Costs," *Reinforced Plastics,* 45 (2001): 22-23.
5. Jonas, S., and Thorsten, J., "New Rohacellê Development for Resin Infusion Processes," Proceedings *of the 7th International Conference on Sandwich Structures*, Aalborg, DK (2005): 1-10.
6. Grove, S.M., Popham, E., and Miles, M. E., "An Investigation of the Skin/Core Bond in Honeycomb Sandwich Structures using Statistical Experimentation Techniques," *Compoistes: Part A*, 37 (2006): 804-812.
7. Kruckenberg, R. and Paton, R., "Resin Transfer Molding for Aerospace Structures," *Chapman & Hall:* (1998).
8. Holemans, P., "Liquid Molded Hollow Cell Core Composite Articles," *United States Patent 6780488 B2,* 2004.
9. Ebonee, P. M. W., Brian, S. H., and James, C. S., "VARTM Processing of Honeycomb Sandwich Composites: Effect of Scrim Permeability," *33rd International SAMPE Technical Conference*, Seattle, WA (2001): 1-7.
10. Sarah, B., "Getting to the Core of Composite Laminates," *Composites Technology*, (2003): 1-3.
11. ASTM D3171, "Standard Test Methods for Constituent Content of Composite Materials," *ASTM International* (2006): 1-10.
12. Chongxin, Y., Min, L., Zuoguang, Z., and Yizhuo, G., "Experimental Investigation on the Co-Cure Processing of Honeycomb Structure with Self-adhesive Prepreg," *Applied Composite Materials,* 15 (2008): 47-49.

13. Grimes, G. C., "The Adhesive – Honeycomb Relationship," *Applied polymer symposium*: 3 (1996): 157-190.
14. ASTM C297, "Standard Test Method for Flatwise Tensile Strength of Sandwich Constructions," *ASTM International* (2004): 1-6.
15. ASTM C365, "Standard Test Method for Flatwise Compressive Properties of Sandwich Cores," *ASTM International* (2005): 1-7.
16. Abrate, S., "Impact on Composite Structures," London, *Cambridge University Press,* (1998).
17. ASTM C364, "Standard Test Method for Edgewise Compressive Strength of Sandwich Constructions," *ASTM International* (2007):1-8.
18. ASTM C393, "Standard Test Method for Core Shear Properties of Sandwich Constructions by Beam Flexure," *ASTM International* (2006): 1-8.
19. ASTM D7250, "Standard Practice for Determining Sandwich Beam Flexural and Shear Stiffness," *ASTM International* (2006): 1-8.

Table 1. Core Properties

Property	**Gilcore HK 1033**
Bare Compression N/m^2 (psi)	4819 (699)
Stabilized Compression N/m^2 (psi)	5454 (791)
L Shear N/m^2 (psi)	4268 (619)
L Modulus GPa (ksi)	0.216 (31.4)
W Shear N/m^2 (psi)	2282 (331)
W Modulus GPa (ksi)	83 (12.1)

Table 2. Fiber Volume Fraction Test Results

	Density (g/cm^3)	**Fiber Volume Fraction (%)**	**Void Content (%)**
1	1.564	59.68	0.62
2	1.566	59.38	0.39
3	1.563	59.09	0.54
4	1.560	59.54	0.88
Average	1.563	59.42	0.61
Standard Deviation	0.002	0.26	0.21

Table 3. Ultimate Flatwise Tensile Strength

Sample	**Ultimate Strength (MPa)**
1	1.036
2	0.958
3	1.077
4	0.971
5	1.021
Average	1.013
Standard Deviation	0.049

Table 4. Flexural Test Results

Sample	**Flexural Stiffness ($N\text{-}m^2$)**	**Transverse Shear Rigidity (kN)**
1	816.96	72.97
2	847.41	70.16
3	836.44	75.52
4	825.47	69.52
Average	831.57	72.04
Standard Deviation	13.23	2.76

Table 5. Low Velocity Impact Test Results

Properties	**3J**	**6J**	**10J**
Energy Absorbed (J)	2.55 ± 0.03	5.63 ± 0.06	10.03 ± 0.07
Maximum Contact Force (kN)	1.72 ± 0.06	1.69 ± 0.09	1.65 ± 0.02
Contact Duration (ms)	8.93 ± 0.12	11.40 ± 0.4	17.56 ± 0.42
Peak Velocity (m/s)	-0.33 ± 0.02	-0.35 ± 0.04	0.05 ± 0.02
Maximum Displacement (mm)	2.3 ± 0.04	4.28 ± 0.25	9.73 ± 0.40

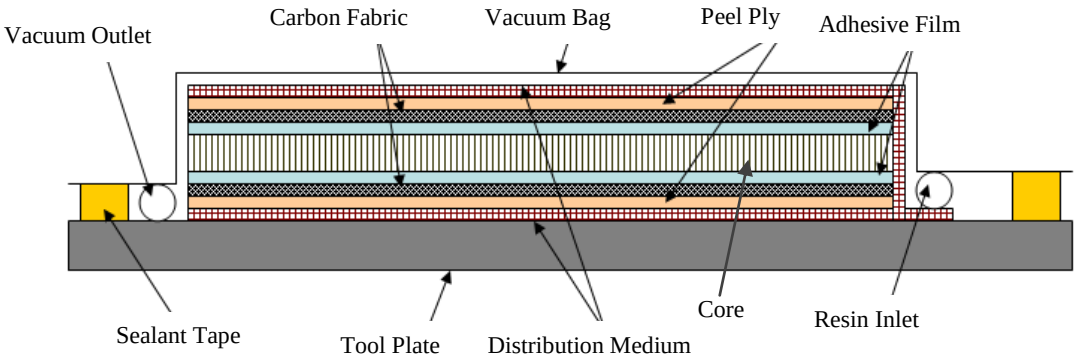

Figure 1. Schematic Representation of Out-of-Autoclave Bagging Procedure

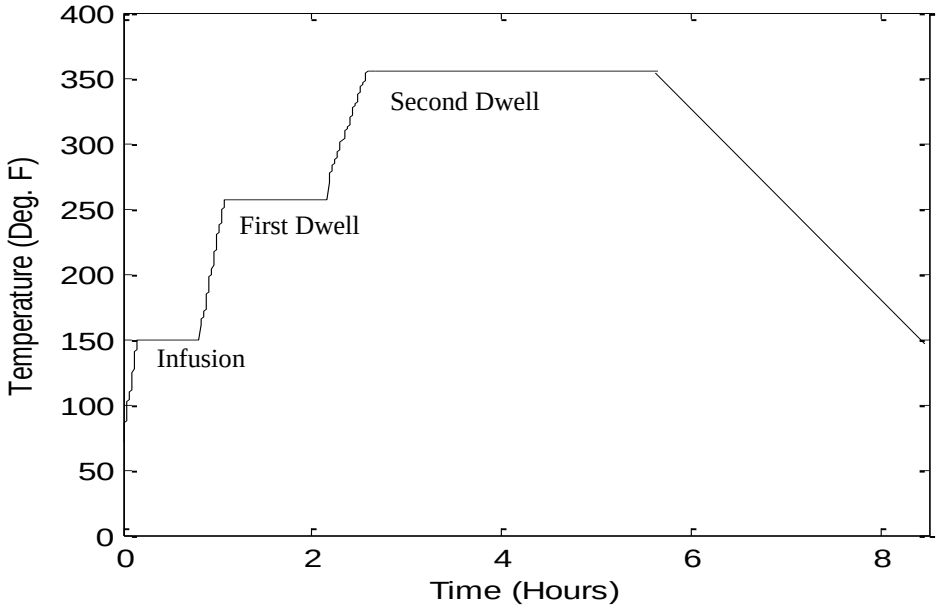

Figure 2. Cure Profile of VARTM Manufacturing

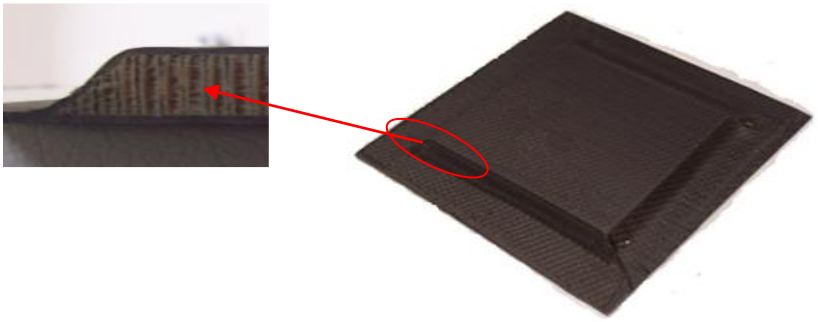

Figure 3. Sandwich Composites Manufactured using VARTM Process

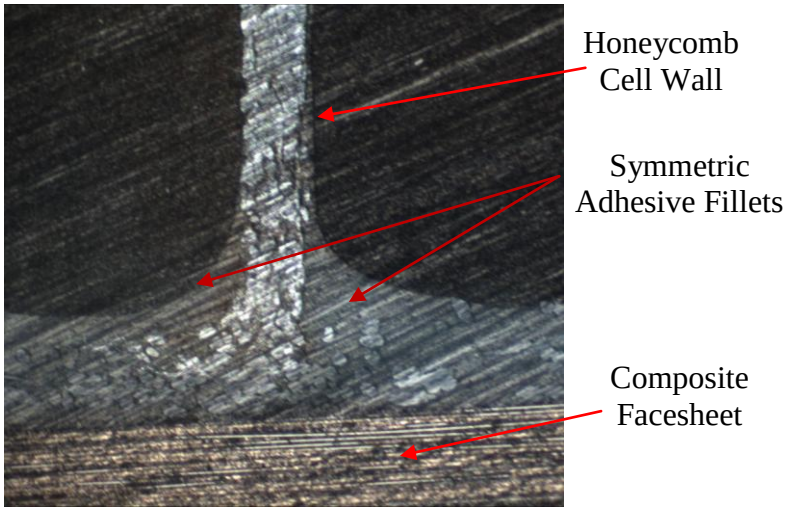

Figure 4. Photomicrograph (x20) of Core-to-Facing Adhesive Bond

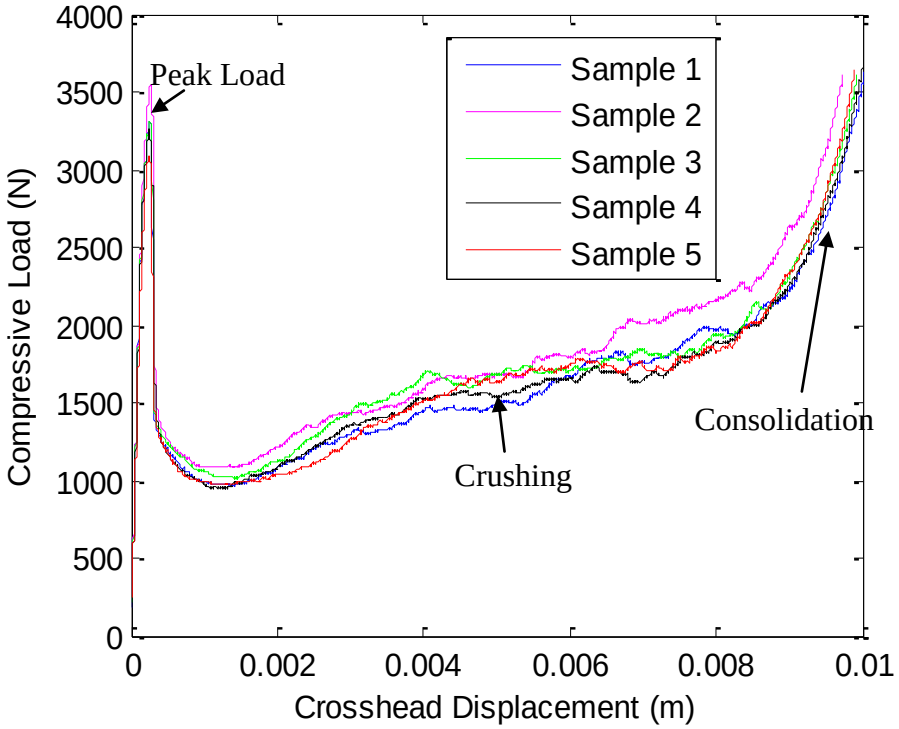

Figure 5. Flatwise Compression Behavior of Honeycomb Sandwich Composites

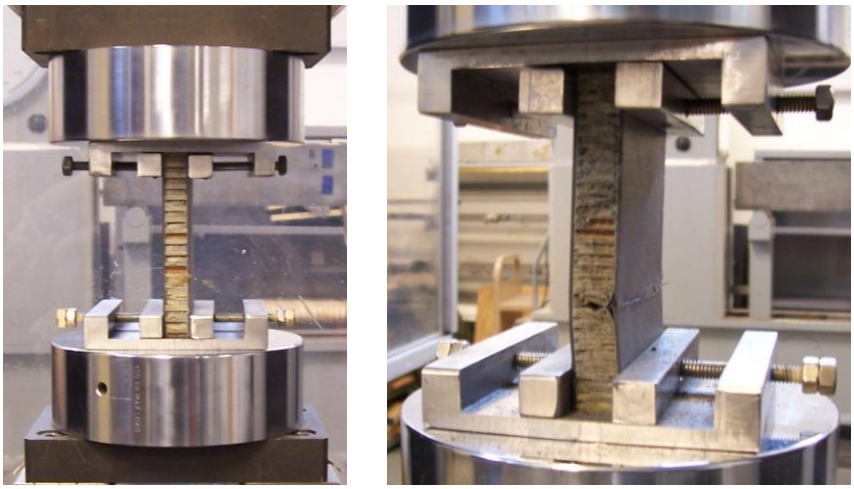

(a) **(b)**

Figure 6. Edgewise Compression Testing (Left); Facesheet Buckling Failure (Right)

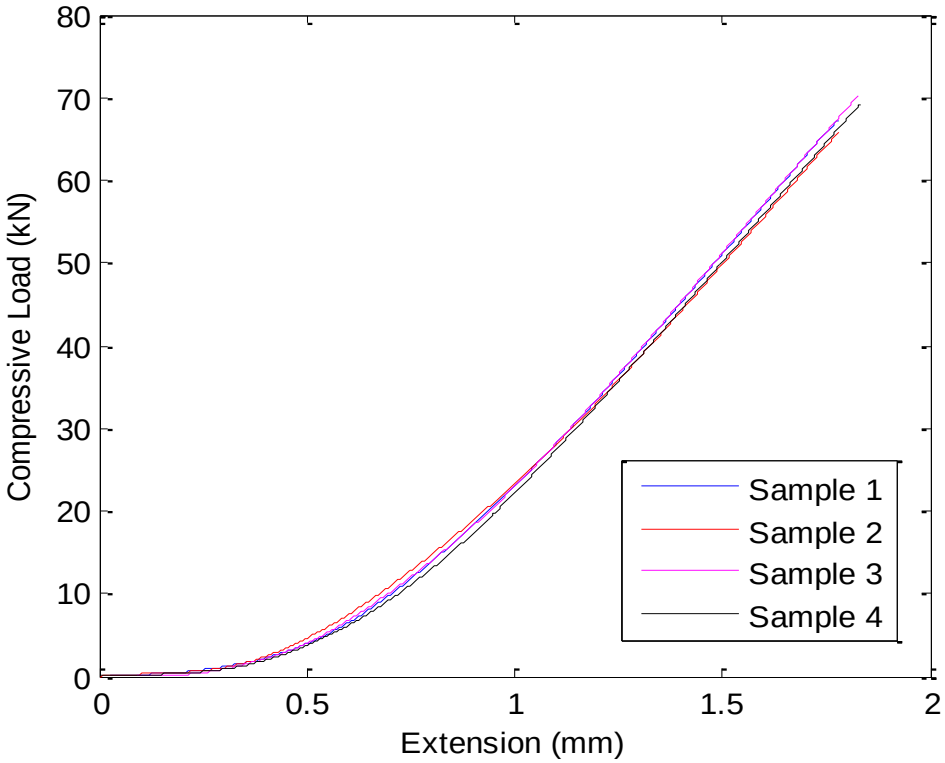

Figure 7. Edgewise Compression Load Deflection Curves of Sandwich Composites

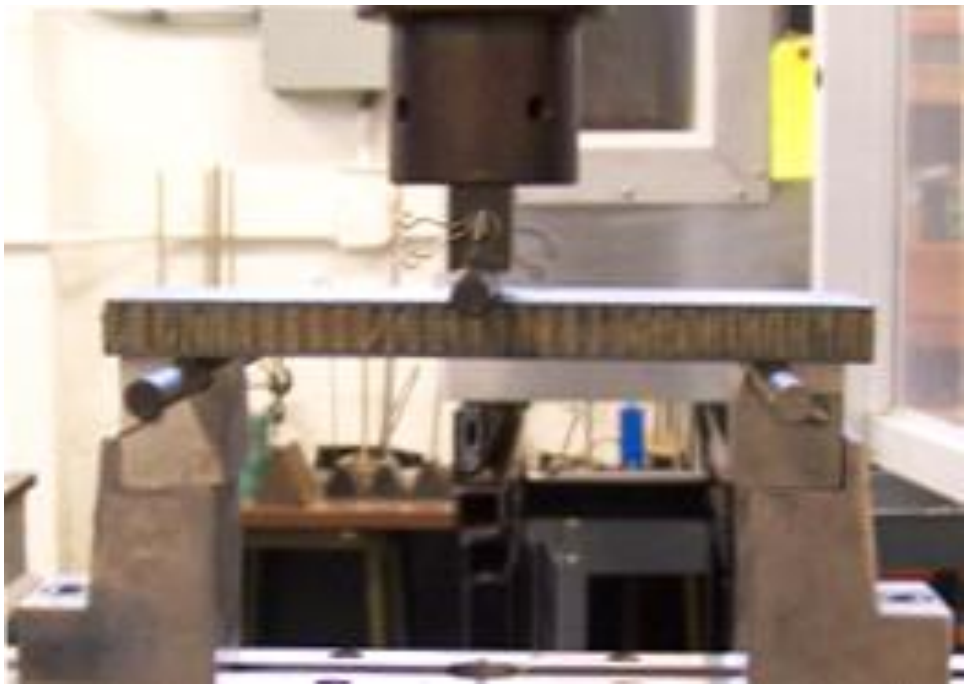

Figure 8. Three Point Bending Test Set-up

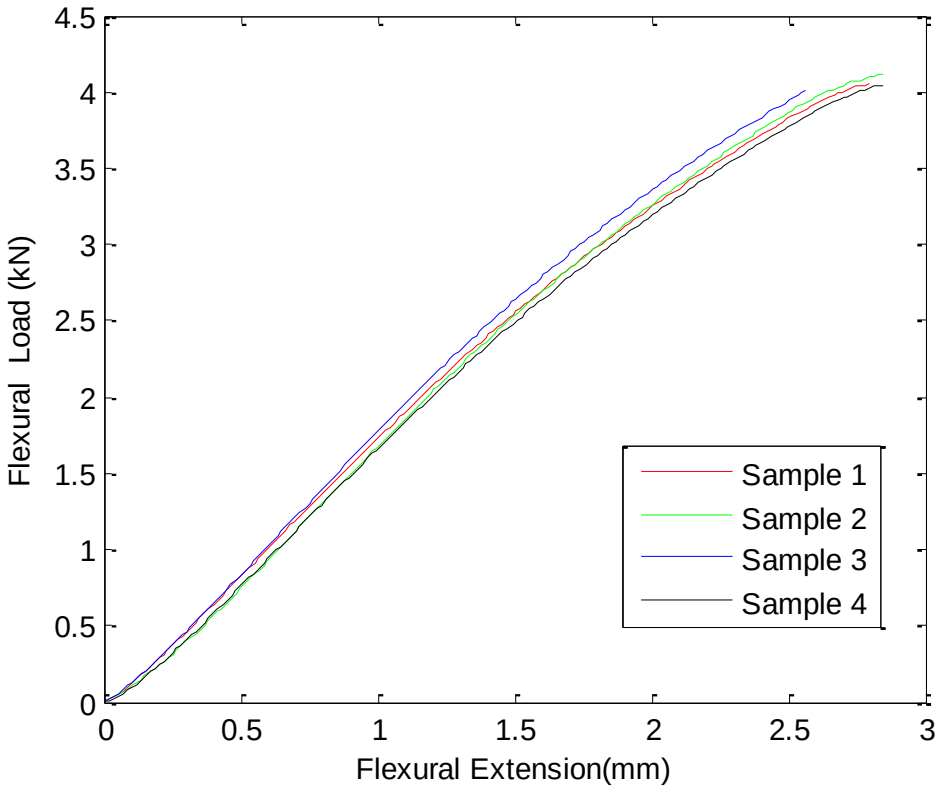

Figure 9. Three-Point Bending Load Deflection Curves of Sandwich Composites

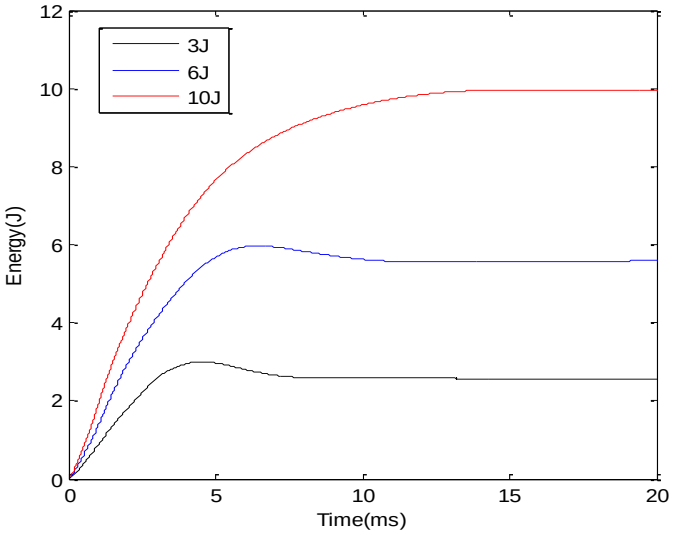

(a)

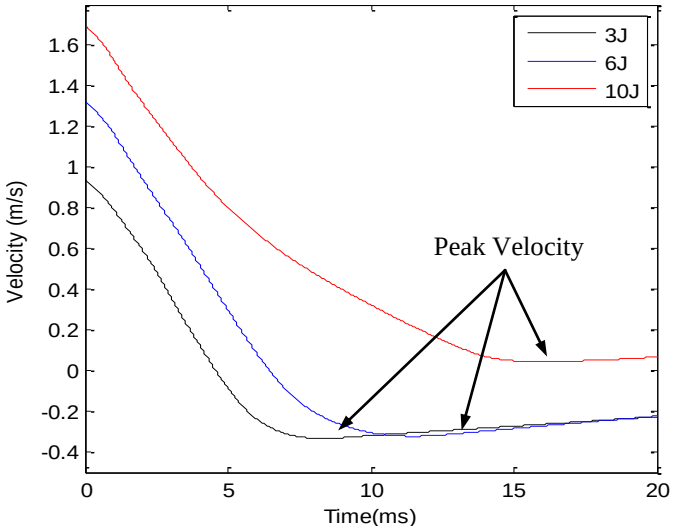

(b)

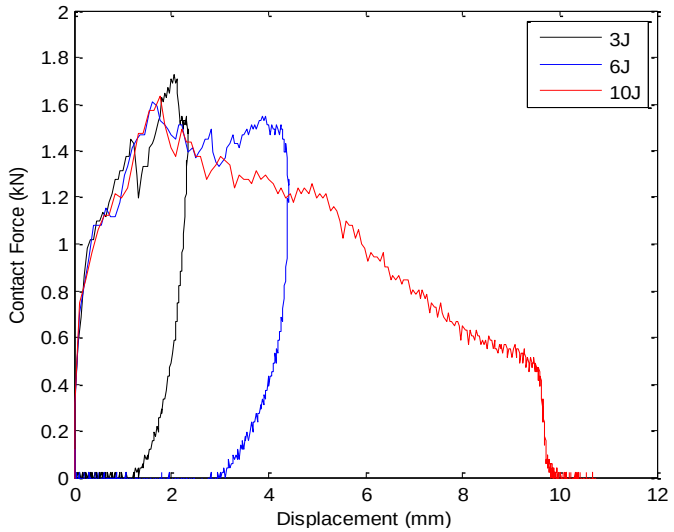

(c)

Figure 10. Impact Test Results (a) Impact Energy History Curve, (b) Velocity History Curve, (c) Contact Force vs. Displacement

III. COMPOSITES USING OUT-OF-AUTOCLAVE PREPREGS

V.G.K. Menta and K. Chandrashekhara
Missouri University of Science and Technology, Rolla, MO 65409

ABSTRACT

Autoclaves have commonly been used to manufacture high performance composites for aerospace applications. However, high capital and tooling costs make these composites very expensive. Vacuum- bag-only cure out-of-autoclave (OOA) composite manufacturing process is potentially a lower-cost alternative to autoclave manufacturing. The OOA process does not require the positive pressure of an autoclave but still produces high quality composite parts. In the present study, high performance carbon/epoxy composite (MTM45-1/CF2412 carbon fabric) laminates have been manufactured using the OOA process. Density, fiber volume fraction and void content have been evaluated using sulphuric acid digestion method. The carbon composites manufactured using OOA process had less than 0.25% void content. Mechanical tests were performed on the manufactured samples. The low velocity impact resistance behavior of the composites has been investigated using statistical design and analysis tools. A Design of Experiments (DoE) approach is used in designing experiments to examine the influence of size, lay-up configuration, thickness and their interactions on the impact behavior of the composites. A full factorial 2^3 (Three factors each at two levels) DoE was used for the study. Energy absorbed, Peak force, contact duration, maximum displacement and velocity were considered as output parameters for the study. Analysis of Variance (ANOVA) was used to analyze the test data. The results show that all the factors considered in the study are significant. These results can be used to simplify and gain more insight into the low-velocity impact study of composites.

1. INTRODUCTION

In spite of numerous application possibilities, the usage of composites has been limited because of high costs. While the material costs sum to 8-10% of the total costs, manufacturing and processing costs contribute to the majority of the overall costs of the composites [1]. Cost savings of up to 75% have been achieved by using low-cost composite manufacturing techniques and by making integral parts [2]. Hence, several studies have been devoted over the past few decades in developing non-autoclave manufacturing techniques that can significantly reduce the manufacturing costs of composites. Bond et al. [3] presented a comparative summary of physical, mechanical and thermal performance of composites manufactured using different non-autoclave processes developed in the past few decades. In addition to huge capital and tool cost-savings, non-autoclave composite manufacturing processes offer several advantages such as scalability to large parts, and flexibility to manufacture hybrid, complex-shaped parts [4]. The out-of-autoclave (OOA) process is a new generation vacuum-bag-only cure process that uses special prepregs that can be cured in regular ovens instead of an autoclave. Developing low cost advanced composites will allow to fully utilize the advantages of composites and to advance the usage of composites in several applications. However, for the OOA method to be qualified as an aerospace composite manufacturing process, the technique should be able to produce composites with low void and surface pit levels as those of autoclave-cured composites.

Poor out-of-plane load transfer capability of composites has been a major concern regarding the usage of composites. Studies show that impact loads as low as 4J has resulted in strength reductions of up to 50 % [5]. Composites are susceptible to different low velocity impacts such as tool drops, hail stone strikes or low flying objects during the life of a structure. While high velocity impacts produce visible damage, low velocity impacts can cause internal damage with little or no visible outward sign yet causing significant loss in tensile strength and especially compressive strength. The low velocity impact behavior of composites is inherently complex. The extent of literature available on this subject is an evidence of the high importance this subject holds among the researchers around the world. Subjected to impact loads, composites generate several

complex damage modes at the same time. The damage zones can comprise of different modes like indentation, matrix cracking, matrix crushing, fiber-matrix interface failure, delaminations and fiber fracture. Several analytical and experimental studies have been conducted to understand the initiation and growth of impact damage and identifying the governing parameters. Impact response of composites are affected by numerous factors including the properties of fibers; properties of matrix; surface treatment of the fibers; fiber volume fraction of the laminates; geometry of the laminate like size, thickness, stacking sequence, stitching, weave angles, lay-up orientation; boundary conditions; impact variables such as impact energy, impactor and angle of impact; and thermal, environmental conditions. The multitude of variables coupled with the complexity of impact dynamics has made every study on this subject valuable to engineers.

Due to the large number of factors involved in impact behavior of composites, statistical analysis would offer most appropriate tools that can help in simplifying the understanding of impact behavior of composites. Design of experiments (DoE) is a statistical technique used to determine the relationship between factors influencing the process and the response of the process. DoE involves designing a structured set of experiments that includes varying several variables systematically and simultaneously in order to get maximum data with fewest experimental runs. DoE which was first developed for agricultural research has been applied in several disciplines including manufacturing process design and development, process management and other engineering design activities. The results obtained from DoE helps greatly in identifying the variables that most affect the response, variables that do not affect, influencing interactions among the variables, and the process conditions that result in close conformance to optimum target requirements. DoE has been employed used by Sutherland et al. [6] to study the impact behavior of composites.

A brief literature review of low velocity impact of composites is presented in this paper. Complete reviews in this subject can be found in [7-11]. Several factors affect the low-velocity impact performance of composites. Cantwell et al. studied the influence of different stacking sequences: $[((+/-45)_{1,2,4,8,16})_s$, $[(0_2,+/-45)_{1,2,4})_s]$, sizes (25-150mm) and thicknesses (0.5 - 4mm) on CFRP composites [12]. The author concluded the geometrical dependence of impact damage and reported that damage is caused by high local stresses

at the point of impact in short thick beams and in long thin composites damage occurs as a result of splitting between the lower surface fibers. The effect of stacking sequence ($[0]_{10}$, $[0/90/0/90/0]_s$ and $[+45/-45/+45/0/90]_s$) and impact energy (2.36,4.33,5.91 and 10.82J) was presented by Tita et al. The author used load history, displacement history, energy history and NDE images to study the impact dynamics [13].

Atas et al. investigated the effect of weave angle on the impact response of woven fabric glass/epoxy composite plates. The author concluded that the absorbed energy and perforation threshold was significantly improved by using small weaving angle between interlacing yarns [14-15]. Sutherland et al. investigated scaling laws of impact on hand-produced low fiber-volume glass-polyester composite laminates using dimensional analysis approach and verified with experimental results [16]. Gomez-del Rio et al. also studied the influence of low temperatures (varying from -150^{o}C to 20^{o}C) on low velocity impact response of CFRP composites [17].

Hosur et al. has conducted low velocity impact tests at 15, 30 and 45J on 8HS satin weave carbon/epoxy laminates subjected to different moisture conditions of cold-dry and cold-moist conditions for a period of 3-6 months [18]. Shyr et al. considered three types of E-glass fabric: non-crimp fabric, woven fabric, and nonwoven mat as reinforcements to study the effect of type of fabric on the impact behavior of composites and recommended non-crimp fabric to improve the impact resistance of composites [19]. Riccio et al. analyzed the onset of impact induced delaminations in stiffened composite panels by using threshold impact force as the response and investigated the influence of the compressive loading conditions on the damage resistance of composites. The author concluded that variation in stiffness caused the panel to absorb impact energy without any delamination onsets [20].

In the present study, high performance composites have been manufactured employing the OOA manufacturing process. Physical and mechanical tests have been conducted to evaluate the performance of the manufactured composites. Low velocity impact tests were performed on the manufactured composite panels. Residual compressive strength of the impacted panels was evaluated. The influence of size, lay-up configuration and thickness and their interactions on the low velocity impact behavior of

OOA composites has been investigated using 2^3 full factorial DoE approach. "Design Expert", statistical analysis software was used to analyze the results.

Terminology:

A glossary of terms related to low-velocity impact tests and DoE have been presented below:

Impact Energy – Incident kinetic energy

Contact Force – Reaction force applied by the specimen to the impactor

Absorbed Energy – The energy absorbed by the specimen during the impact event

Peak Force – Maximum load recorded during the impact test

Threshold Force – The load at which the first delamination (first discontinuity in the force history curve or slope of the curve)

Threshold Energy – The energy corresponding to the threshold force and is the energy below which no damage is induced in the specimen

Contact Duration – Total duration of impactor tup in contact with specimen from the time it first contacted the specimen.

Perforation Threshold Energy – The energy at which the impactor perforates the specimen

Dent depth – Depth of the depression in the specimen made by the impactor

Factors – Variables or process inputs that are controlled during the experiment

Levels – Different settings each factor can have

Replication – Independent repetitions of experimental runs

2. MATERIALS

MTM45-1/CF2412 carbon prepregs obtained from Advanced Composites Group Inc., Tulsa, OK have been used for the present study. These prepregs contain 6K 5HS AS4C carbon fabric impregnated with MTM 45-1, a variable cure temperature, high performance toughened epoxy resin.

3. MANUFACTURING

Flat composite panels have been manufactured using OOA manufacturing process. The schematic of the bagging procedure employed for the OOA process is shown in the Figure 1. The manufacturing procedure includes laying up the prepregs that were cut to the required dimensions and orientations on to an aluminum mold free from surface defects and already coated with Frekote release agent. Hand pressure and rollers were used to press the prepregs over the mold starting from one side of the prepreg and moving progressively towards the rest of the surface. This process is repeated for all the prepregs to remove entrapped air bubbles as well as folds or wrinkles. Thin glass strings, FEP release film, breather and vacuum outlets were placed and sealed with a vacuum bag. Vacuum line was connected to the vacuum pump and checked for any leaks. A two-stage vacuum pump with a capacity of 5 L s^{-1}(10.6 cfm) and an ultimate vacuum of 0.013 Pa (1 x 10^{-4} torr) has been used to manufacture these panels. The set-up was maintained under vacuum for 12 hours. Medium temperature cure/High temperature post-cure cycle recommended by the prepreg manufacturer was used for curing the composite parts. The lay-up is heated to 180°F and held for 4.5 hours. The temperature is then increased to 250°F and held for 4.5 hours. The part is then cooled down to room temperature, de-molded and post-cured at 350°F for 2 hours. The cure cycled used during the manufacturing process is shown in Figure 2.

4. CHARACTERIZATION

4.1. FIBER VOLUME FRACTION TESTING

Fiber volume fraction tests were conducted on the manufactured OOA composite panel using sulphuric acid digestion method. Four specimens each weighing from 0.50 to 2 grams was cut from the panel. The edges of the specimens were polished thoroughly to facilitate accurate density measurements. The samples were dried in an oven for 1 hour at 120°C to remove any surface moisture and then weighed. The specimens were tested for density. The samples had an average density of 1.5037 g/cm^3. The fiber volume fraction was then calculated from the following formula:

$$V_f = \frac{M_i \times D_c}{M_f \times D_f}$$

where, M_i is initial mass of the specimen before digestion

M_f is the final mass of specimen after digestion

D_c is density of composite

D_f is fiber density (taken as 1.75 g/cm^3)

The Void content was calculated as:

$$V_v = 100 - (V_m + V_f)$$

where, V_m is the matrix volume fraction by volume and V_f is the fiber volume fraction.

Table 1 shows the density, fiber volume fraction, and void content of the composite samples. The samples had an average fiber volume fraction of 53.99 %, and a void content of 0.21 %. The fiber volume fractions obtained are typical of high performance composite parts.

4.2. TENSILE TESTS

Tensile tests were performed on the OOA composites to evaluate the ultimate tensile strength of the composites. Samples of 2.286 mm (0.09 in.) thickness (6 layers) with 25.4 mm (1 in.) and 12.7 mm (0.5 in.) width either slipped or failed in the grips. Hence the thickness of the samples was decreased to 0.064 in (4 layers). While samples with 25.4 mm (1 in.) width failed in the grips without slipping, 12.7 mm (0.5 in.) wide samples failed in the middle. The test results obtained for 12.7 mm (0.5 in.) width and 1.626 mm (0.064 in.) thickness are given below. Composites coupons were cut from the panels were manufactured using 4 layers of MTM45-1/CF2412 OOA prepregs. Tests were conducted on the coupons using Instron 4204 testing machine in accordance with ASTM D 3039. Samples were tested at a crosshead speed of 12.7 mm/min. (0.05 in./min). The ultimate tensile strength, modulus and failure strain are tabulated in Table 2. The samples had an average tensile modulus, strength and strain to failure of 824.79 MPa, 65.20 GPa and 1.27%, respectively.

4.3. FLEXURE TESTS

Static flexure tests were performed on the OOA composites to evaluate the bending properties. Samples of 0.09 in thickness (6 layers) with 12.7 mm (0.5 in.) width manufactured from 6 layers of MTM45-1/CF2412 prepregs were used as test specimens. Tests were conducted on an Instron testing machine according to ASTM D790-03. A span to depth ratio of 40:1 was used to avoid failure by shear. Six specimens were tested at a crosshead speed of 6.096 mm/ min. (0.24 in./min.) The flexural stress-strain curves are shown in Figure 3. The ultimate flexural strength, modulus and stain to failure values are tabulated in Table 3.

4.4. LOW VELOCITY IMPACT TESTS

Low velocity impact tests have been performed on the composite panels manufactured using Out-of-Autoclave (OOA) process. A Dynatup Instron Model 9250 Impact Testing Machine with impulse control and data system was used to carry out the low velocity impact tests. Three different energy levels of 10J, 20J, and 25J were considered. The hemi-spherical impactor had a mass of 6.88 Kg and a diameter of 12.7 mm (0.5 in). The energy-time history, load vs. displacement and velocity-time history plots were shown in Figures 4 - 6 respectively. The impactor penetrated the samples at 30J of energy.

4.5. COMPRESSION-AFTER-IMPACT (CAI) TESTS

CAI tests have been conducted on MTM45-1/CF2412 composites manufactured using OOA process. The tests were performed according to ASTM D7137. Four specimens of size 152.4 mm (6 in.) x 152.4 mm (6 in.) were first subjected to low velocity impact tests and then machined to 152.4 mm (6 in.) x 101.6 mm (4 in.) for the CAI tests. Laminate construction consists of 12 fabric plies with a stacking sequence of $[(+45/-45)/(0/90)]_{3S}$. Impact energy per unit thickness of 6672 J/m, an industry standard for evaluating thick, quasi-isotropic laminates was selected. Just clearly visible impact damage (VID) has been observed at 32J. The CAI test fixture is edge-loaded between the flat platens. Loads were applied at a cross-head speed of 1.27 mm/min. (0.05 in./min). Compression load vs. deflection curves are shown in Figure 7. The ultimate compression-

after-impact strength values of the specimens are tabulated in Table 4. The front view of the tested samples is shown in Figure 8.

5. STATISTICAL ANALYSIS

DoE includes two aspects: process of statistically planning experiments and process of analyzing data by statistical methods to draw meaningful conclusions. The planning procedure includes selection of response variables, factors, levels and finally performing the experiment. Response variable is the output that one would like to observe or study from the experiment. Factors are the controlled input variables that influence the performance of a process or system. The levels of each factor can be amount or magnitude such as considering 25 mm (0.1 in.) and 50 mm (0.2 in.) can be two levels of thickness.

Several response variables obtained from the impact tests are: impact energy, contact force, displacement, velocity, contact duration, threshold force, threshold energy and perforation threshold energy. The ANOVA results show that the statistical model for velocity was not significant and hence excluded. While all other responses are included in the study, threshold force and energy cannot be obtained for few samples. The statistical analysis of a response restricts that all data is available to retain the balance and the analysis is not possible for insufficient data. Therefore, the response variables considered for this study are: amount of energy absorbed by the composite, peak force, contact duration, and maximum deflection of the impactor.

The factors selected for the study are: size (in-plane dimensions) of the panel, thickness and lay-up configuration. Studies have shown that all these variables are significantly affect the impact response of the composites. Two levels were considered for each factor. The levels of each factor are shown in Table 5 and the experimental treatments are given in Table 6. Each experiment was replicated twice. A 2^3 factorial design with two replications has been used for the present work.

6. EXPERIMENTATION

A Dynatup Instron Model 9250 Impact Testing Machine with impulse control and data system was used to carry out the low velocity impact tests. The maximum physical drop height of the machine is 1.25 m and the machine can simulate a drop height of 20.4 m. The impact test instrument has a motor and twin screw drive for rapid crosshead retrieval after impact. The impulse control and data system includes impulse software controller panel for test set-up and high-speed impulse signal conditioning unit. The impulse data software can calculate total energy, contact force, impactor displacement and impactor velocity as a function of time. 127 mm (5 in.) x 127 mm (5 in.) and 50mm (2 in.) x 50mm (2 in.) fixtures were used for the tests. The hemi-spherical impactor had a mass of 6.88 Kg and a diameter of 12.7 mm (0.5 in.). All the experiments were conducted at a fixed energy level of 20 J. The energy level was selected such that it causes a maximum dent depth yet without penetrating any of the samples. Each specimen was selected randomly and clamped in the fixture. The impactor mass was then raised to the desired drop height corresponding to the energy of impact. The impactor was dropped onto the clamped specimen. As the impactor makes contact with the specimen, the impulse control data acquisition system is triggered to start acquiring data.

7. RESULTS AND DISCUSSION

Figures 9 - 11 show the energy vs. time history, contact force (or simply ‘load’) history and load vs. deflection plots of the test panels, respectively. The loading phase of the energy history curve indicates the amount of energy absorbed by the specimen and the unloading phase is a measure of the amount of energy given by the specimen to the impactor. The net absorbed energy is given by the flat region of the curve. The contact force history curve gives the information of threshold force, peak force and contact duration. While some specimens show mountain like load-deflection curves with sharp peak loads, other curves exhibited flat region at the peak load. The ascending section of the curve gives the information on bending stiffness history of the composite under impact loading and the descending portion of the load-deflection curve gives the information about rebounding of the impactor and softening of the composite. The load vs. deflection curve will be an open curve when the impactor penetrates through the

composite with horizontal section representing the friction between the impactor and the composite specimen. The area under the curve gives the absorbed energy. The maximum deflection of the impactor as it comes in contact with the target can also calculated from the load vs. deflection curve or can be obtained from displacement history curve.

The p-values obtained from the ANOVA results are summarized in Table 7. The p-values signify the effects that are statistically significant based on the experimental results. An effect is considered to be significant if the p-value is less than or equal to 0.05. The R^2 values given in Table 7 show that the statistical model fits very well with the data.

The P-values for all the three main effects and interaction effects of size, lay-up and thickness are less than 0.05 indicating that all effects are significantly influencing the absorbed energy at 95% confidence level. Absorbed energy for all the samples varied from 10.94 J to 19 J. The main and interaction effect plots of size, lay-up and thickness are shown in Figures 12 - 13.

For a given lay-up configuration, and thickness, larger samples absorbed lower energies. However for a given lay-up and size, the change in the thickness of the sample did not show one trend. For 50 mm (2 in.) x 50 mm (2 in.) panel, absorbed energy increased slightly with increase in thickness whereas absorbed energy decreased considerably with increase in thickness in the case of 127 mm (5 in.) x 127 mm (5 in.) panel. From the size vs. thickness interaction plots, it is observed that with the increase in aspect ratio (width/thickness), the ability of the composite to absorb energy decreased. Similar observations were made by Cantwell et al. [12]. Cantwell et al. observed that while increasing the size of the panels has resulted in absorbing more energy, doubling the dimensions did not yield the same response.

Highest energy was absorbed by 50 mm (2 in.) x 50 mm (2 in.) and $[45/0/45]_s$ while the lowest energy was absorbed by $[0/45/0]_s$ and 127 mm (5 in.) x 127 mm (5 in.). While significant changes were not observed in the absorbed energy for thin samples, changing the lay-up from $[45/0/45]_s$ to $[0/45/0]_s$ lay-up resulted in considerable decrease in thick samples. Similarly, the change in absorbed energy is not as pronouncedly observed in 50 mm (2 in.) x 50 mm (2 in.) samples as observed in 127 mm (5in.) x 127 mm (5in.) samples. Stacking sequence, size and thickness all govern the flexural stiffness

of the composite and hence the absorbed energy. Table 7 shows that among all the main effects and interaction effects, only main factors of size and thickness and the interaction of size and thickness have a significant effect on peak force, contact duration and maximum deflection. Figure 14 shows the plots of significant main effects and Figure 15 shows the significant interaction effect plots. In case of peak force, thinner and larger samples have minimum peak force while both 127 mm (5 in.) x 127 mm (5 in.) and 50 mm (2 in.) x 50 mm (2 in.) samples absorbed same amount of peak force at 5 mm (0.2 in.) thick. The significant main effect and interaction effect plots of size, thickness on the contact duration are shown in Figures 16 and 17 respectively. Contact duration decreased with increase in thickness. Panels with 127 mm (5 in.) x 127 mm (5 in.) displayed higher contact duration for both thin and thick panels. Hence, the lowest contact duration was observed for 5 mm (0.2 in.) thick and 50 mm (2 in.) x 50 mm (2 in.) panels. The significant main effect plots and interaction plots on maximum displacement are shown in Figures 18 and 19 respectively. Thicker panels showed less displacement at maximum energy. The displacements are more pronounced in 5 in x 5 in samples.

8. CONCLUSIONS

High performance carbon composites were successfully manufactured using new generation and low-cost OOA vacuum-bag-only cure prepreg process. Fiber volume fraction tests showed that the composites have void content less than 0.25%. Tensile, flexure, impact, and compression-after-impact tests were conducted on the manufactured panels. The influence of size, lay-up configuration and thickness on the low velocity impact behavior of carbon composites was investigated using DoE techniques. The test results were analyzed using ANOVA. The results show that all the identified geometric parameters and their interactions have significant effect on the amount of energy absorbed by the specimen. Whereas, only size, thickness, and size vs. thickness have significant effect on peak force, contact duration and maximum deflection. Only size has a significant effect on the velocity. These results can be used to simplify and gain more insight into the low-velocity impact study of composites.

9. REFERENCES

1. National Materials advisory Board, "New Materials for next generation transport," Washington, D.C., The National Academic Press, p. 38,1996.
2. Tatum, S., "VARTM Cuts Costs," *Reinforced Plastics*, 45(5) (2001): 22.
3. Bond, G. G. Griffith, J. M., Hahn, G. L., "Non-Autoclave Prepreg Manufacturing Technology," *40th International SAMPE Fall Technical Conference*, Memphis, TN (2008): 25
4. Rhodes, M. D. and Williams, J. G., "Effect of resin on impact damage tolerance of graphite-epoxy laminates," *NASA TND 8411*, 1977.
5. Schoeppner, G.A., Abrate, S., "Delamination threshold loads for low velocity impact on composite laminates," *Composites: Part A*, 31(2000): 903–915.
6. Sutherland, L. S., and Guedes Soares, C., "The Effects of Test Parameters on the Impact Response of Glass Reinforced Plastic using an Experimental Design Approach," Composites Science and Technology, 63 (2003): 1-18.
7. Abrate, S., "Impact on Composite Structures," London, Cambridge University Press, (1998).
8. Abrate, S., "Impact on Laminated Composite Materials," *Applied Mechanics Reviews*, 44 (1991): 155-190.
9. Abrate, S., "Impact on laminated composites: Recent Advances," *Applied Mechanics Reviews*, 47 (1994): 517-544.
10. Cantwell, W. J. and Morton, J., "The impact response of composite materials – A Review," *Composites*, 22 (1991): 347 – 362.
11. Richardson, M. O. W., Wisheart, M. J., "Review of Low-velocity Impact Properties of Composite Materials," *Composites – Part A*, 27 (1996): 1123 – 1131.
12. Cantwell, W. J. and Morton, J., "Geometrical Effects in the Low Velocity Impact Response of CFRP," *Composite Structures*, 12 (1989): 39-59.
13. Tita, V., Carvalho, J. D., Vandepitte, D., "Failure Analysis of Low Velocity Impact on Thin Composite Laminates: Experimental and Numerical Approaches," *Composite Structures*, 83 (2008): 413 – 428.

14. Atas, C., and Sayman, O., "An Overview of Impact Response of Woven Fabric Composite Plates," *Composite Structures,* 82 (2008): 336 – 345.
15. Atas, C., and Liu, D., "Impact Response of Woven Composites with Small Weaving Angles," *International Journal of Impact Engineering*, 35 (2008): 80 – 97.
16. Sutherland, L. S., and Guedes Soares, C., "Scaling of Impact on Low Fibre-Volume Glass-Polyester Laminates," *Composites: Part A*, 38 (2007): 307 – 317.
17. Gomez-del Rio,T., Zaera, R., Barbero, E., and Navarro, C., "Damage in CFRPs Due to Low Velocity Impact on Low Temperature," *Composites: Part B,* 36 (2005): 41 – 50.
18. Hosur, M. V., Jain, K., Chowdhury, F., Jeelani, S., Bhat, M. R., and Murthy, C. R. L., "Low-Velocity Impact Response of Carbon/Epoxy Laminates Subjected to Cold-Dry and Cold-Moist Conditioning," *Composite Structures,* 79 (2007): 300 – 311.
19. Shyr, T. W., and Pan, Y. H., "Impact Resistance and Damage Characteristics of Composite Laminates," *Composite Structures,* 62 (2003): 193 – 203.
20. Riccio, A., and Tessitore, N., "Influence of Loading Conditions on the Impact Damage Resistance of Composite Panels," *Composites and Structures,* 83 (2005): 2306 – 2317.

Table 1. Fiber Volume Fraction Test Results of MTM45-1/CF2412

Specimen	**Density (g/cc)**	**Fiber volume fraction (%)**	**Void content (%)**
1	1.5021	53.6185	0.1629
2	1.5052	54.5352	0.3616
3	1.5018	53.7553	0.2569
4	1.5059	54.0799	0.0738
Average	1.5037	53.9972	0.2138

Table 2. Tensile Properties of MTM45-1/CF2412

	Ultimate Tensile Strength (MPa)	**Tensile Modulus (GPa)**	**Failure Strain (%)**
1	877.38	65.02	1.35
2	795.56	65.64	1.24
3	820.17	60.40	1.26
4	857.17	65.84	1.3
5	826.27	69.09	1.19
Average	824.79	65.20	1.268
Standard Deviation	25.34	3.11	0.061

Table 3. Flexural Test Results of MTM45-1/CF2412

	Sample #						Average
	1	**2**	**3**	**6**	**7**	**8**	
Strength (MPa)	821.65	842.60	810.55	875.53	844.20	873.52	844.68
Modulus (GPa)	52.73	51.66	51.34	54.90	53.37	53.23	52.87
Failure Strain (%)	1.70	1.707	1.69	1.77	1.78	1.86	1.75

Table 4. CAI Strength Values at 32J Energy Level of MTM45-1/CF2412

	Compression After Impact Strength (MPa)
Sample - 1	240.2
Sample - 2	233.6
Sample - 3	244.9
Sample - 4	241.3
Average	240.0
Standard Deviation	4.7

Table 5. DOE Factors and their Levels

Factor	Higher Level	Lower Level
Size of the panel	127mm (5in.) x 127mm (5in.)	50mm (2 in.) x 50mm (2 in.)
Layup	$[45/0/45]_s$	$[0/45/0]_s$
Thickness	5mm (0.2 in.)	2.5mm (0.1in.)

Table 6. Experimental Treatments for Testing

Run	Factors/Levels		
	Size	**Lay-up**	**Thickness**
1	50 mm (2 in.) x 50 mm (2 in.)	$[45/0/45]_s$	2.5mm (0.1 in.)
2	127 mm (5 in.) x 127 mm (5 in.)	$[45/0/45]_s$	2.5mm (0.1 in.)
3	50 mm (2 in.) x 50 mm (2 in.)	$[0/45/0]_s$	2.5mm (0.1 in.)
4	127 mm (5 in.) x 127 mm (5 in.)	$[0/45/0]_s$	2.5mm (0.1 in.)
5	50 mm (2 in.) x 50 mm (2 in.)	$[45/0/45_2/0/45]_s$	5mm (0.2 in.)
6	127 mm (5 in.) x 127 mm (5 in.)	$[45/0/45_2/0/45]_s$	5mm (0.2 in.)
7	50 mm (2 in.) x 50 mm (2 in.)	$[0/45/0_2/45/0]_s$	5mm (0.2 in.)
8	127 mm (5 in.) x 127 mm (5 in.)	$[0/45/0_2/45/0]_s$	5mm (0.2 in.)

Table 7. Analysis of Variance (ANOVA), p-values

Source	**Energy Absorbed (J)**	**Peak Force (kN)**	**Contact Duration (ms)**	**Maximum Deflection (mm)**
Size	**<0.0001**	**0.0169**	**<0.0001**	**0.0063**
Lay-up	**0.0002**	0.4751	0.1538	0.3773
Thickness	**<0.0001**	**<0.0001**	**<0.0001**	**<0.0001**
Size*Lay-up	**0.0019**	0.8489	0.0700	0.3351
Size*Thickness	**<0.0001**	**0.0331**	**0.0004**	**0.0135**
Lay-up*Thickness	**0.0001**	0.4510	0.0658	0.3545
Size*Lay-up*Thickness	**0.0013**	0.9239	0.0785	0.3611
R^2 (%)	99.89	99.47	99.53	95.38
Standard Deviation	0.1400	0.1300	0.2900	0.6800

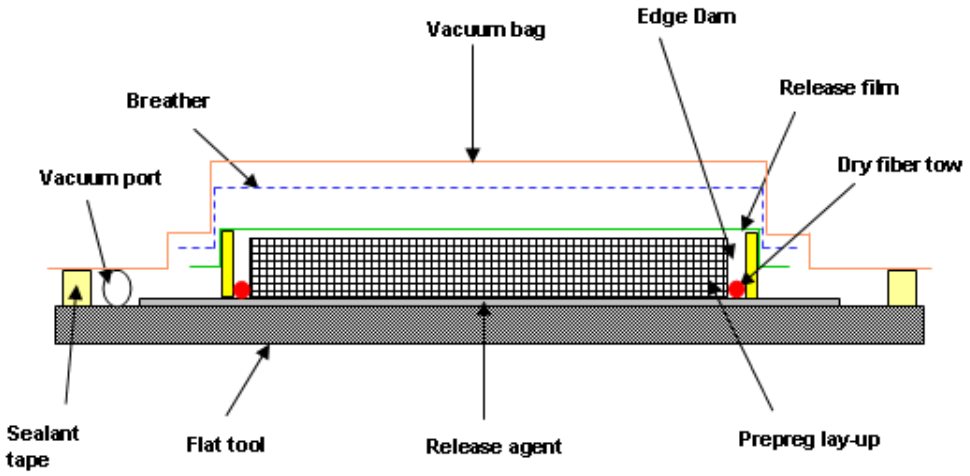

Figure 1. Schematic of Out-of-Autoclave Bagging Procedure

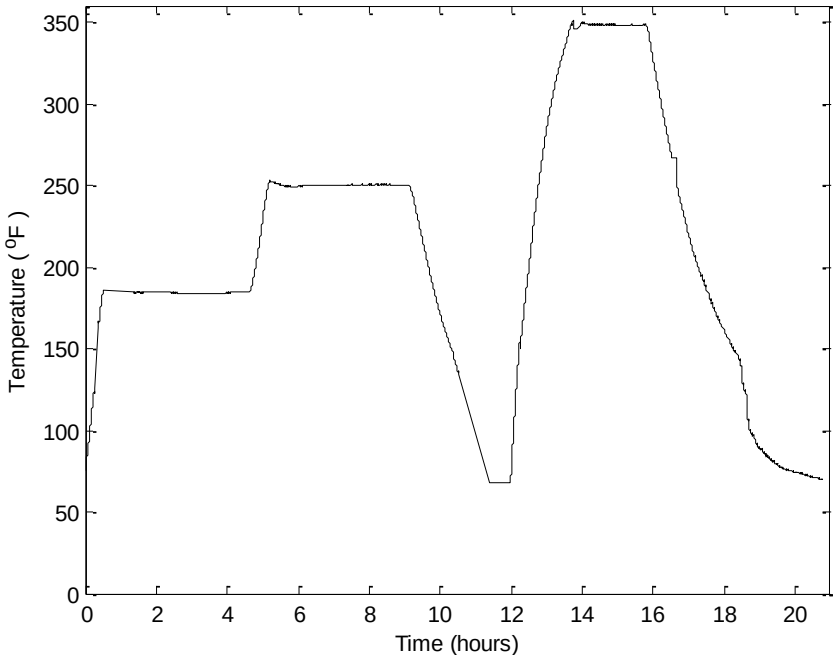

Figure 2. Cure Cycle for Out-of-Autoclave Process

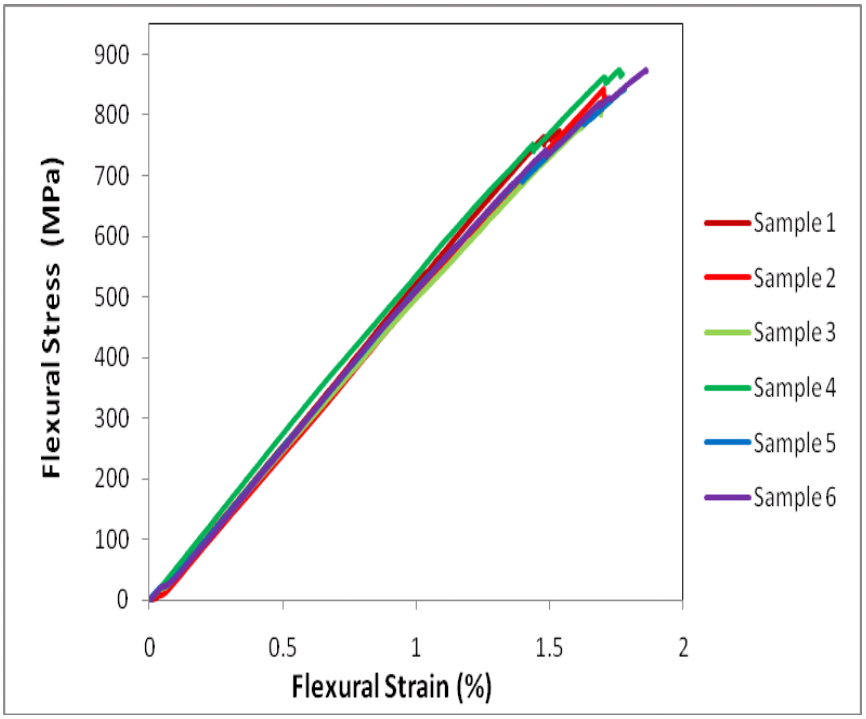

Figure 3. Flexural Stress-Strain Curves of MTM45-1/CF2412 Composites

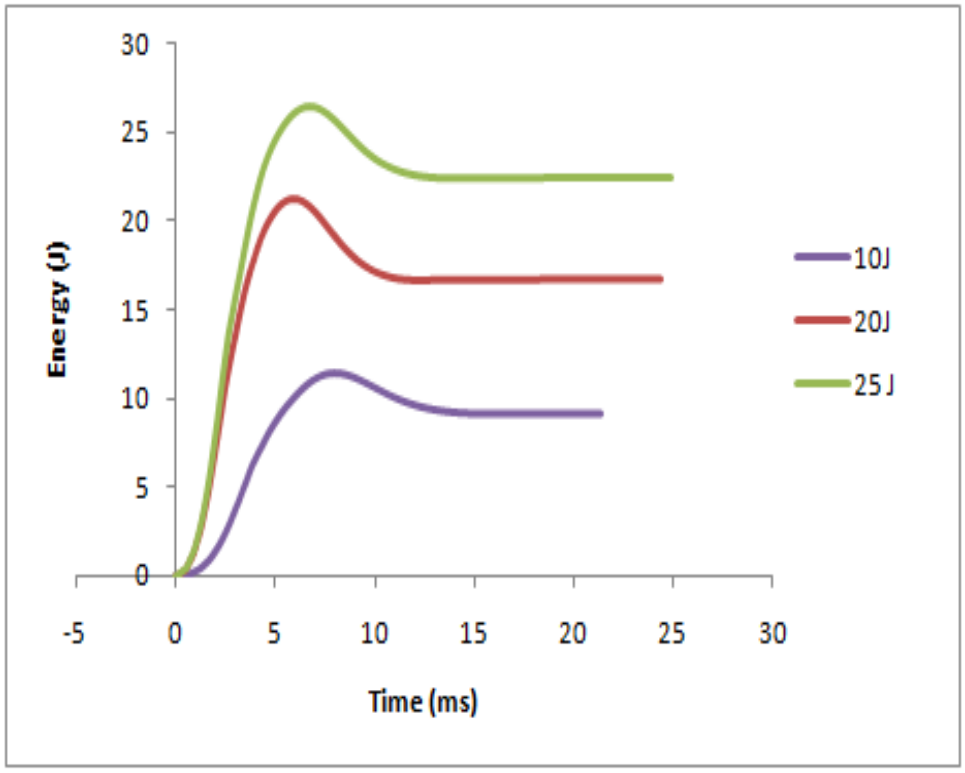

Figure 4. Energy-Time History of MTM45-1/CF2412 Composites

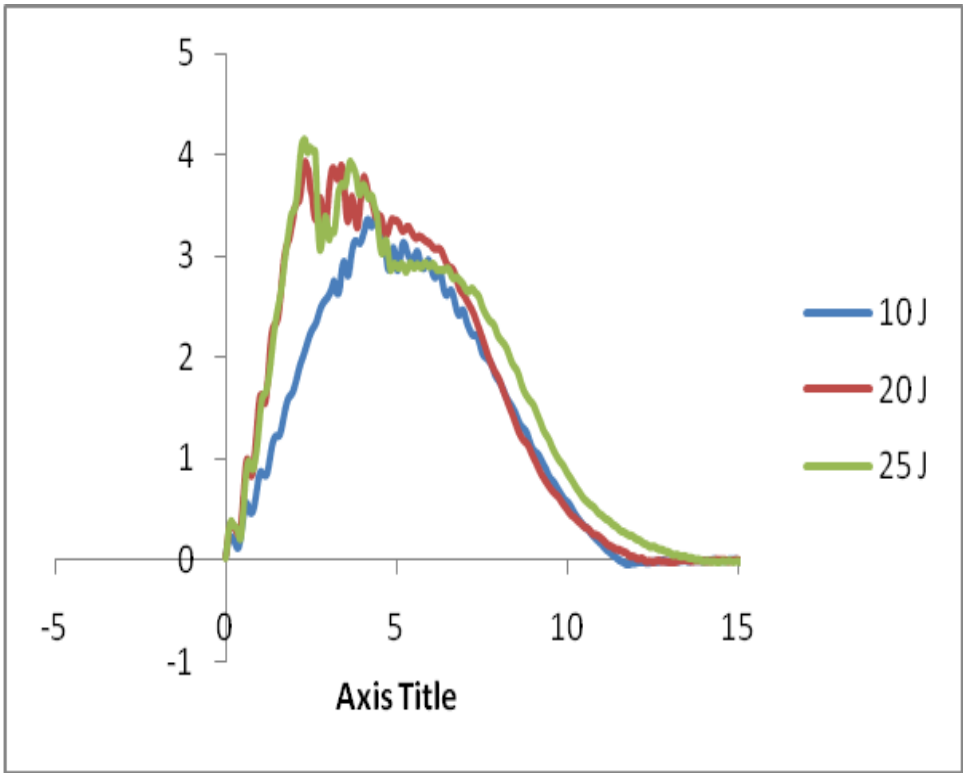

Figure 5. Impact Load vs. Deflection of MTM45-1/CF2412 Composites

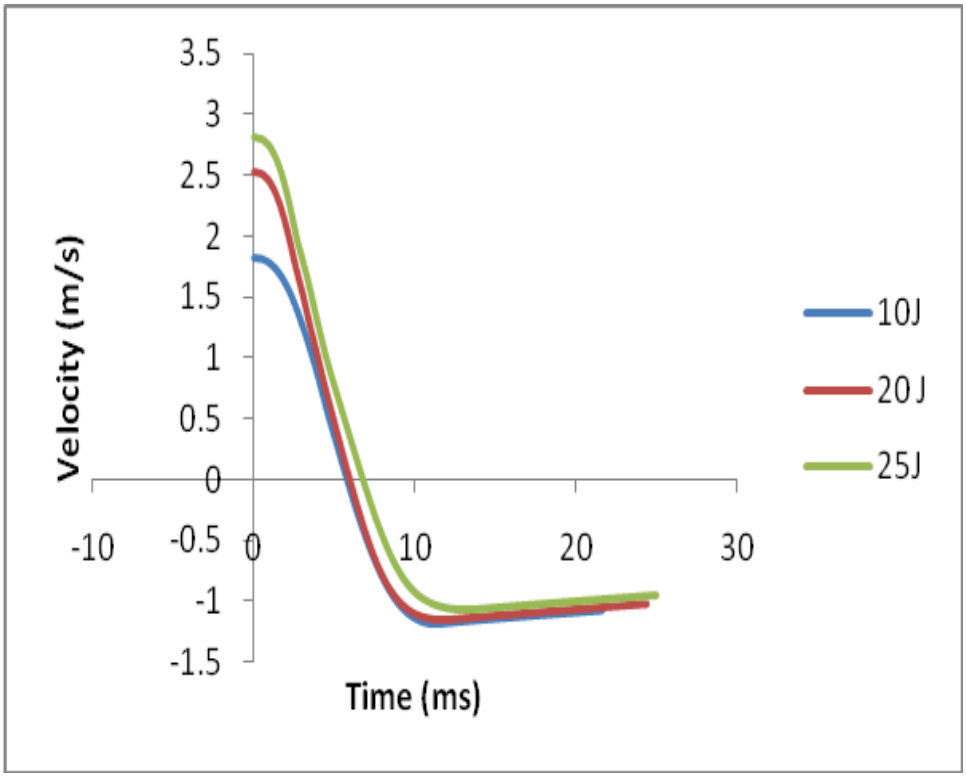

Figure 6. Velocity-Time History of MTM45-1/CF2412 Composites

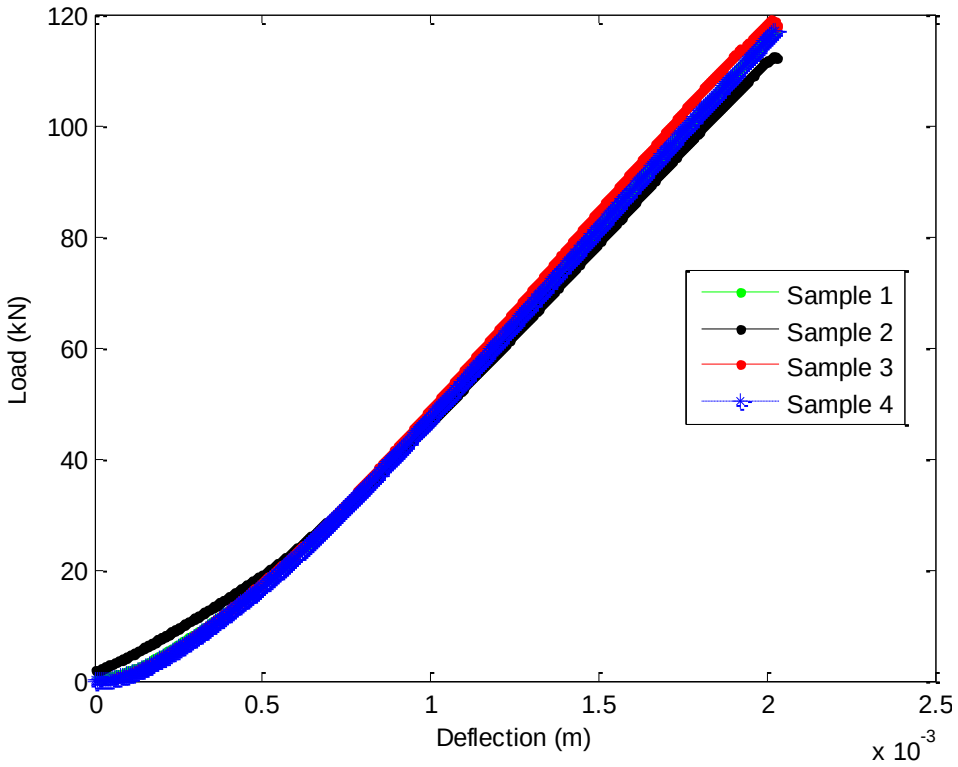

Figure 7. Load vs. Deflection of MTM45-1/CF2412 Composites during CAI Testing Process

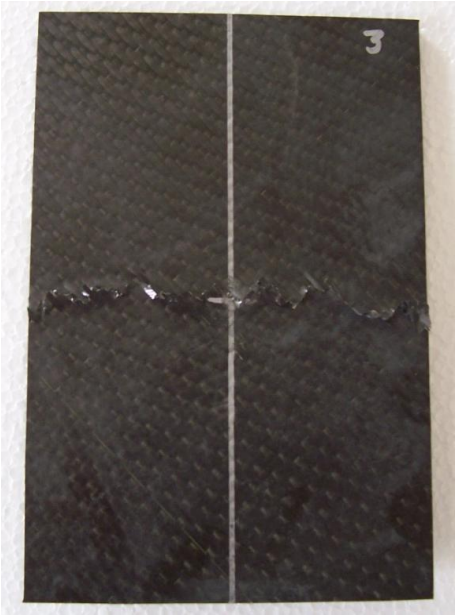

Figure 8. Front View of MTM45-1/CF2412 Composite Sample under CAI Testing

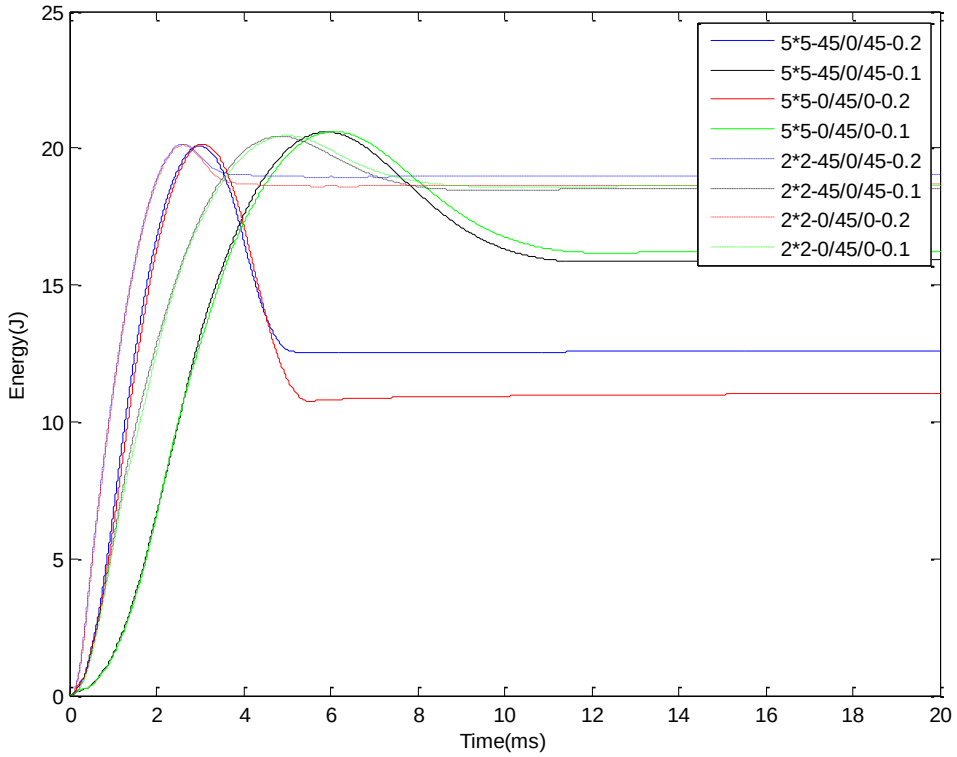

Figure 9. Impact Energy vs. Time of MTM45-1/CF2412 Composites

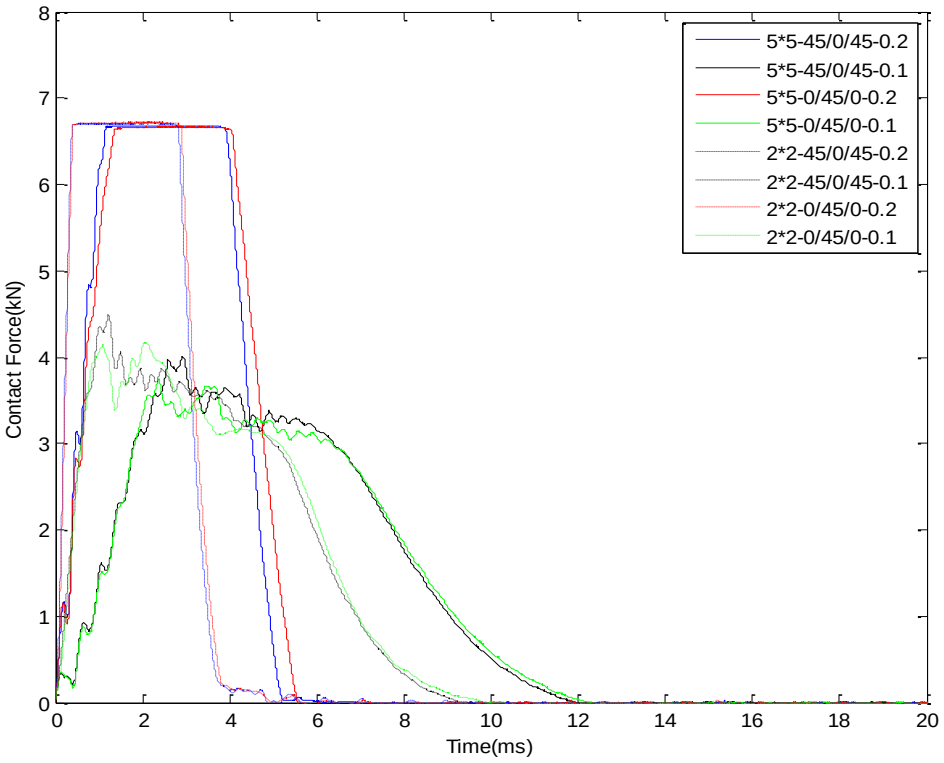

Figure 10. Contact Force vs. Time of MTM45-1/CF2412 Composites

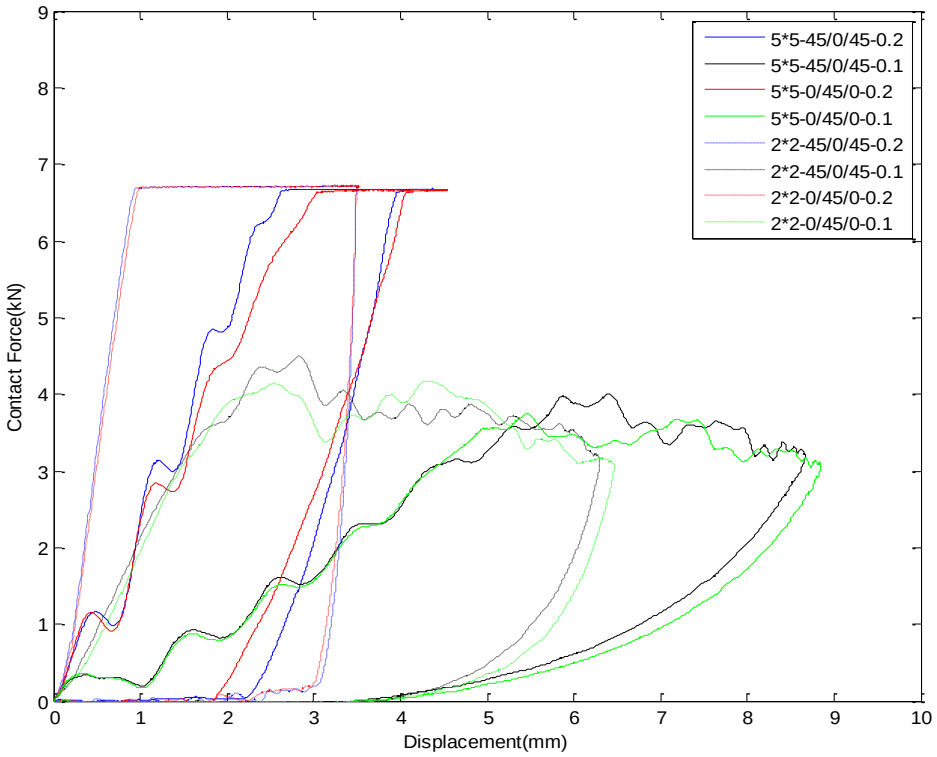

Figure 11. Contact Force vs. Displacement of MTM45-1/CF2412 Composites

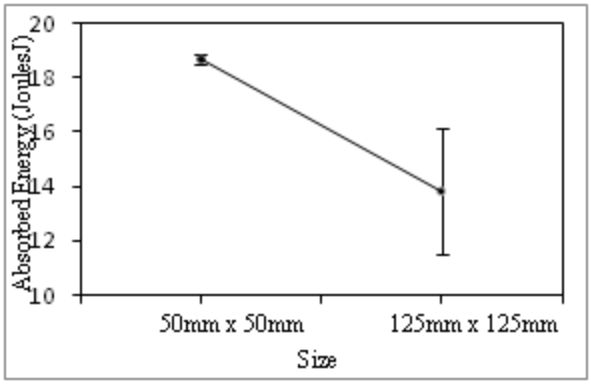

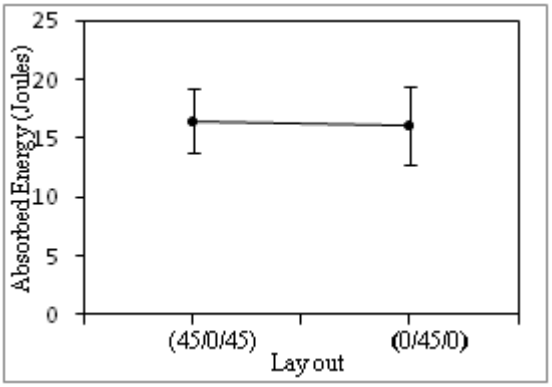

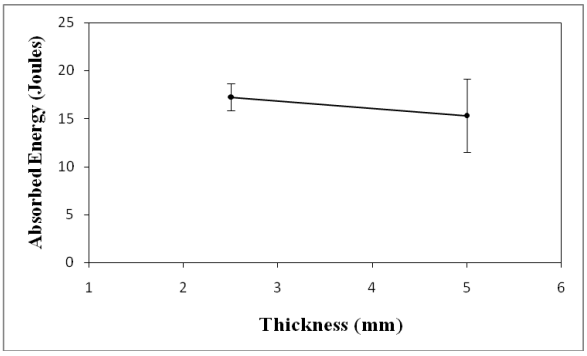

Figure 12. Main Effect Plots for Absorbed Energy

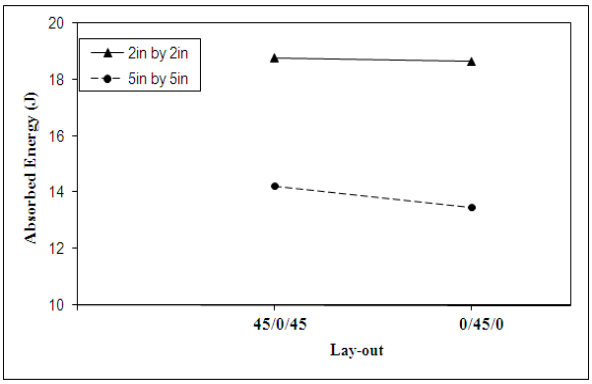

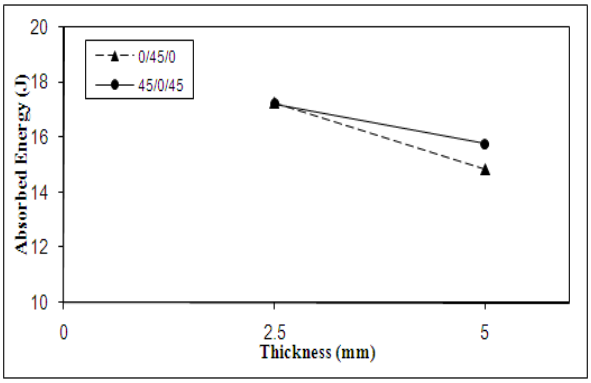

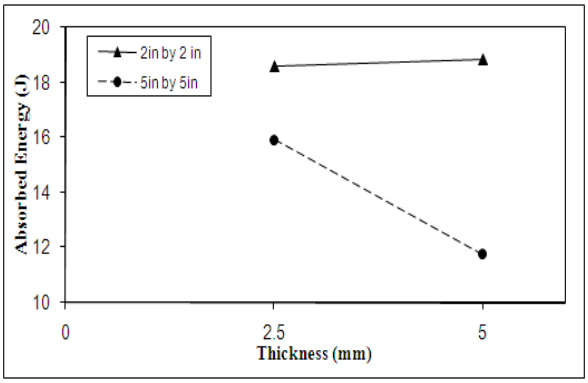

Figure 13. Interaction Effect Plots for Absorbed Energy

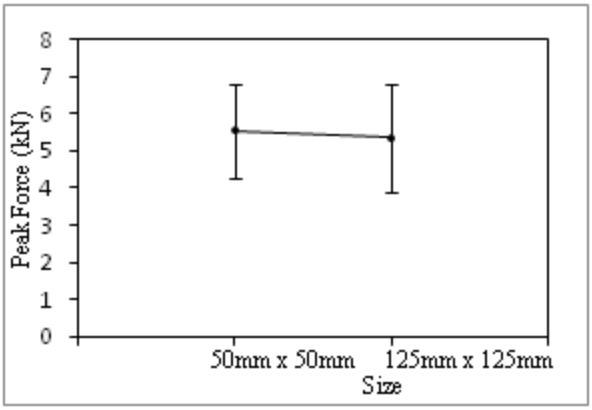

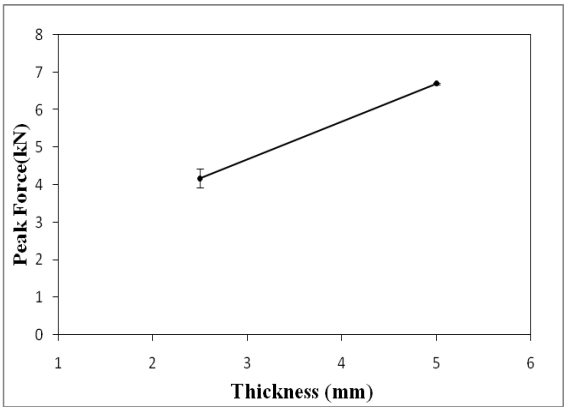

Figure 14. Significant Main Effect Plots for Peak Force

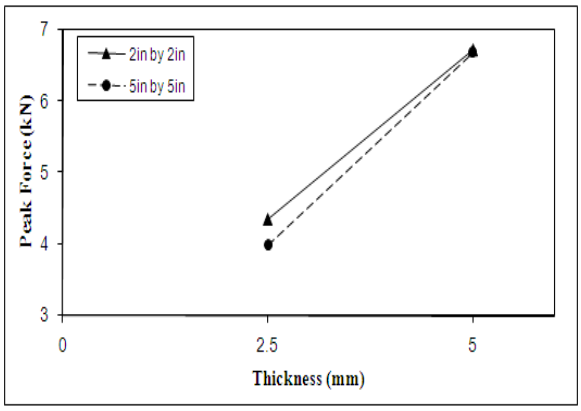

Figure 15. Size vs. Thickness Interaction Effect Plot for Peak Force

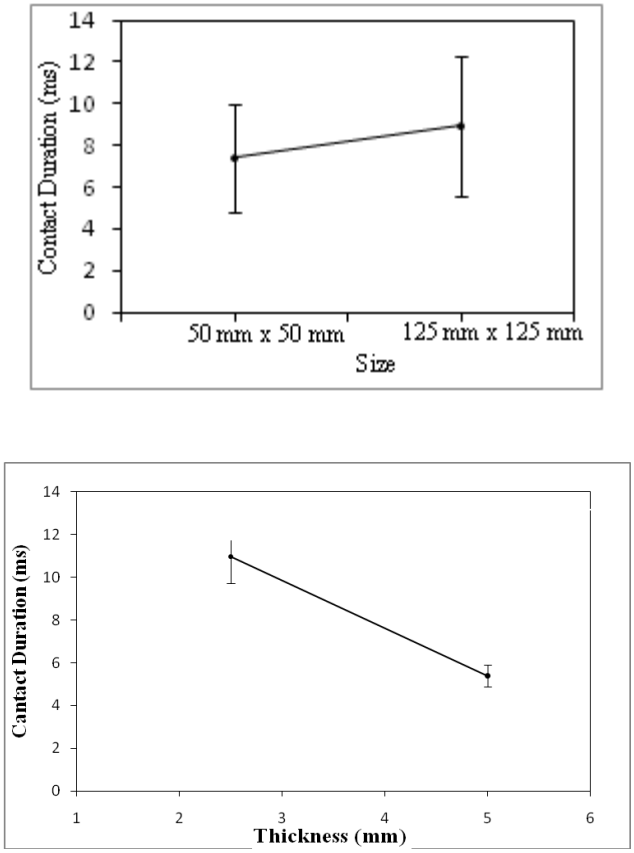

Figure 16. Significant Main Effect Plots for Contact Duration

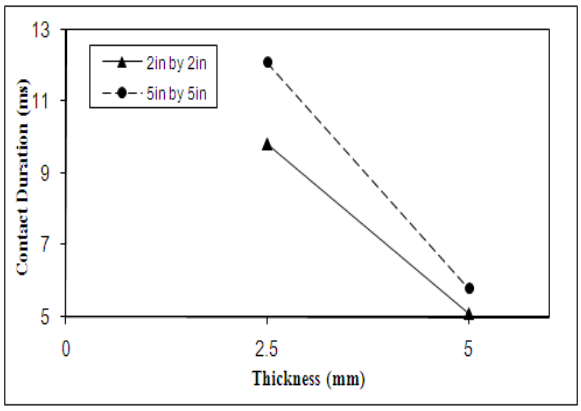

Figure 17. Size vs. Thickness Interaction Effect Plot for Contact Duration

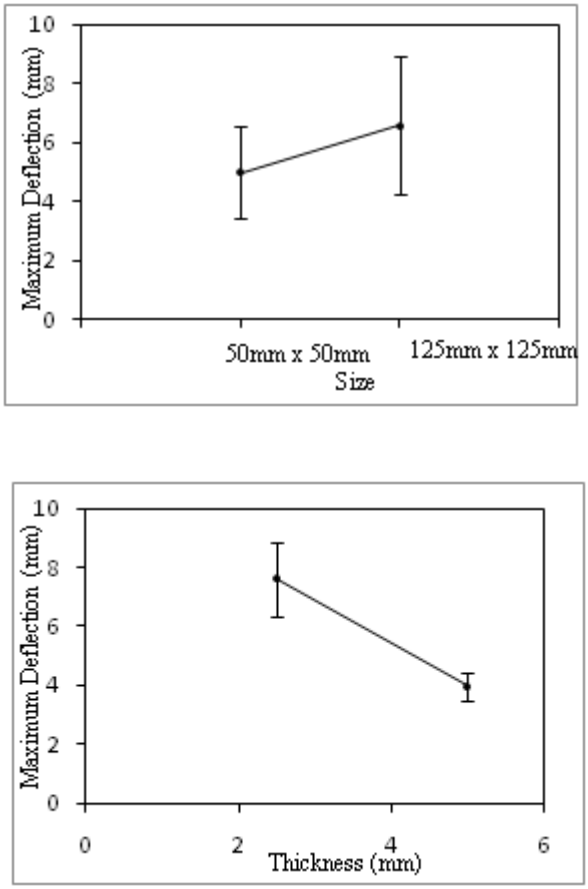

Figure 18. Significant Main Effect Plots for Maximum Deflection

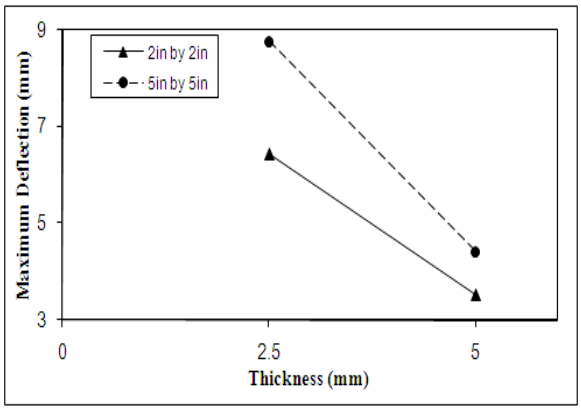

Figure 19. Size vs. Thickness Interaction Effect on Maximum Deflection

SECTION

3. CONCLUSIONS

The dissertation presents the development and characterization of advanced composites using non-autoclave processes. The first paper offers the details of the set developed to manufacture elevated-temperature composites. The challenges of the process and the procedures followed to address them were presented. Two vacuum bagging processes: SCRIMP and DVBI processes were evaluated. Composite panels manufactured using DVBI process were evaluated to be of low void content, high fiber volume contents and uniform thickness. A database of physical and mechanical properties of the resin system and manufactured composites was developed from tensile, flexure, short beam shear, impact, compression after impact and open hole compression tests. Viscosity and Differential scanning calorimetric (DSC) tests were conducted to evaluate the infusion and cure behavior of the resin system. Density and fiber volume fraction tests showed that composites with void content less than 1% were performed to evaluate the quality of the manufactured parts. A database of these properties will help manufacturers and designers to employ low cost elevated-temperature VARTM process. A three dimensional flow simulation of VARTM process was developed and implemented in ABAQUS commercial code. The flow simulation results are compared with the experimental findings for a flat panel and the simulation results are in good agreement with experimental results

In the second paper, open-cell honeycomb core sandwich composites were manufactured using a modified one-step VARTM process. Manufacturing open-cell core composites using low cost VARTM process result in significant cost savings. The details of the manufacturing process and the set-up developed were presented. The manufactured sandwich composites were free from any resin inside the core. The adhesive fillet formation was studied using photomicrographs.The quality of the adhesive bond was evaluated using flatwise tensile tests. Flatwise/edgewise compression, three-point bending and low velocity impact test results were also presented. Fiber volume fraction and optical microscopy test results show that the facesheets have very low void content. The work shows that the currently available moisture barrier adhesive films can be used

to implement a resin infusion process for honeycomb or open-cell core sandwich composite manufacturing.

In the third paper, a new oven cure vacuum-bag-only OOA process was evaluated for the manufacturing of aerospace composites. High performance carbon composites were successfully manufactured. Fiber volume fraction tests showed that the composites have void content less than 0.25%. Tensile, flexure, impact, and compression-after-impact tests were conducted on the manufactured panels. The influence of size, lay-up configuration and thickness on the low velocity impact behavior of carbon composites was investigated using DoE techniques. The results show that all the identified geometric parameters and their interactions have significant effect on the amount of energy absorbed by the specimen. Whereas, only size, thickness, and size vs. thickness have significant effect on peak force, contact duration and maximum deflection. Only size has a significant effect on the velocity.

The results from the present work show that non-autoclave processes are very promising in producing parts that have part qualities comparable to autoclave manufactured parts. The research presented here could be extended in several ways. The non-autoclave processes can be explored to manufacture complex and integral parts thus resulting in further cost reductions. And also the simulation can be improved to include cure and compaction models. Finally, the flow simulation can be extended to implement for large complex parts.

BIBLIOGRAPHY

1. B.D. Agarwal, L. J. Broutman, and K. Chandrashekhara, "Analysis and performance of Fiber Composites," 2006.
2. Alan A. Baker, Stuart Dutton, D. Kelly, Donald W. Kelly "Composite Materials for Aircraft Structures," Second Edition, AIAA, 2004.
3. D. Gay, S. V. Hoa, "Composite Materials: Design and Applications," Second Edition, CRC Press, 2002.
4. February 2005 market report, Global Composites Market 2004-2010, published by E-Composites Inc.
5. Bitzer, T., "Honeycomb Technology: Materials, Design, Manufacturing, Applications and Testing," *Chapman & Hall:* (1998).
6. Menta, V. G. K., Sundararaman, S., Chandrashekhara, K., Phan, N., and Nguyen, T., "Hybrid Composites using Out-of-Autoclave Process for Aerospace Sub-structures," *SAMPE International Symposium*, 53 (2008): 1-11.
7. Khan, S., and Loken, H. Y., "Bonding of Sandwich Structures - The Facesheet/Honeycomb Interface – A Phenomenological Study," *39rd International SAMPE Technical Conference*, Baltimore, MD (2007): 1-9.
8. Holemans, P., "Liquid Molded Hollow Cell Core Composite Articles," *United States Patent 6780488 B2*, 2004.
9. Loren R. Thomas, Alan K. Miller, Allan L. Chan, "Fabrication of Complex High-Performance Composite Structures at Low Cost using VARTM," SAMPE 2002 - Long Beach, CA, May 12 - 16, 2002.
10. M. P. Groover, "Fundamentals of Modern Manufacturing: Materials, Processes, and Systems," John Wiley and Sons, 2010.
11. J. Hu, S. Sundararaman, V.G.K. Menta and K. Chandrashekhara, "Failure Pressure Prediction of Composite Cylinders for Hydrogen Storage using Thermo-mechanical Analysis and Neural Network," Advanced Composite Materials, Vol. 8, No. 2, 2009
12. K. T. Hsiao, J. W. Gillespie,Jr. and S. G. Advani, "Role of Vacuum Pressure and Port Locations on Flow Front Control for Liquid Composite Molding Processes," Polymer Composites, Vol. 22, pp. 660-667, 2001.

13. Tatum, S., "VARTM Cuts Costs," *Reinforced Plastics*, 45(5) (2001): 22.
14. Bond, G. G. Griffith, J. M., Hahn, G. L., "Non-Autoclave Prepreg Manufacturing Technology," *40th International SAMPE Fall Technical Conference*, Memphis, TN (2008): 25
15. V. G. K. Menta, R. R. Vuppalapati, K. Chandrashekhara, Gary G. Bond, and N. Phan, "Low Velocity Impact of Composites Manufactured using Out-of-Autoclave Process," Proceedings of SAMPE Conference, SAMPE 2009, Baltimore, MD, May 18 -21, 2009.
16. K. Kang, W. I. Lee, and H. T. Hahn, "Analysis of the Vacuum Bag Resin Transfer Molding Process," Composites, Part A, Vol. 32, pp. 1535-1560, 2001.
17. National Materials advisory Board, "New Materials for Next Generation Transport," Washington, D.C., *The National Academic Press*: (1996).
18. W. D. Brouwer, E. C. F. C. van Herpt, and M. Labordus, "Vacuum Injection Molding for Large Structural Applications," Composites Part A: Applied Science and Manufacturing, Vol. 34, pp. 551-558, 2003.
19. Brosius D, "Boeing 787 Update," High Performance Composites, May 2007.
20. Fu, X., Zhang, C., Liang, R., Wang, B. and Fielding, J. C., "High Temperature Vacuum Assisted Resin Transfer Molding of Phenylethynyl Terminated Imide Composites," *Polymer Composites*, (2010) In Advance of Print, doi: 10.1002/pc.21015
21. Kruckenberg, R. and Paton, R., "Resin Transfer Moulding for Aerospace Structures," *Chapman & Hall:* (1998).
22. Jonas, S., and Thorsten, J., "New Rohacellê Development for Resin Infusion Processes," Proceedings *of the 7th International Conference on Sandwich Structures*, Aalborg, DK (2005): 1-10.
23. Ebonee, P. M. W., Brian, S. H., and James, C. S., "VARTM Processing of Honeycomb Sandwich Composites: Effect of Scrim Permeability," *33rd International SAMPE Technical Conference*, Seattle, WA (2001): 1-7.

VITA

Venkatagireesh Menta was born in Nellore, Andhra Pradesh, India on March 12th 1983. He received his Bachelor of Engineering degree in Mechanical Engineering in 2004 from Sri Venkateswara University, Tirupati, India. He joined Mechanical Engineering program at Missouri University of Science and Technology (Formerly: University of Missouri – Rolla), Rolla, Missouri, USA and obtained M.S. degree in August 2007. He later enrolled for his Ph.D. in Mechanical Engineering at Missouri S&T since August 2007. He has held the position of Graduate Research Assistant through his M.S and Ph.D. degrees since August 2005.